Suspended Cohesive Particle Characteristics in the Connecticut River Estuary

Author: Katherine Lavallee

SUSPENDED COHESIVE PARTICLE CHARACTERISTICS IN THE CONNECTICUT RIVER ESTUARY

Katherine D. Lavallee

A thesis
submitted to the Faculty of
the department of Earth & Environmental Sciences
in partial fulfillment
of the requirements for the degree of
Master of Science

Boston College
Morrissey College of Arts and Sciences
Graduate School

August, 2017

Suspended Cohesive Particle Characteristics in the Connecticut River Estuary

Katherine D. Lavallee
Advisor: Dr. Gail C. Kineke

ABSTRACT

To determine the role of cohesive suspended particle characteristics on sediment transport patterns in an energetic estuary floc size, density, and settling velocity were investigated in the Connecticut River estuary over three years spanning varying fluvial discharge regimes. Concurrent measurements of in-situ floc size, flow, bed stress, salinity and suspended-sediment concentration (SSC) were used to identify primary influences on floc size variability. Water discharge ranged from 202 to 910 m^3/s between the three sampling campaigns, and the timing of major sediment discharge events preceding measurement periods from 23 to 162 days. Two distinct particle populations were observed under high and low sediment discharge regimes. With abundant fluvial sediment input, flocculation occurred resulting in large, loosely-packed flocs dominating the suspended signal (median sizes of 194-209 μm; median excess densities of 13-17 kg/m^3). Following an extended period of low sediment discharge, small, dense aggregates resuspended from the bed were observed throughout the water column (median size of 171 μm and excess density of 60 kg/m^3). The timing of and partial decoupling of water and sediment discharge led to inter-annual patterns of cohesive particle characteristics controlled by fresh sediment supply. The large, light flocs with lower settling velocities characteristic of high sediment supply regimes likely bypass the estuary. Smaller compact aggregates dominated the low-sediment discharge regimes. However, the similar disaggregated size distribution of the two regimes suggests the same fine source material is reintroduced to the estuary with the intrusion of the salt wedge, which extends farther up-estuary during low discharge regimes and ultimately supplies the off-channel bays and coves.

TABLE OF CONTENTS

List of Tables:

List of Figures:

Acknowledgements

First and foremost I would like to thank my advisor, Dr. Gail Kineke, for her guidance, support, encouragement and unfailing ability to find the right equation when needed. Without you, I would not be here.

Massive thanks are needed to my mentor and floc extraordinaire Tim Milligan. Thank you for letting me poke around your instruments four years ago and for helping me tell this story.

I would also like to thank my thesis committee: Dr. Noah Snyder and Dr. Corinne Wong. Your insight and edits not only helped shape my approach to my project, but your coursework challenged me to be a better scientist.

I also would not be here without the unwavering support and friendship from my lab group- Kendall Valentine Cole, Lisa Kumpf, Kevin Simans, Ellen Kristiansen, and Michelle Mullane. Thank you for always being there to bounce ideas off, de-bug code, and lend a hand if OBSes (or my brain) needed calibrating. I cannot imagine my time at BC without you.

And finally I would like to thank my family for their love, support, and willingness to listen to me talk on and on about these little particles floating in the water.

This project was funded by National Science Foundation grant OCE-1234164.

1. INTRODUCTION

Understanding the processes that control sediment transport within the estuarine system is vital to proper management and preservation, with consequences for maintenance of harbors, navigation channels, management of commercial fisheries, shoreline erosion, turbidity and water quality (Mehta, 1989; Dyer, 1995). Fine-grained sediments are of particular interest in estuaries because they impact the fate of contaminants (Milligan and Loring, 1997). Pollutants such as trace metals, organic pollutants and radionuclides are often associated with the smallest suspended particles, as cohesive aggregates preferentially incorporate dissolved and suspended chemical constituents (Eisma, 1986; Mehta, 1989; Xia et al., 2004). Understanding the transport and trapping of fine-suspended sediment can have important implications for predicting toxin residence times and planning pollution remediation efforts (Kranck and Milligan, 1992; Dyer, 1995). Additionally, suspended-sediment transport patterns such as localized trapping and rapid deposition can lead to shoaling which impacts dredging (Woodruff et al., 2001; Ralston et al., 2012).

The fate of fine-grained, cohesive sediments in estuaries is largely determined by the settling velocity of the sediment. Flocculation of fine sediments, or the formation of aggregates composed of silts and clays through inter-particle collision and adhesion, is a major control on the effective settling velocity of these muddy sediments (Kranck, 1980; Winterwerp, 1998; Fugate and Friedrichs, 2003). Once flocs, or agglomerations of smaller particles, form, they are held together by intermolecular Van der Waals forces as well as organic coatings and can be difficult to break up entirely (Eisma, 1986; Hill et al., 2000). Flocs can range from 10 μm to several mm in diameter, resulting in settling

velocities up to several orders of magnitude greater than those of individual grains and can limit dispersal of fine sediments (Kranck, 1973; Manning and Bass, 2006).

In dynamic environments like estuaries, flocculation may vary widely in both time and space (Winterwerp, 2002). The interaction of tides and riverine flow in estuaries result in complex circulation patterns and can result in the formation of strong density fronts, where the convergence of bottom flows and dampening of turbulence can lead to sediment trapping (Traykovski et al., 2004; Ralston et al., 2012; Woodruff et al., 2013).

Flocs have been observed in virtually all marine environments, however floc properties can vary widely between sites and even temporally at a single location (Kranck and Milligan, 1992; Markussen and Andersen, 2013; Fettweis and Baeye, 2015). Methods such as digital imaging and video settling columns, laser transmissometry, and water sampling tubes have increased the accuracy of in-situ measurements by reducing floc disruption during sampling, however the heterogeneous nature of suspended sediment necessitates conducting site-specific investigations (Mehta, 1989; Mikkelsen et al., 2005; Manning and Schoellhamer, 2013). Sediment-transport models are widely used as management tools in estuarine settings, however the complexity of settling patterns and circulation dynamics can cause errors, particularly if flocculation dynamics are left out (Manning and Bass, 2006; Smith and Friedrichs, 2015).

The primary objective of this study is to quantify cohesive suspended-particle dynamics in the Connecticut River estuary to determine their importance to fine-sediment transport and trapping in a highly stratified, seasonally-varying estuarine system. Observed changes in concentration, floc size, density and settling velocity will influence the relative importance of transport mechanisms within the system. Spatial and seasonal

measurements of floc size, density, constituent particles, salinity, suspended-sediment concentration (SSC) and bottom stress have been collected to determine the relationship between suspended-sediment particle characteristics and suspended-sediment transport pathways in the Connecticut River estuary.

2. Background

2.1 Flocculation processes

In natural systems inorganic, fine, suspended particles such as clays have negative surface charges (Eisma, 1986). Particles smaller than 63 μm are considered fine grained, though cohesion becomes important for particles less than 20 μm (Mehta, 1989). These negative forces must be overcome in order for aggregates to form. Flocculation is controlled by five primary mechanisms: (a) adsorption of positively charged ions, such as salt ions, to compensate for negative surface charges, (b) adsorption of organic matter, sometimes creating organic coatings, that glue particles together, (c) Brownian motion, or the random movement of particles in a fluid, leading to particle collisions, (d) particle collision through differential settling, when larger particles with faster settling velocities overtake smaller particles with slower settling velocities causing collisions, and (e) turbulent shear in the water column, where turbulent eddies cause particle collisions (van Leussen, 1988; Fugate and Friedrichs, 2003; Winterwerp and van Kesteren, 2004). Flocs can range from 10 μm to several mm in diameter, resulting in settling velocities up to several orders of magnitude greater than their component particles (Kranck, 1973; Manning and Bass, 2006).

Suspended-sediment concentration and shear in the flow also influence floc size. At low concentrations, flocs are typically small. With increased concentrations more collisions between particles and 'microflocs' (flocs < 160 μm in diameter) form, leading to the building of larger flocs sometimes reaching the mm scale, or 'macroflocs' (Fig. 1; Manning and Dyer 1999; Uncles et al. 2006; Manning and Scheollhamer, 2013). In natural settings, turbulent stresses can disrupt flocs (Winterwerp and van Kesteren, 2004;

McCave, 2005). At low shear stresses, concentration effects dominate and flocs can grow by increasing the likelihood of collision, while at higher stresses (> 0.1 Pa) floc breakup occurs (Winterwerp, 1997). In addition, large flocs are more easily disrupted by stresses than small flocs. Shear intensity also affects the floc size distribution. At low and high stresses modal distribution is narrow, where at moderate shear a wide range of floc sizes is possible due to simultaneous growth and breakup processes (Burban et al., 1989; Winterwerp, 1998).

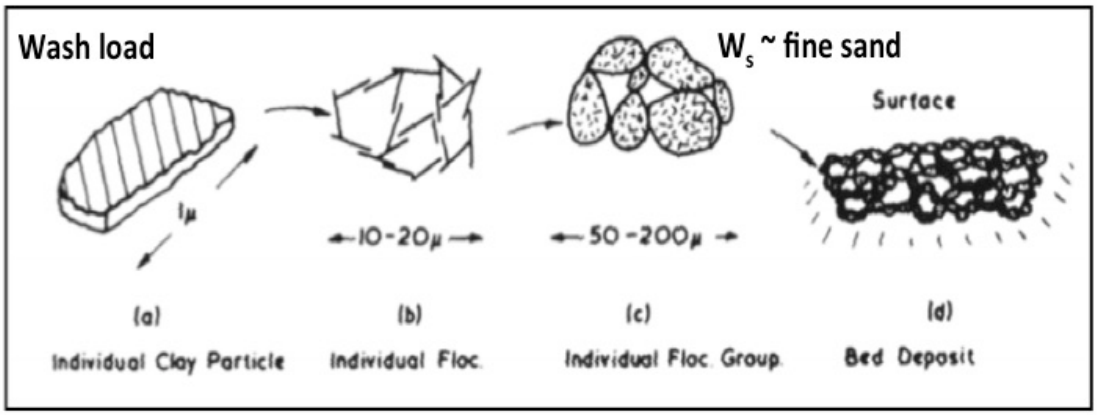

Figure 1. Size range and structure of cohesive sediments, modified from Van Leussen (1997).

2.2 Estuarine circulation and sediment transport

Estuaries are influenced by a combination of factors including the input of sediment from rivers, and the mixing of fresh and salt waters due to tides (Wright et al., 1989; Blake et al., 2001). This mixing causes estuaries to display intense horizontal gradients of fluid properties, or fronts. In particular, estuaries have the strongest density gradients of any marine environment (Geyer et al., 2012). High river discharge and weak tidal currents result in salt-wedge, or highly-stratified, estuaries that possess strong salinity fronts along the bottom of the estuary, marking the landward limit of the salinity

intrusion (Fig. 2; Geyer and Farmer, 1989; Horne and Patton, 1989). Multiple fronts can occur within an estuary due to flow alterations from channel constriction or changes in bathymetry. The presence of fronts can affect the circulation and sediment transport within an estuary. The convergence of bottom flows and damping of turbulence due to stratification, can lead to suspended-sediment trapping at fronts (Traykovski et al., 2004; Woodruff et al., 2012).

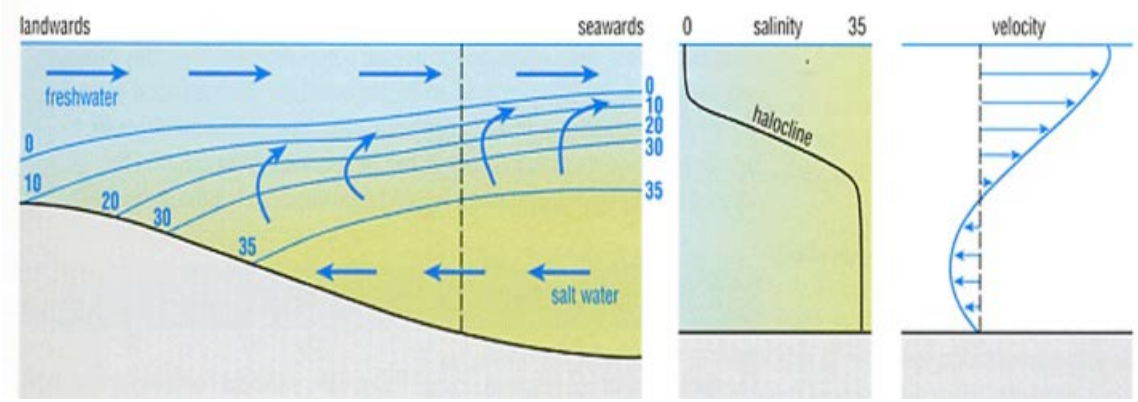

Figure 2. Typical salinity and velocity structure within a salt-wedge estuary. The freshwater flowing over the intruding salt water causes stratification in the form of a steep halocline. Near-bed tidal-averaged velocity is net landward, while surface flow is net seaward. Modified from Open University (1999).

Suspended-sediment concentrations in estuaries are typically high, with sediment input from the river and the sea (Dyer, 1995). Bottom stress and the structure of turbulence near the bed are important factors in the patterns of sediment transport within an estuary. The erosion and deposition of sediment at the bed and its entrainment and transport in the water column are controlled by the stress at the bed (Kim et al., 2000). The frictional drag from flow over the bed creates a velocity gradient, or shear, that produces turbulence (Dyer, 1997). The energy for mixing and erosion at the bed comes from the dissipation of kinetic energy in the boundary layer (Winterwerp, 1998).

Measuring the settling velocities of fragile flocs whose densities may vary as their diameters change is challenging but well studied (Eisma, 1986; Van Leussen, 1998; Fugate and Freidrichs, 2002; Manning and Bass, 2006), and important to accurately estimate suspended-sediment transport patterns. Flocculation is a major control on the settling velocity (w_s) of cohesive sediments in suspension, controlling the settling component of the two-dimensional time-dependent advection-diffusion equation (Harris and Wiberg, 2002):

$$\frac{\partial C}{\partial t} = -u\frac{dC}{\partial x} + \frac{\partial}{\partial x}\left(K_x \frac{\partial C}{\partial x}\right) + w_s \frac{\partial C}{\partial z} + \frac{\partial}{\partial z}\left(K_z \frac{\partial C}{\partial z}\right) \quad (1)$$

where C is suspended-sediment concentration, u is current velocity, t is time, and K_x and K_z are the horizontal and vertical turbulent diffusion coefficients respectively. The vertical coefficient K_z, is also called the eddy diffusivity, and is dependent on bed stress and height above the bed. This equation calculates C as a function of four mechanisms: advection ($-u\frac{dC}{\partial x}$), horizontal diffusion ($\frac{\partial}{\partial x}\left(K_x \frac{\partial C}{\partial x}\right)$), settling ($w_s \frac{\partial C}{\partial z}$), and vertical diffusion ($\frac{\partial}{\partial z}\left(K_z \frac{\partial C}{\partial z}\right)$) where diffusion is due to turbulent mixing.

2.3 Motivation and previous work

Issues associated with fine-sediment deposition such as predicting toxin residence times, planning pollution remediation efforts, localized trapping and rapid deposition which can lead to shoaling were discussed in Section 1 (Kranck and Milligan, 1992; Dyer, 1995; Traykovski et al., 2004). The complex and dynamic behavior of flocs during transportation underscore the importance of studying cohesive suspended-sediment properties over both tidal and seasonal time scales. While the former has been widely investigated, there are few flocculation studies that span multiple years (Manning and Bass, 2006; Fetteweis and Baeye, 2015).

Prior studies suggest complicated sediment transport patterns within the Connecticut River estuary, some postulating that fine sediments bypass the estuary and are delivered to Long Island Sound (Horne and Patton, 1989), while more recent work has found localized regions of rapid accumulation of fine sediments in off-channel coves (Woodruff et al., 2013; Yellen et al., 2017). Additionally, strong salinity fronts have been observed in the Connecticut River estuary making it a natural laboratory for the study of flocculation and trapping processes related to frontogenesis (Geyer et al., 2010).

2.4. Objectives

The goal of this study is to quantify suspended-sediment particle characteristics in the Connecticut River estuary to determine their importance to fine-sediment transport and trapping in a highly stratified, seasonally-varying estuarine system. Observed changes in suspended-sediment concentration (SSC), floc size, density and settling velocity will influence the relative importance of transport mechanisms within the system. In situ suspended-sediment and hydrodynamic measurements were taken over varying discharge regimes to determine the relationship between suspended-sediment particle characteristics and suspended-sediment transport pathways in this energetic, shallow estuary.

3. METHODS

3.1 Study site description

The Connecticut River is the third largest river on the east coast of the United States, originating at the border between Canada and New Hampshire and discharging into Long Island Sound (Fig. 3). The Connecticut River drains an area of 29,000 km^2 and has a mean annual discharge of 465 m^3/s. Maximum discharge (~2500 m^3/s) typically occurs with the spring snow melt in April, delivering high fine-grained sediment loads on the order of 10^6 tons per year, which is the largest sediment load of rivers in the northeastern U. S. (Horne and Patton, 1989). Low discharge generally occurs during late summer (September), with baseline flows of ~140 m^3/s occurring approximately 10% of the time (Yellen et al., 2017). According to Patton and Horne (1992) and Woodruff et al. (2013), above the extent of tidal influence, suspended-sediment concentration follows discharge according to a power-law relationship, leading the bulk of the sediment load to be transported to the estuary during seasonal high discharge from March to May. Yellen et al. (2014) found that late summer-fall hurricanes can have significant, though rare, effects on the sediment discharge, delivering loads exceeding the yearly average over the span of several days.

Long Island Sound has semi-diurnal tides resulting in a tidal influence extending nearly 100 km upstream, although the tidal amplitude is under 2 m making it a microtidal estuary. The fluctuations in salinity distribution, tidal range and river discharge patterns have caused the estuary to be classified as a partially-mixed estuary during low to moderate discharge (Garvine, 1974) as well as a salt-wedge estuary during moderate to high discharge (Meade, 1966; Garvine, 1975; Ralston et al., 2016).

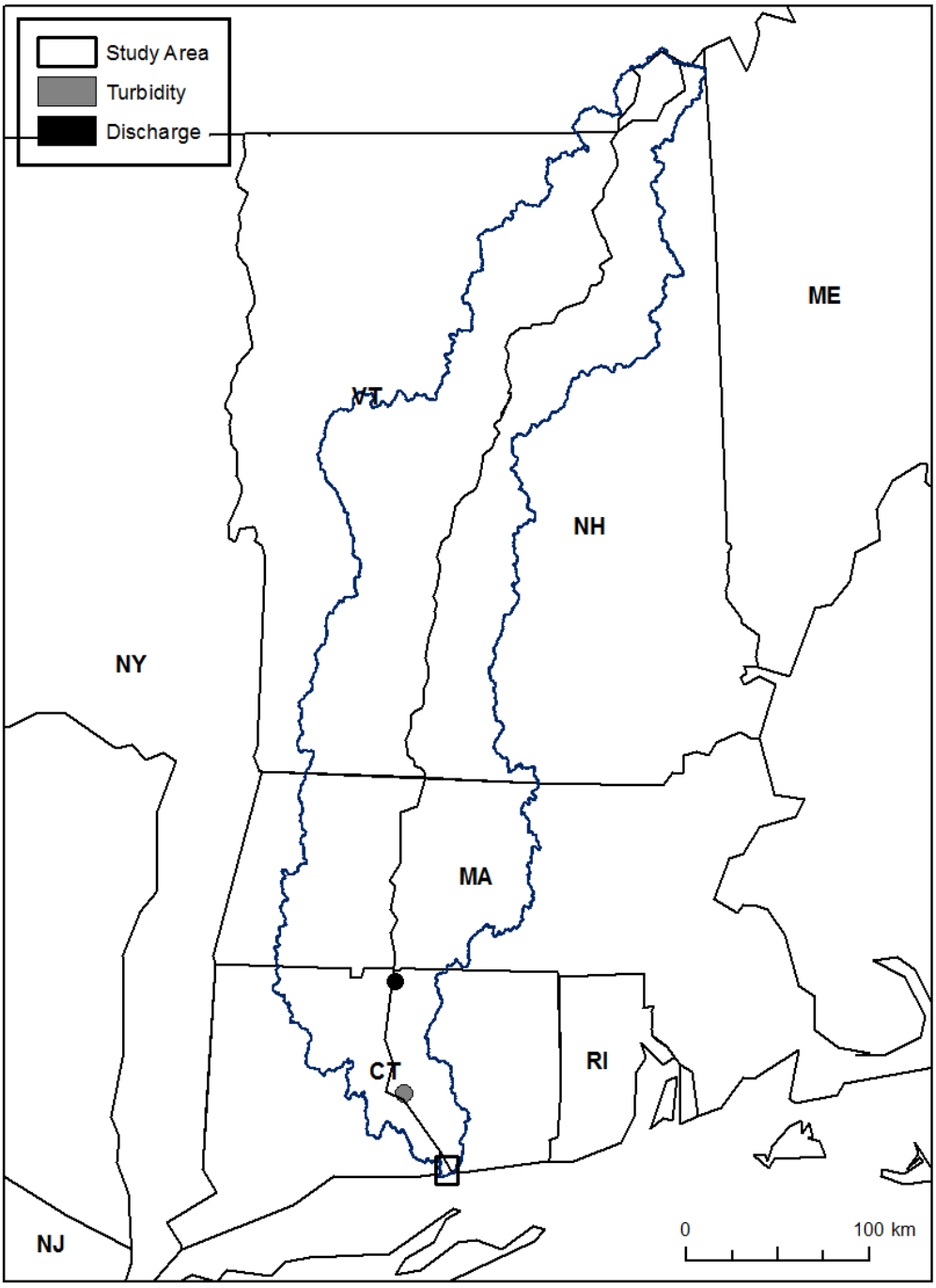

Figure 3. The Connecticut River watershed, the largest on the east coast of the U.S. spans from southern Quebec south to Long Island Sound. The study area is marked in the black rectangle along with the location of long-term Connecticut River turbidity (USGS gage 1193050, Middle Haddam, CT) and water discharge (USGS gage 1193050, Thompsonville, CT).

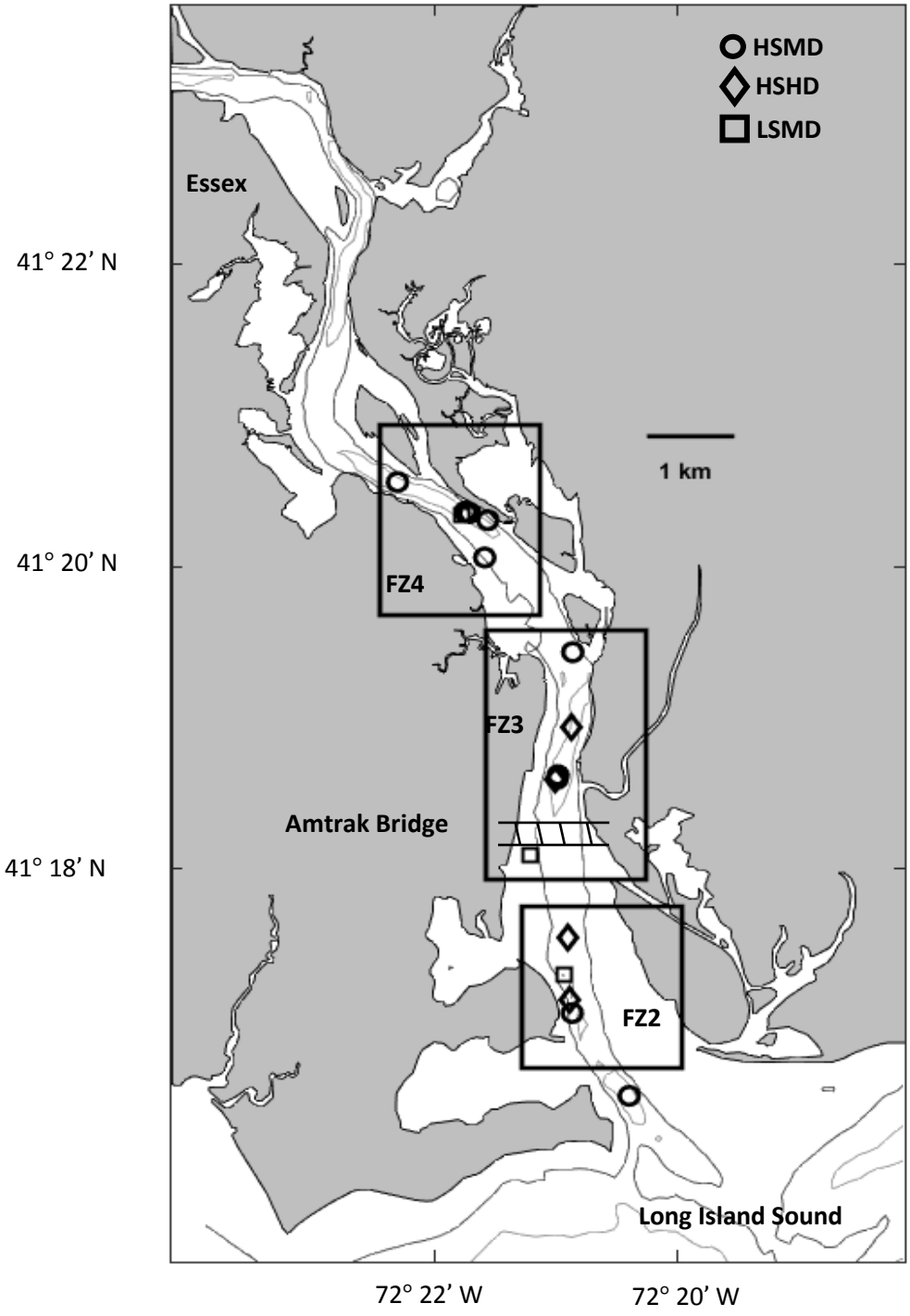

Figure 4. Site map of the Connecticut River estuary. Measurements were taken at fifteen anchor stations under three different hydrologic regimes from Essex, CT south to the mouth at Long Island Sound. Known regions of convergence, or frontal zones, are indicated by black boxes and are labeled in ascending order from south to north. Circle, diamond and square markers correspond to HSMD, HSHD, and LSMD regimes respectively. This symbol convention will be used throughout the paper.

The study area extends from Essex, CT downstream to the estuary mouth where the river discharges into Long Island Sound (Fig. 4). The upper estuary from Essex to the Amtrak railroad bridge to the south is described by Horne and Patton (1989) as bedrock-confined with a meandering thalweg 4 to 9 m deep. The lower estuary is a coastal-plain estuary with wider shoals and a shallower channel.

3.2 Anchor station measurements

The field program for this project consisted of three sampling periods over three years, spanning high and low water and sediment discharge regimes (Table 1). Water-column data were collected at three locations within the upper and lower estuary, where two instrumented packages were alternately deployed while at anchor for water-column profiles. Anchor-station locations were chosen based on previous observations of salinity fronts within the estuary (Geyer et al., 2010). Frontal zones are labeled in ascending order from south to north (Fig. 4).

Table 1. Summary of hydrologic conditions preceding and during each field survey.

	November 2013 (HSMD)	**May 2014 (HSHD)**	**Sept.-Oct. 2015 (LSMD)**
Mean daily discharge during observations (m^3/s)	578	638	507*
Cumulative discharge (m^3 per two weeks before cruise)	2.7×10^8	13.8×10^8	2.3×10^5
Mean change in discharge per day two weeks prior to cruise, $\frac{dQ}{dt}$ (m^3/day)	2480	7930	2550 (2120 excluding 10/2/15)
Mean annual discharge, year preceding cruise (m^3/s)	502	585	467
Days above mean flow during prior year	113	118	119
Days above Q + 1 std	52	57	43
Days above Q + 2std	21	20	17
Tidal range (m)	1.2	1.2	1.1

* S15 cruise coincided with a major discharge event, Hurricane Joaquin. From 9/30/15 to 10/02/15, discharge increased from 80 to 1047 m^3/s.

Frontal Zone 4 (FZ4) is the farthest upstream sampling location, approximately 8 km north of the mouth. This reach is characterized by a narrow channel (0.5 km cross-channel), with a thalweg, 7 m depth on average. Large, 2 m amplitude, ebb-oriented sand waves have been observed at this location (Valentine, 2015). Extending 3 to 5 km from Long Island Sound, Frontal Zone 3 (FZ3) is a shallower (mean depth 6 m) and wider (0.75 km cross-channel) section of the estuary, with 1.0 to 1.5 m, ebb-oriented bedforms. Here the thalweg follows the east bank of the river, and two large bridges span the channel. Frontal Zone 2 (FZ2) is the farthest downstream location, located 2 km from the mouth, with a wide (1.2 km), shallow (5 m depth) channel and small 0.5 m flood-oriented bedforms.

3.2.1. Water and flow measurements

A profiling tripod (modified after Sternberg et al., 1991; Fig. 5A) was mounted with an RBR XR-620 Conductivity, Temperature and Depth profiler (CTD), a Campbell Scientific Optical Backscatterance Sensor (OBS), a Nortek Acoustic Doppler Velocimeter (ADV), an Aquatec AQUAScat 1000 Acoustic Backscatterance Sensor (ABS) and an in-situ pump system. The tripod was lowered to the bed and remained in place, oriented with the flow for 13 minutes. The programmed pumps collected three timed samples 15 cm above the bed, the same height above the bed as the OBS (Table 2). Additionally, a RDI-Teledyne Acoustic Doppler Current Profiler (ADCP) and Knudsen Engineering Dual-Frequency Echo Sounder were mounted to the ship's hull and sampled continuously.

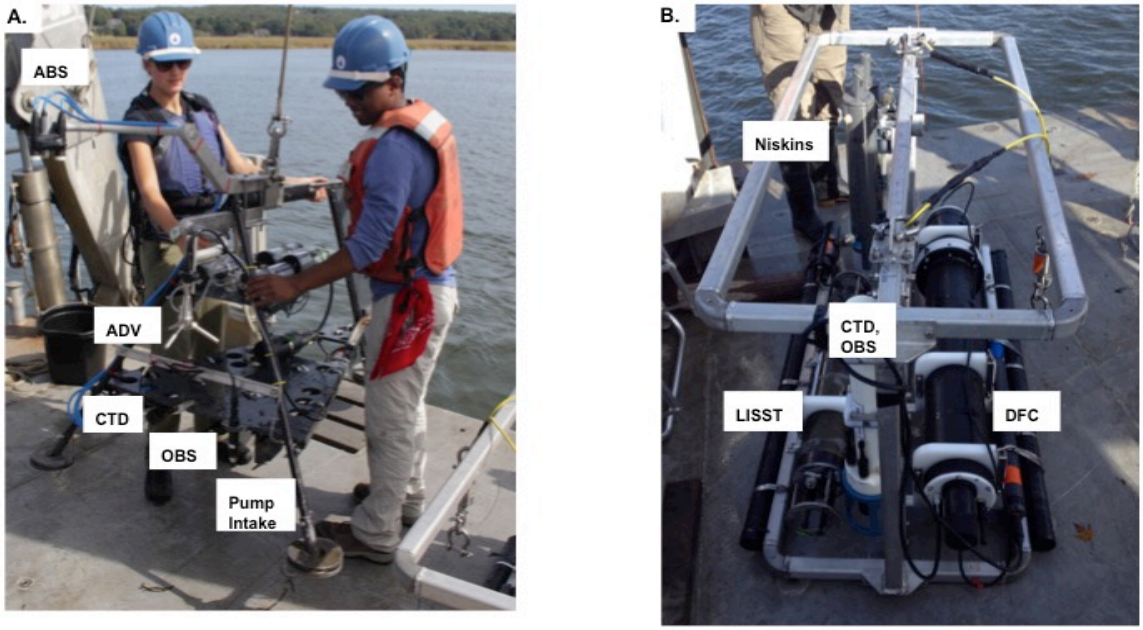

Figure 5. (A). Instrumented profiling tripod used to measure currents, water properties and SSC. **(B).** Particle Characteristics Package (PCP), used to measure in-situ floc properties.

Table 2. Instrumentation summary.

Instrument	**Elevation above bed (cm)**	**Sampling Interval**
Profiling Tripod		***Profiling, stationary on bed 10-13 minute intervals***
Acoustic Doppler Velocimeter (ADV)	75	16 Hz
Conductivity-Temperature-Depth Sensor (CTD)	24	6 Hz
Optical Backscatterance Sensor (OBS)	16	6 Hz
Pump	15	Pumping 10s every 3 mins
PCP		***Profiling, recording up and down cast***
Laser-in-situ-Scattering-and Transmissometry Sensor (LISST)	40	Continuous
Digital Floc Camera (DFC)	30	1 image every 5 s
CTD	60	6 Hz
OBS	60	6 Hz

3.2.2. Particle characteristics

The second instrument package was designed to investigate in-situ characteristics of suspended particles and aggregates (Particle Characteristics Package, PCP; Fig. 5B). The steel frame contained a Digital Floc Camera (DFC), a Sequoia Scientific LISST-100x (Laser In-Situ Scattering and Transmissometry), RBR CTD, Seapoint turbidity sensor, and two Niskin bottles that collected samples at 5 m and 10 m depths. A third water sample was collected at the surface during each cast. Each cast lasted three to five minutes as the package was lowered to the bed, collected data for one minute on average, approximately every 15 minutes.

Particle size distributions, concentrations and density were measured by the DFC and LISST-100x separately, then merged during post-processing (Mikkelsen et al., 2005). The delicate nature of flocs requires field methods that will minimize floc breakup (Van Leussen, 1988; Winterwerp and Van Kesteren, 2004). The DFC and LISST are methods that have been tested and found effective for in-situ quantification of cohesive suspended particles (Agrawal and Pottsmith, 2000; Smith and Freidrichs, 2015; Fetteweis and Baeye, 2015; Yang et al., 2016) The pressure-triggered DFC took silhouette images of a 4 by 3 by 2.5 cm deep slice of the water column every five seconds once reaching water depths of 0.2 m or greater. Particles are illuminated by a strobe LED flash, 'freezing' the particles in suspension, causing particles to appear black against a white background in images (Fig. 6). The LISST recorded continuously at 6 Hz, with logging started manually at the beginning of each cast.

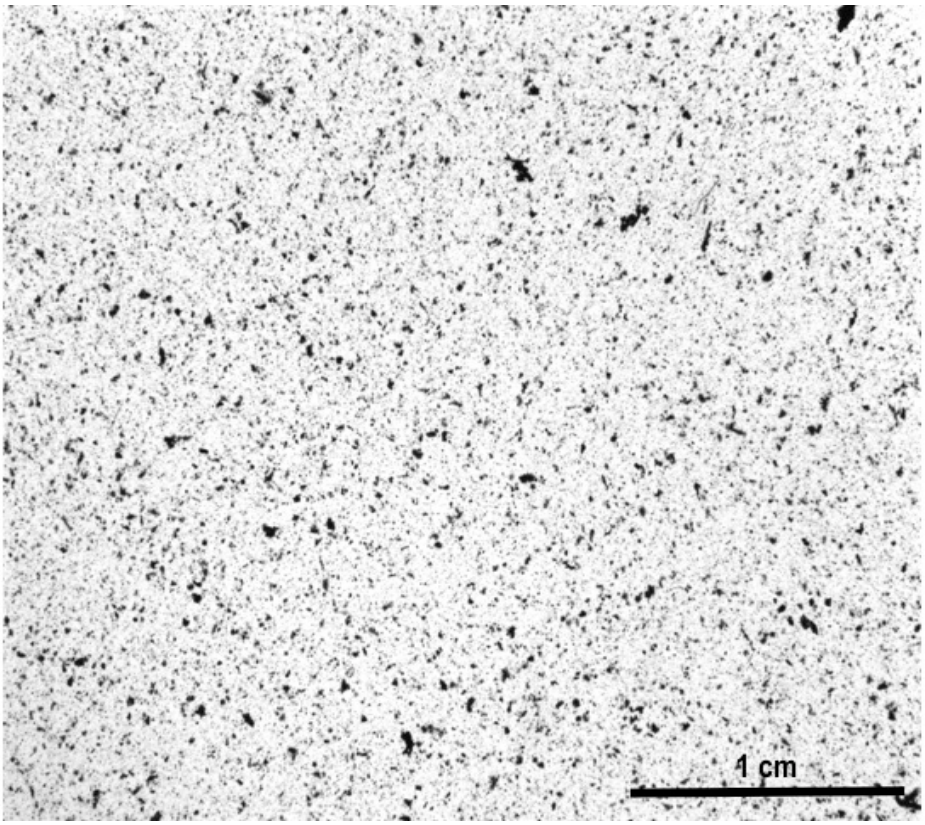

Figure 6. Example of in-situ silhouette image captured by the DFC on September 28, 2015 at 09:05 in FZ4. Particles appear black against white background.

3.3. Laboratory methods

Water samples from both packages were filtered using pre-weighed 0.45 or 8 μm Millipore filters using a vacuum filtration system to obtain concentrations in milligrams per liter. The 8 μm filters have similar retention efficiency to filters with much smaller nominal pore sizes while allowing the collection of sufficient material for grain size analysis (Sheldon, 1973). These concentrations were used to provide an in-situ calibration of the OBS, enabling the optical reading in volts to be converted to mass per volume (Sternberg et al., 1991; Table 3; Fig. 7).

The disaggregated inorganic grain size (DIGS) distributions of suspended sediment from water samples collected with both packages were analyzed using a

Beckman-Coulter Multisizer 3 at the Bedford Institute of Oceanography following the methods of Milligan et al. (2007). Organic material and the filter were combusted in a low temperature plasma asher and then treated with 35% H_2O_2. The residue was suspended in 1% NaCl and disaggregated with a sapphire tipped ultrasonic probe just prior to analysis on the Multisizer. Results are expressed as log concentration in parts per million versus log diameter.

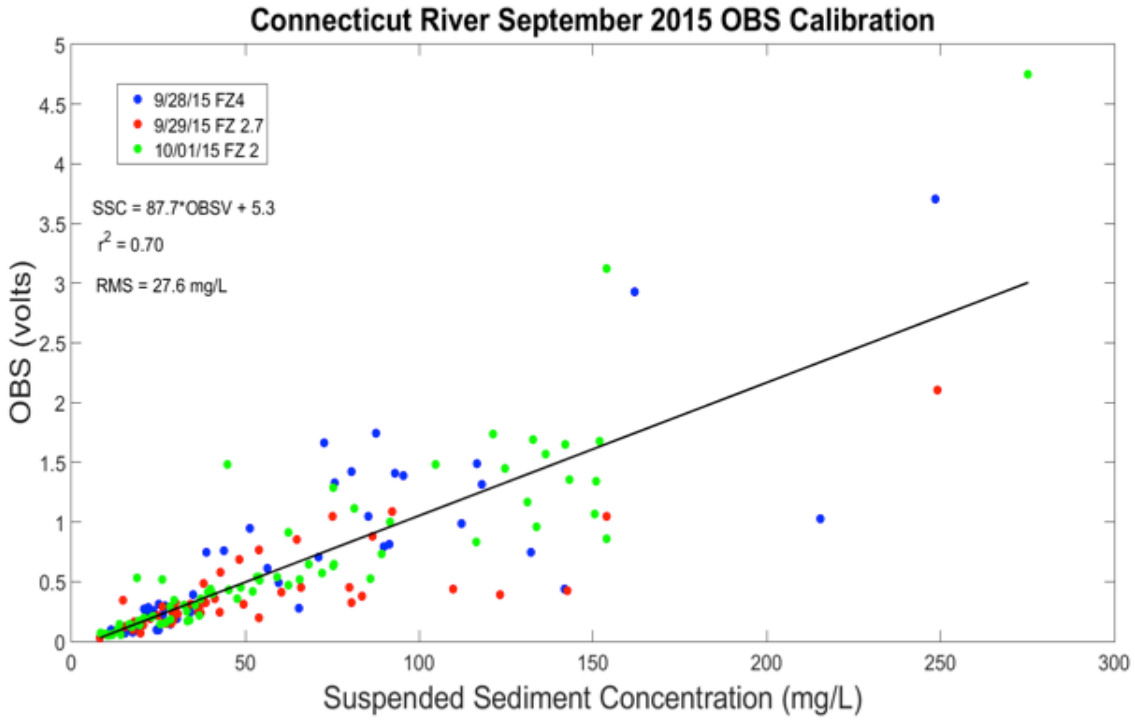

Figure 7. Example OBS calibration, using September 2015 data. Pumped samples are matched with OBS readings, with no significant difference in the calibration curve for each location.

Table 3. Summary of OBS calibrations used for each season, using the calibration equation: $SSC = m * OBS + b$.

	m	**b**	**r^2**	**RMS (mg/L)**	**n**
November 13	52.97	1.37	0.80	26.7	229
May 14*	1.92	0.16	0.83	31.1	159
September 15	87.7	5.3	0.70	27.6	170

*M14 calibration in NTUs, N13 and S15 in Volts.

3.4. Analyses

3.4.1. Merging LISST and DFC data

Data from the DFC and LISST were matched and merged to create one complete suspended particle-size distribution for each image taken during PCP casts. Full floc size distributions were obtained by merging particle size data from the LISST with data from the DFC (Mikkelsen et al., 2005). Image analysis to derive particle area from the DFC images was carried out using ImageJ (Schneider et al., 2012) and particle size and volume concentration was calculated in MATLAB. In ImageJ the threshold grayscale value was defined using the triangle algorithm. Particle areas were then converted to volume concentration assuming an equivalent spherical diameter. Particle size spectra derived from DFC images were binned into the same logarithmic size classes as the LISST. Particle size data generated from the DFC (> 45 μm) were then merged with those of the LISST to produce continuous grain size spectra.

The LISST-100x records scattering intensity over 32 logarithmically-spaced ring detectors, the width of which determine the size classes of the measured particles. The raw intensity captured by each ring is inverted mathematically to produce an area distribution of particles, which can then be multiplied by median diameter in each size class to obtain a full volume size distribution (Agrawal and Pottsmith, 2000; Fig. 8). This factory-standard inversion algorithm is weighted for size classes, resulting in total volume concentrations which are insensitive to grain size distribution of the sediment in suspension (Fugate and Friedrichs, 2002). Based on Mie Theory of laser diffraction, small angle scattering is dominated by light diffraction of the particles, rather than light transmitted through the particle, making LISST measurements mainly independent of

composition (Agrawal and Mikkelsen, 2009). The LISST size spectra range from 2.5-500 μm, though scattering can still be captured at sizes outside that range, potentially causing an overestimate of particle volumes in the smallest or largest size classes (Davies et al., 2012). To account for this excess scattering, sizes larger than 103 μm DFC data were used exclusively and the smallest five LISST size bins (<5 μm) were excluded. The region of overlap (53-88 μm) was averaged to merge the two datasets into one distribution (Fig. 9). The final result is a volume size spectrum over a size range from 5 μm to centimeter-scale. Results are plotted as the log of particle diameter (μm) versus the log of volume concentration (ppm).

The negative effects of schlieren (optical anomalies caused by the changing refractive indices of density gradients) were considered when processing the LISST data (Fig. 10A; Mikkelsen et al., 2008; Markussen and Andersen, 2013). The excess signal caused by the LISST scattering off density interfaces has been described by Mikkelsen et al. (2008), and LISST data for this study were assessed in a similar method. Distributions affected by schlieren were excluded from the final analysis by (Fig. 10B).

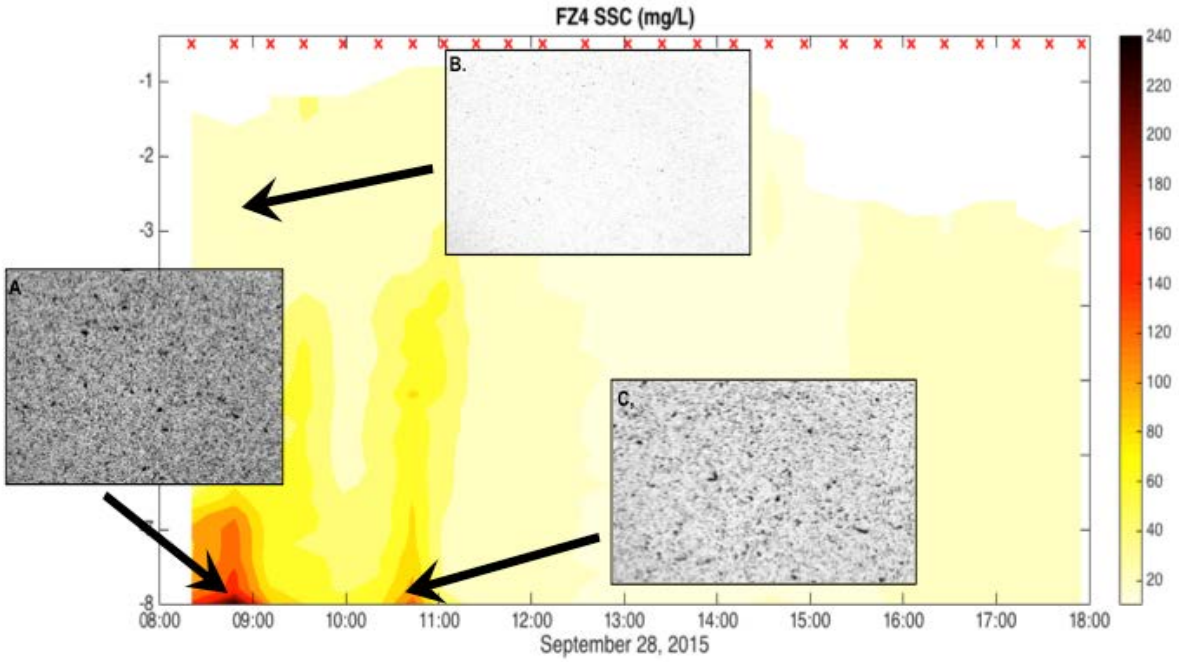

Figure 8. Example floc camera images taken at one anchor station (FZ4 on September 28, 2015), at different heights above the bed and different times in the tidal cycle. Image A captured the highest concentrations, while image B is from the surface during the same cast as A, showing much lower surface concentrations. Image B was taken 0.3 m above the bed during the second highest near-bed SSC observations.

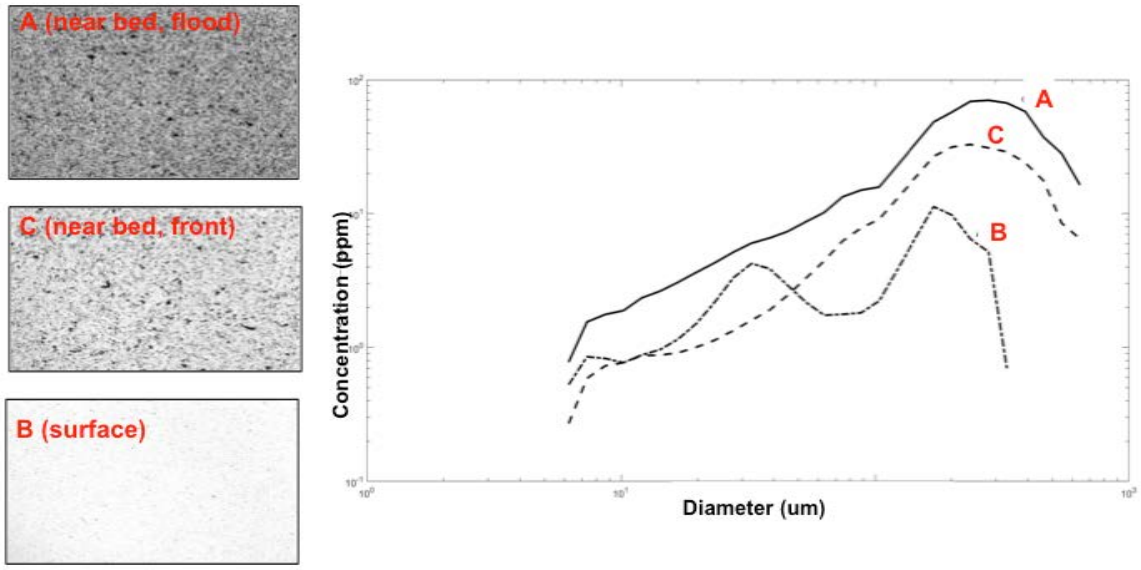

Figure 9. The resulting full size distributions from merging the DFC images in Figure 8 with the corresponding LISST measurements.

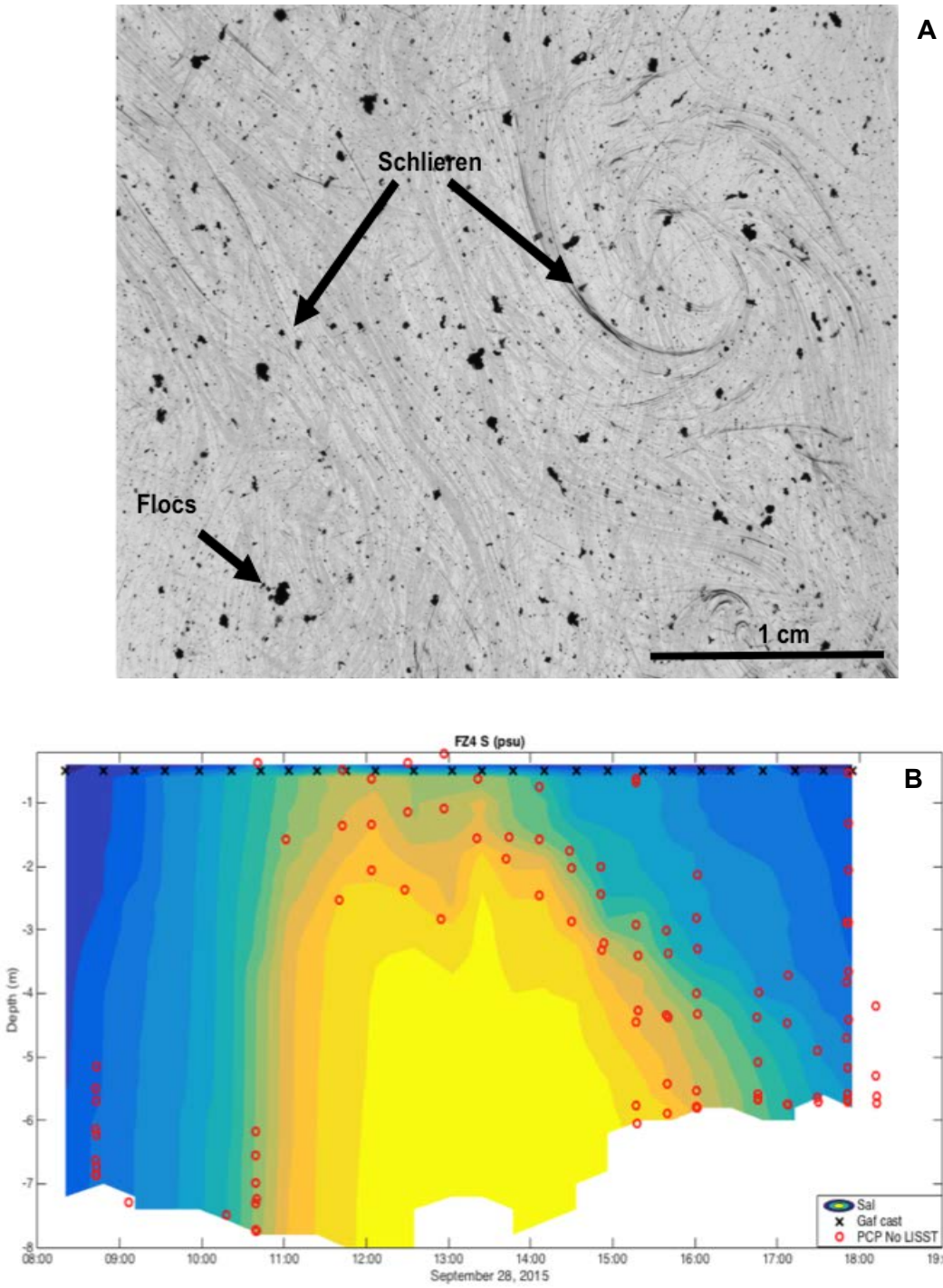

Figure 10. (A). DFC image captured the effects of schlieren. The scattering off density interfaces in the water column inhibits the image analysis of particle cross-sectional area. **(B).** LISST measurements marked in red were effected by schlieren. The majority of bad data points fall along the pycnocline, where scattering off the density interface is likely enhanced. These data points were excluded from particle characteristics analysis.

3.4.2 Particle data analysis

Median floc diameter (D_{50}), maximum floc diameter (D_{95}, defined as 95% of the sample particles are the same or smaller than this size), total volume concentration in parts-per-million (C_V), and Sauter Mean Diameter (*SMD*) were all determined from the full size spectra (Table 4).

Sauter Mean Diameter is defined as the size of spherical particles that would have the same surface area to volume ratio as the observed particles and is the ratio of total particle volume concentration (C_V) to total particle surface area concentration (C_A),

$$SMD = 1.5\frac{C_v}{C_A} \quad (2)$$

where 1.5 is a correction coefficient (Agrawal and Mikkelsen, 2009). *SMD* is description of mean particle size that is typically more informative of aggregate particle packing and response to stress than D_{50} (Filippa et al., 2012). The larger *SMD* indicates larger, loosely- packed, less-dense flocs. *SMD* will be used as the principal particle size descriptor in this study.

Floc apparent density, ρ_a, defined as the total mass of particles in suspension divided by the total wet volume of particles, was calculated following the method of Hurley et al. (2016), assuming beam attenuation of the LISST-100 (c_p) is proportional to the suspended-sediment concentration,

$$\rho_a = \frac{c_p}{c_v} \quad (3)$$

in kg/m^3. Floc effective density, ρ_e, a more commonly used quantity, is related to ρ_a through the relation:

$$\rho_e = \rho_s - \rho_w = \frac{\rho_s - \rho_w}{\rho_s}\rho_a \quad (4)$$

and defined as the density of particles (in this case, flocs), in excess of the density of water (Winterwerp and Van Kesteren, 2004; Hurley et al., 2016). Floc density is typically inversely correlated with floc size. The larger the floc, the more loosely bound and thus less dense. This relationship has been observed in numerous studies and results in a significant control on floc settling velocity (Van Leussen, 1988; Winterwerp and Van Kesteren, 2004).

3.4.3. Floc settling velocity

The settling velocity of flocs is a function of their size and density. Winterwerp (1998) adjusted the classic Stokes mass balance between frictional drag forces and gravitational forces to include parameters descriptive of flocs' fractal and sub-spherical structure:

$$w_s = \frac{1}{18}\theta g \frac{\rho_s - \rho_w}{\mu} d_c^{3-F} * \frac{D^{F-1}}{1+0.15Re^{0.687}} \quad (5)$$

requiring inputs of: θ, the particle shape factor, g, acceleration due to gravity ρ_s, sediment (component particle) density, ρ_w, fluid density, d_c, median diameter of component grains in floc, F, fractal dimension, D, floc diameter, and Re, floc Reynolds number (Winterwerp and Van Kesteren, 2004), allowing adjustments for the non-spherical, varying-density flocs. For Euclidean (θ = 1), spherical (F = 3) flocs, Eq. 5 simplifies to the familiar Stokes settling equation,

$$w_s = \frac{(\rho_s - \rho_w) g D^2}{18\mu} \quad (6)$$

While Eq. 5 can be practical in numerical models, field measurements are required for accurate, site-specific investigations. Thus, in-situ methods of indirectly measuring settling velocity are used in this study.

Floc settling velocity (w_s) varies through time and space with changes in floc size, density and shape. Numerous methods have been used to determine the settling velocity of in-situ suspended particles, including in-situ video methods reliant on visual particle tracking, modeling based on empirical relationships (Manning and Schollenhamer, 2013; Smith and Friedrichs, 2015; Yang et al., 2016), and fitting of acoustic data (Fugate and Freidrichs, 2002).

The latter two methods were used to quantify floc settling velocity in this study. In Method 1, calibrated backscatter from the ADV was used to estimate in-situ particle settling, using a modified expression of Reynolds turbulent diffusion:

$$K\frac{dc}{dz} = -\overline{\langle w'c' \rangle} \quad (7)$$

where *w'* and *c'* are fluctuating components of vertical velocity and concentration, the angle brackets indicate an average of the turbulent components and the overbar represents a time-average for each cast. The slope of the best-fit regression allows for an estimation of w_s without having to estimate the eddy diffusivity, *K*, directly. The intercept for each regression was set at $\langle w'c' \rangle = 0$ to represent the background concentration of particles too small to settle to the bed. One regression for each discharge regime will produce estimates of average w_s of all particles observed.

The high resolution of the ADV allows for the measurement of turbulent fluctuations in backscatter and vertical velocity, however does not capture variations in concentration across individual size classes. For Method 2, the LISST-derived ρ_e can be used in a Stokes' settling approximation, assuming particle sphericity (Fox, 2003):

$$w_s = \frac{g}{18\mu}\rho_e {D_{50}}^2 \quad (8)$$

where g is the acceleration due to gravity (m/s) and μ is molecular viscosity (kg/ms), allowing for a calculation of bulk effective settling velocity for each LISST-DFC image pair.

3.4.4. Near-bed stress

Near bottom along-channel mean velocity measured by the ADV (at 75 cm above the bed) was used to calculate bed shear stress using the Quadratic Stress Law (QSL). The QSL is an empirical relationship between boundary shear stress and mean near bottom velocity:

$$\tau_b = C_D \rho u^2 \quad (9)$$

where τ_b is boundary shear stress, u is a mean near-bottom velocity, ρ is the density of the fluid and C_D is the drag coefficient, that relates u with the force exerted by the fluid on the bed, a factor of bed roughness (Sternberg, 1972; Dyer, 1997). C_D remains constant for a specific bed condition, thus one value of C_D can be used to estimate τ_b from one mean velocity measurement at a specified height above the bed (Sternberg, 1972). Though Sternberg (1972) found a range in C_D values up to a factor of two over beds with different sediment characteristics, he proposed that the mean value of 3.1×10^{-3} could be accurately used in cases without high sediment transport rates or large bedforms. Valentine (2015) estimated changes in C_D during sampling periods in 2012 to 2014 in the Connecticut River estuary (two of which are included in this study) and found that though values ranged from 10^{-4} to 10^{-2} across three different methods and four locations within the estuary, using the generalized C_D estimate did not significantly affect bed stress estimates. A secondary check comparing the calculated stresses from near-bed ADV velocity measured at 0.75 meters above the bed (mab) and an estimated bed stress at 1.0

mab (to match the generalized C_D standardized for 1.0 mab), determined that measured stresses were slightly underestimated, however not significantly so (n=53, RMSE = 0.003 Pa; see Appendix II).

The QSL is derived from the Karman-Prandtl Equation and estimates boundary shear stress through a mean velocity profile close to the bed. In unstratified conditions, the velocity profile can be described by:

$$\frac{u_z}{u_*} = \frac{1}{\kappa} ln \frac{z}{z_0} \quad (10)$$

where u_z is the mean velocity at z, height above the bed, u_* is shear velocity, defined as

$$u_* = \sqrt{\frac{\tau_b}{\rho}} \quad (11)$$

k is von Karman's constant (0.41), and z_0 is roughness length, dependent on the roughness of the bed (Dyer, 1995).

3.4.5. Suspended sediment concentration

Suspended-sediment concentrations determined from the in-situ pumped samples were used to calibrate indirect measurements of concentration from the OBS, LISST and ADV. Optical readings were matched with measured filtered suspended-sediment concentrations to produce a linear calibration to convert backscatterance in volts to suspended-sediment concentration in mass/volume (Fig. 7). Calibrations varied based on instrument and anchor station location, but the differences in slopes for individual locations were not significant for a single OBS. One calibration for each OBS for field season was applied (Table 3). The same ADV and LISST were used each field survey allowing for one calibration for all measurement periods.

In addition to the OBS, the pumped samples were used to calibrate adjusted acoustic backscatter from the ADV (r=0.86, n=139, p<0.001) and LISST transmissivity

(beam c, r=0.51, n=142, p<0.001) and volume concentration, C_v (r=0.47, n=142, p<0.001). Figure 11 shows the comparisons of these three indirect measures of SSC. While the pumped samples and calibrated OBS will be the primary source of SSC data presented throughout the study, the calibrated ADV backscatter and LISST beam c were used to measure rapid fluctuations and relative volumetric changes in concentration respectively to estimate in-situ settling velocity. Care was taken to quality check the data following the process of Valentine (2015), eliminating erroneous points with non-standard pitch, roll, and heading that would indicate the tripod was not fully stationary on the bottom.

Optical, acoustic, and laser diffraction methods of indirect SSC measurements all vary depending on particle characteristics. Optical backscatterance sensors emit a beam of light and record the amount of light that is scattered back to the sensor, effectively measuring the particle cross-sectional area per unit area (Kineke and Sternberg, 1992). This makes optical methods sensitive to particle size distribution; for example a concentration of small particles will have a greater optical response than the same concentration composed of larger particles. Acoustic sensors emit pulses of sound that are scattered by particles in suspension, somewhat analogous to the scattering of light. However acoustic methods are dependent on particle density and packaging due to the relatively large wavelength of sound compared to particle diameter, potentially scattering off individual particles within flocs or aggregates and the floc as a whole (Fugate and Friedrichs, 2002). Laser diffraction is unaffected by both the composition of particles (by measuring the light diffracted rather than transmitted through the particle), and the LISST specifically accounts for particle size by measuring scattering over the 32 ring detectors

(Agrawal and Mikkelsen, 2009). In addition to measuring volume concentration and size spectra, the LISST transmissometer, located in the center of the ring detectors, measures beam transmission (beam c), which can serve as a check on total concentration (Agrawal and Pottsmith, 2000).

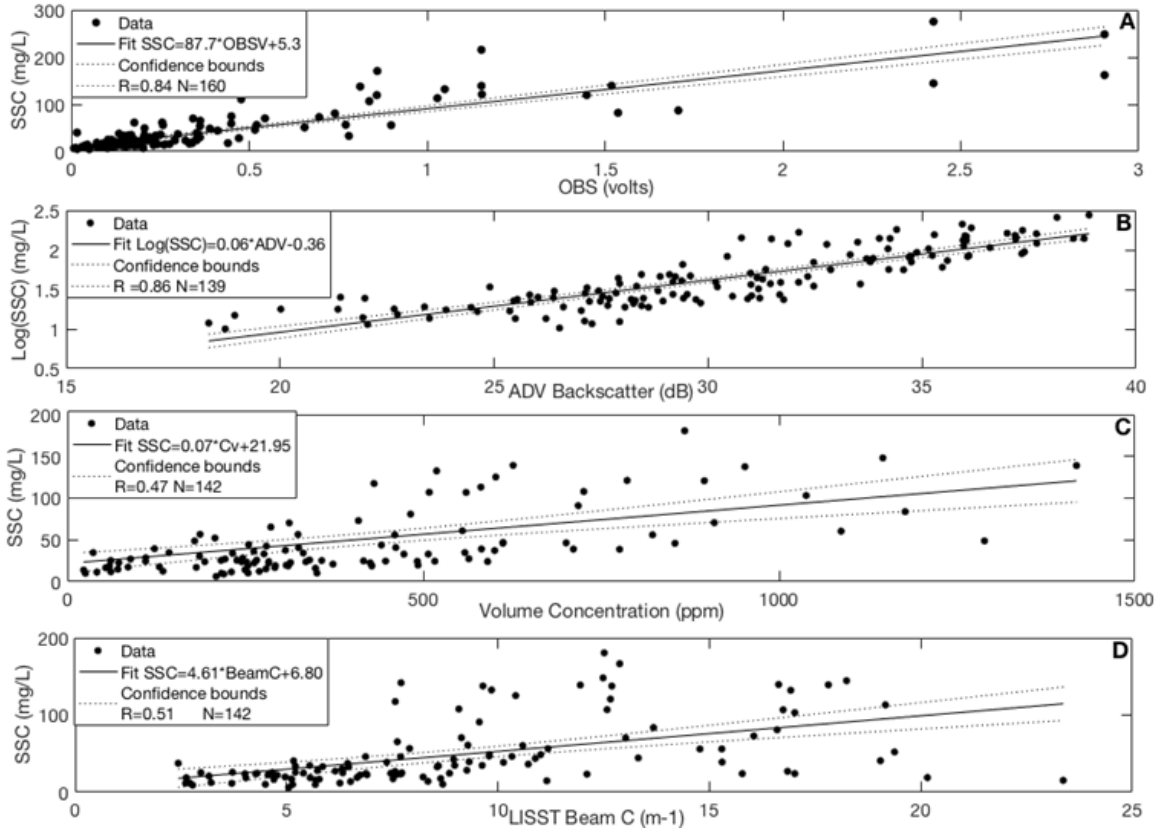

Figure 11. Comparison of near-bed SSC measured from pumped samples with indirect measures of concentration. **(A)** OBS, **(B)** ADV backscatter (signal-to-noise ratio in dB), **(C)** volume concentration measured by the LISST-DFC, **(D)** and LISST beam c (m^{-1}, bottom).

Table 4. Dataset summary.

Variable	Method	Dataset
D_{50}, D_{95}, C_V, C_A, *SMD*, ρ_a Median floc diameter Maximum floc diameter Total volume concentration Total surface area concentration Sauter mean diameter Floc apparent density	Matched LISST and DFC	PCP November 2013 (5 AS) May 2014 (3 AS) September-October 2015 (3 AS) Both 0.5 LISST transmission threshold and 0.4 threshold datasets
S, ρ_w, *T*, *depth* Salinity Water density Temperature Pressure (water depth)	CTD	Profiling Tripod and PCP CTD data
SSC Suspended-sediment concentration	OBS; in-situ pump samples	Profiling Tripod
τ_b, u_*, $\frac{du}{dz}$, *u'v',w'* Bed shear stress Shear velocity Velocity shear Fluctuating components of velocity	ADV, ADCP	Profiling Tripod and ship-mounted, continuous ADCP

*AS = Anchor Station

3.4.6. Flow conditions

Mean daily discharge of the Connecticut River over the duration of all sampling periods was collected from USGS Gage 1193050 at Thompsonville, CT, located approximately 80 km north of the study area (Fig. 3). To assess the effects of discharge on suspended-particle characteristics, the following analyses were completed:

1. Cumulative discharge two weeks prior to each survey (Q_{cw}) and one year prior (Q_{cy}) was calculated in cubic meters.
2. The slope of the cumulative discharge curve ($\frac{dQ}{dt}$, the average change in mean daily discharge two weeks prior to the survey, in m^3/day) for the two

preceding weeks of each cruise was calculated to assess the timing of recent discharge events.

3. The mean annual flow $\bar{Q}$ in m^3/s was calculated for the 365 days preceding each cruise. The number of days during that time with flow exceeding $\bar{Q}$ (and flow exceeding $\bar{Q}$ + 1σ and $\bar{Q}$ + 2σ) were calculated to compare high discharge events from year to year.
4. The number and magnitude of major discharge (Q >1500 m^3/s) and turbidity events (T > 50 NTU) observed in relation to the study period. High turbidity events represent an event that 'charges' the estuary with new sediment.

Continuous turbidity data were not available at the Thompsonville station during the study period, thus daily mean turbidity values (in NTU) were taken from USGS gage 1193050 at Middle Haddam, CT, approximately 65 km south of Thompsonville and 35 km upstream of Essex, the northern extent of the study site (Fig. 3).

4. RESULTS

4.1. Hydrodynamics

Mean discharge during each cruise did not vary significantly over the three sampling periods, with all falling around the long-term mean of ~500 m^3/s (Table 1). The mean discharges ($\bar{Q}$) were 578 m^3/s, 638 m^3/s, and 507 m^3/s during the November 2013, May 2014, and September 2015 cruises respectively. However, to put the results of the three sample periods into the context of the overall system, a much longer record is required (Fig. 12).

November 2013 had moderate mean daily discharge during the survey but was falling over the course of the sampling period ($\bar{Q}$ = 578 m^3/s, $\frac{dQ}{dt}$ of -2480 m^3/day; Fig. 13). Flow surpassed the annual mean discharge plus one standard deviation ($\bar{Q}$+σ) on 52 days during the one year prior to the survey, and exceeded $\bar{Q}$+2σ on 20 days. Two of the four largest precipitation events (>100 mm/day) and turbidity events (>100 NTU) recorded between January 2013 and October 2015 (the three years surrounding the field surveys) occurred during 2013 (Fig. 14). Mean turbidity during the year prior was 7 NTU, with a modal turbidity of 2 NTU and maximum of 180 NTU on July 3, 2013. The last peak turbidity event occurred 34 days prior to the survey period.

A typical spring freshet was captured in the May 2014 survey, with cumulative discharge two weeks prior to the survey increasing sharply to 13.8 x 10^8 m^3 ($\frac{dQ}{dt}$ of 7930 m^3/day). The high discharge was maintained throughout the 5-day survey with mean daily discharge nearly 100 m^3/s higher than either of the other sampling periods. The year prior to the May 2014 survey included 57 days of flow above $\bar{Q}$+σ, and 20 days with flow greater than $\bar{Q}$+2σ. Mean turbidity during the year prior was 9 NTU, with a mode of 12

NTU and peak of 180 NTU. A major discharge event with flow reaching 2570 m^3/s and turbidity peaking at 85 NTU occurred 24 days before the survey, on April 11, 2014.

The September 2015 survey was preceded by a low flow period lasting 157 days, with mean daily discharge nearly half as high as the historical median. Cumulative discharge two weeks prior to the survey was three orders of magnitude smaller than in May 2014 and daily flow surpassed $\bar{Q}$+σ only 43 days the year prior, and surpassed $\bar{Q}$+2σ on 17 days. It should be noted however, a fall storm typical of the northeast U.S. was captured at the end of the 2015 survey, as hurricane Joaquin hit Long Island Sound on October 1-2, 2015, causing a significant amount of precipitation (~40 mm in 24 hours and turbidity spiked from to 1 to 43 NTU) and an increase in discharge during the final day of the sampling period ($\frac{dQ}{dt}$ drops from 2550 to 2120 m^3/day if discharge on October 2 is excluded). No PCP measurements were taken on October 2 however, so this event is excluded from the characterization of the September 2015 field survey. Removing Hurricane Joaquin, mean turbidity over the year prior was 4 NTU, with a modal turbidity of 1 NTU and maximum of 59 NTU. An estimated 162 days without a major turbidity event preceded the survey period.

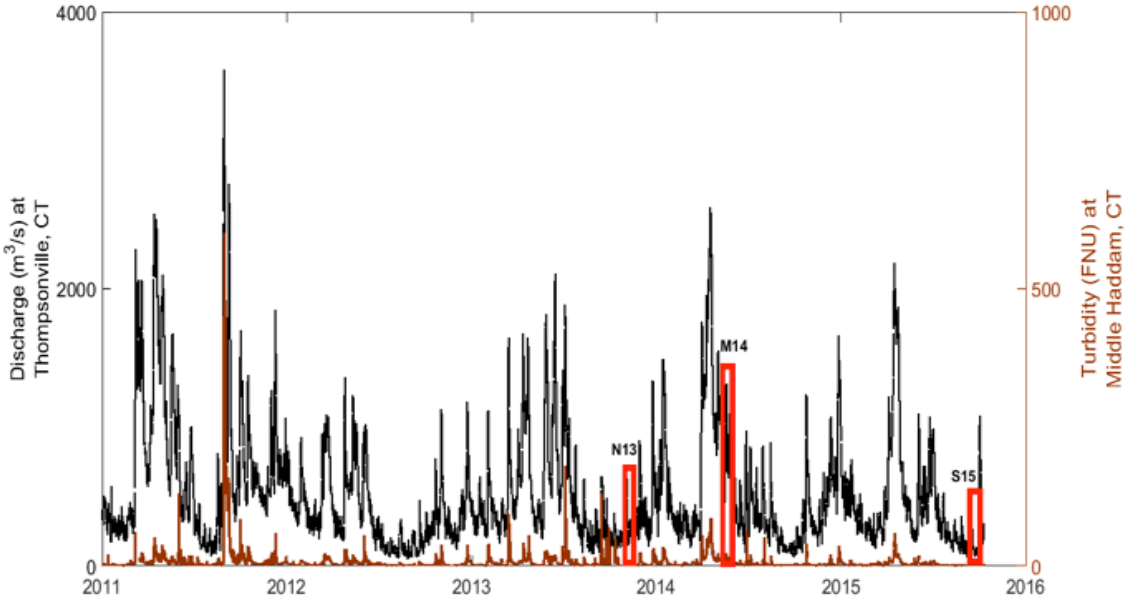

Figure 12. Daily discharge and daily turbidity recorded at Thompsonville, CT and Middle Haddam, CT respectively, from January 2011 to October 2015. The duration of the three field surveys are marked in red.

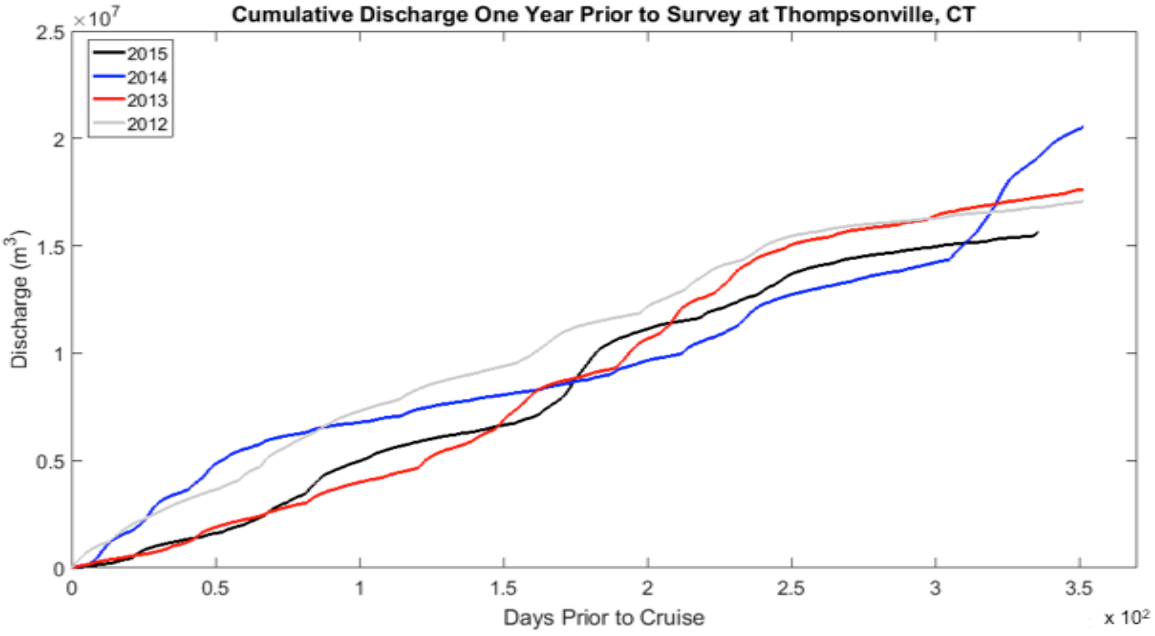

Figure 13. Cumulative discharge (m^3) measured at USGS gaging station (01184000) at Thompsonville, CT for one year prior to the survey. Water year 2012 is included for context.

4.1.1. Seasonal characterization of field surveys

Using the timeseries presented in Figure 14 and previously observed seasonal patterns of the Connecticut River, the hydrologic and climatic settings of the three cruises can be classified. The fall survey in November 2013 did not capture any late-season storm events, however it was preceded by an unusual number of high-discharge and turbidity events; the most of any cruise. The Connecticut River and estuary were charged up with sediment from the multiple large events that occurred over the year. The May 2014 survey occurred during typical freshet conditions (Yellen et al., 2017), though with fewer large events occurring over the year prior compared to November 2013 (indeed the same maximum turbidity event for May 2014 was the July 3, 2013 event). The higher than average flow and high fluvial sediment input characterize this survey. The September 2015 cruise occurred during a typical late-summer low discharge period. Additionally, not only were there no large water or sediment discharge events during the preceding year, the spring 2015 freshet signal was smaller than the two previous years (Fig. 12). These factors compounded to result in a low fluvial sediment supply.

The timeseries of water and sediment discharge over this three-year time period suggests that the timing of high water discharge and high sediment discharge events are partially decoupled. Because not every high water discharge event is accompanied by a high sediment event, the use of a 'seasonal' characterization becomes problematic. Also, the conditions of the system in weeks and months prior to the time of measurements has a significant impact on the observations. To highlight the important forcings on the conditions that effect our observations, though somewhat awkward, a naming scheme reflecting this decoupling will be used. Throughout the remainder of this study,

November 2013 ‘charged up’ conditions will be referred to as ‘high sediment supply, moderate discharge’ (HSMD). The freshet captured in the May 2014 survey will be named ‘high sediment supply, high discharge’ (HSHD). The extended low turbidity signal and lack of major events qualify the September 2015 conditions as ‘low sediment supply, moderate discharge’ (LSMD).

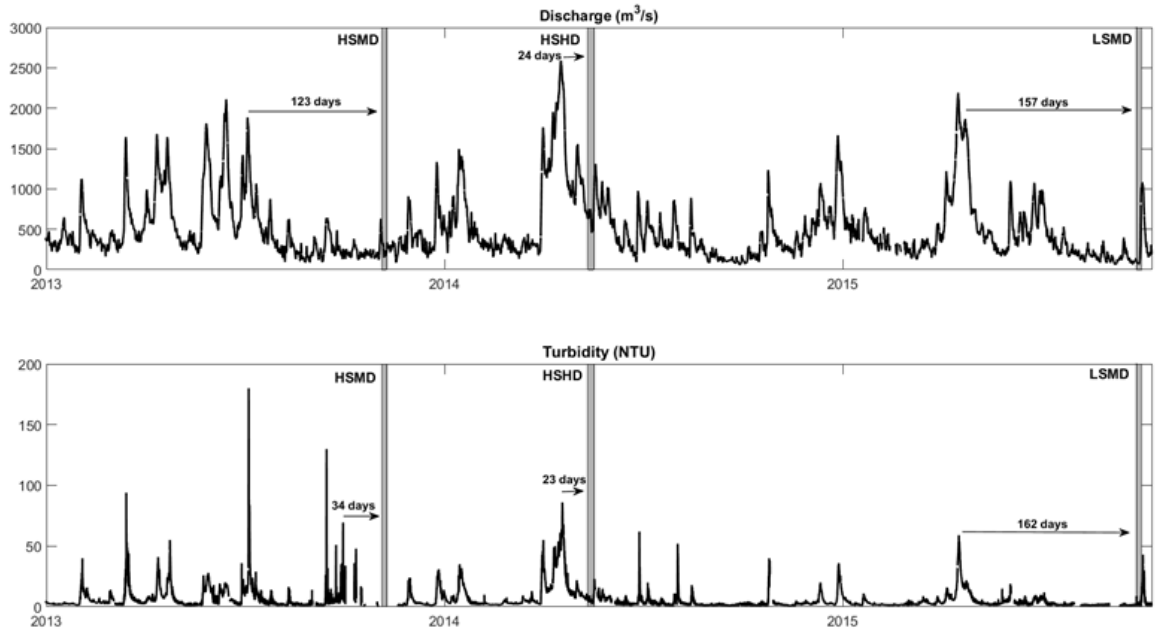

Figure 14. Connecticut River discharge (top, m^3/s) and turbidity (bottom, NTU) from January 2013-October 2015. The periods of measurements are marked by vertical bars. Arrows indicate duration since peak discharge event (>1500 m^3/s) and peak turbidity event (>50 NTU).

4.2. Hydrodynamics: tidal patterns

Measurements of particle characteristics, flow and water column conditions were taken at 11 anchor stations over the course of the three-year study (Fig. 4). Anchor station time series typically captured the initiation of flooding currents, the flooding front, slack after flood, and the initiation of ebbing currents. Figures 15-17 illustrate three water column measurement timeseries measured by the profiling tripod at anchor over each

survey in FZ3 and FZ4. Anchor stations lasted 6 to 8 hours and captured the flood to ebb transition. Figures 15-17 are annotated to provide context to the following tidal terminology. The flooding front, the strongest horizontal salinity gradient associated with the incoming flood tide, is a dominant feature at each frontal zone with near-bed salinity at times increasing by 20 psu or more in less than one hour. The mixing and stratification throughout the estuary changes with discharge conditions. Under the moderate conditions of LSMD and HSMD, the water column is generally well-mixed during flood, as the salt wedge propagates up-estuary and the salt reaches the surface. During HSHD, the surface remains fresh even at peak flood at FZ2, resulting in the pycnocline remaining 1-2 m below the surface (Fig. 16). During slack and the early ebb, freshwater begins to flow over the higher salinity bottom water, resulting in a stratified water column. The pycnocline is pushed down towards the bed, until it ultimately intersects the bed typically 3-4 hours following slack. The stratification during ebb is greatest during HSHD conditions, where the increased freshwater flow causes an approximate 15 psu increase over 2 m depth.

At all locations during each survey, the highest SSC was observed close to the bed, most frequently concurrently with the flooding front (Fig. 15-17; Table 5). Maximum bottom SSC of the entire study was observed at FZ2 during HSHD, with concentrations reaching 275 mg/L. Maximum surface SSC was an order of magnitude smaller than near-bed concentrations. FZ4 had the second highest SSC, with 211 mg/L during HSMD. During all seasons, the water column cleared during slack, with background concentrations on the order of 10-20 mg/L. As the ebb began and bed

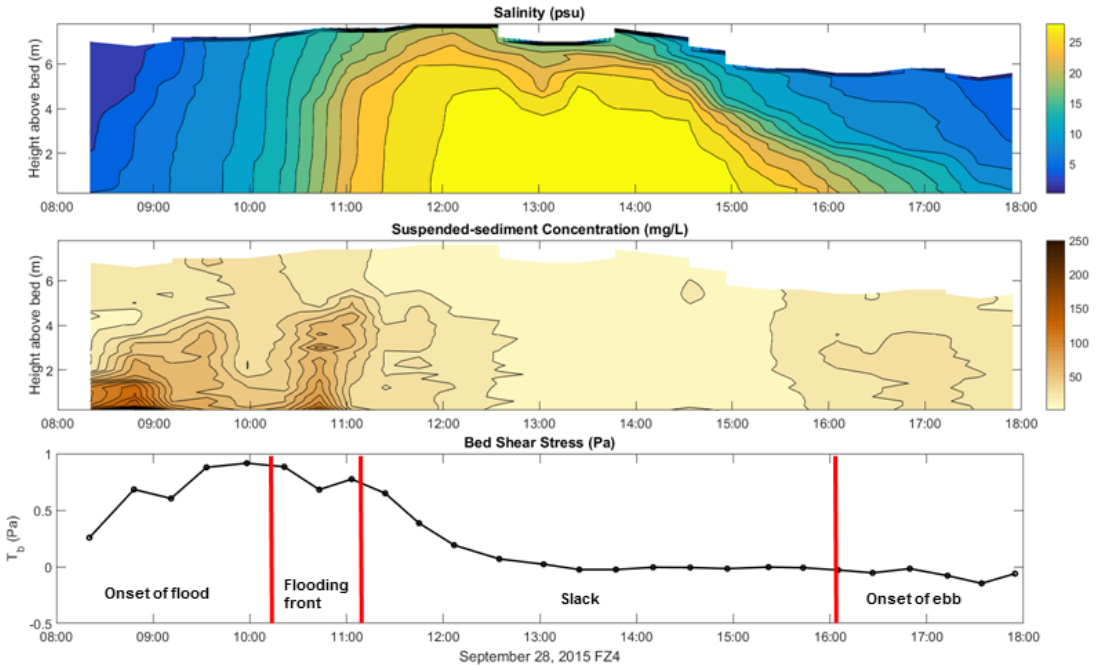

Figure 15. Example anchor station timeseries from the LSMD survey located at FZ4 on September 28, 2015. The terminology applied to the tidal patterns in near-bed flow and salinity structure will be used throughout.

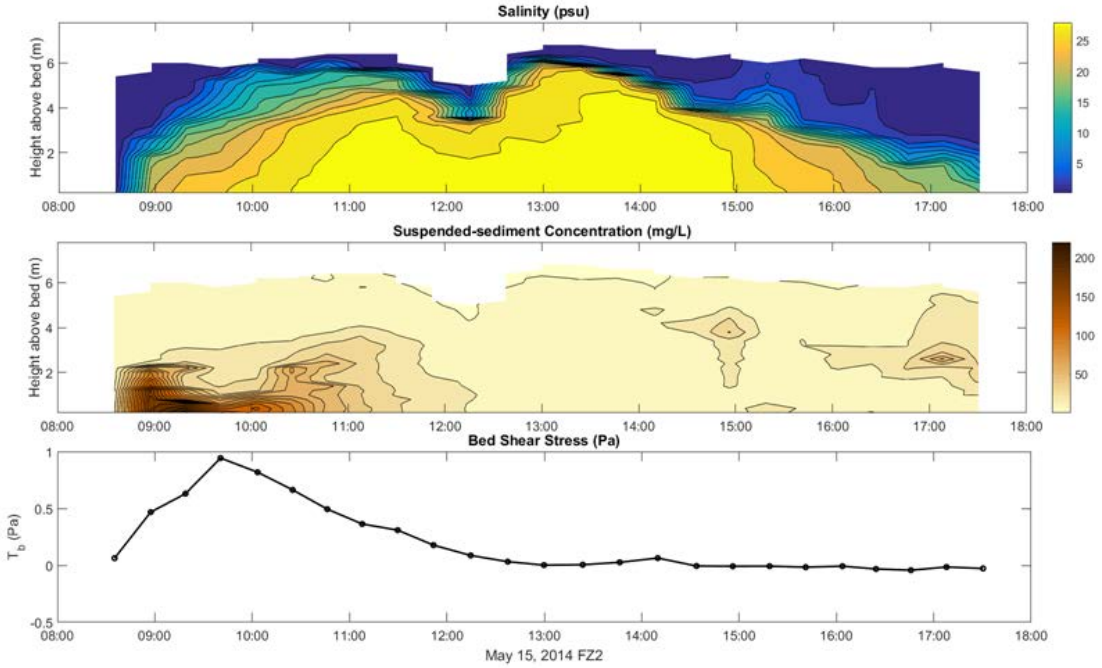

Figure 16. Example anchor station timeseries from the HSHD survey located at FZ2 on May 14, 2014.

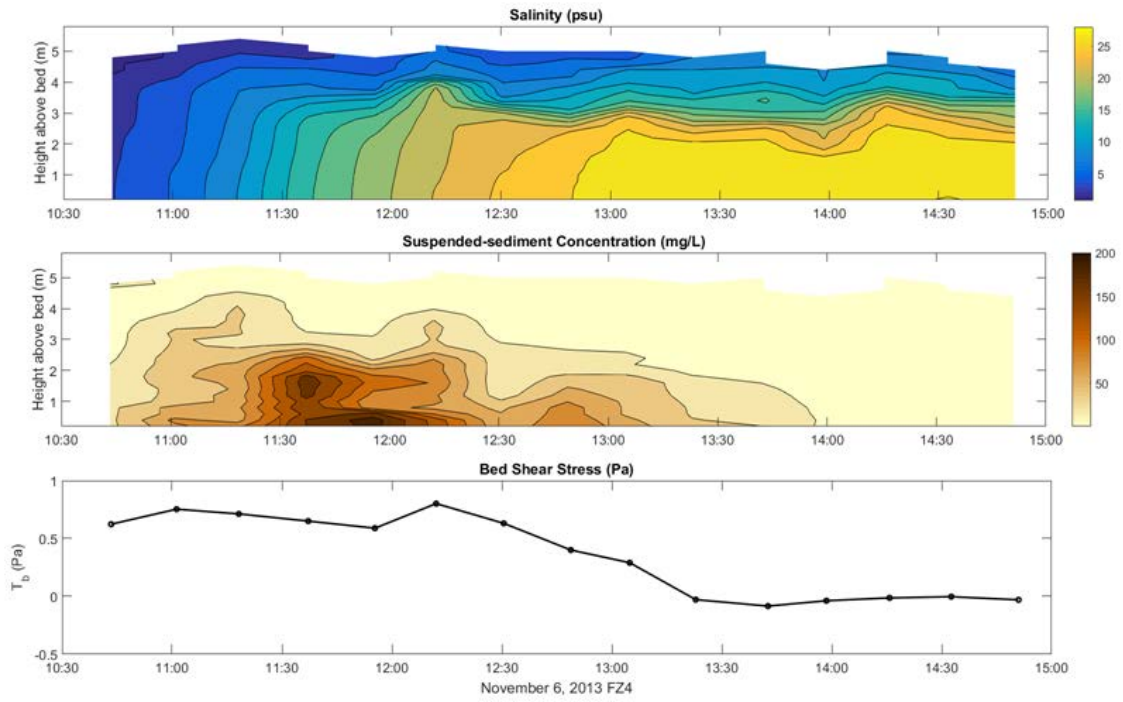

Figure 17. Example anchor station timeseries from the HSMD survey taken at FZ4 on November 6, 2013.

stresses started to increase, suspended sediment extended from the bed to mid-water column at the longer anchor stations that captured the ebbing phase following slack. These concentrations were always less than those observed during flood, and ranged from 50-80 mg/L.

The fastest near-bed current velocities reached 0.75 m/s at 0.62 m above the bed, with corresponding bed stresses of 1.79 Pa in FZ2 during LSMD. The highest stresses most often occurred during peak flood, though only one full ebb tide was captured in this study. Maximum SSC was not always observed with maximum stress. This lack of a relationship between SSC and τ_b was observed predominantly during the LSMD regime (Fig. 15). Peak SSC instead coincided with the onset of the flood, once stresses reached

~0.5 Pa. Near bed SSC (less than 2 mab) at peak flood currents was less than pre- or post-maximum flood velocities (Fig. 15).

4.3. Suspended-sediment particle characteristics

Table 5 summarizes the patterns of suspended-sediment particle characteristics over the three hydrodynamic regimes in each location in the estuary. SMD for the flocs measured with the combined LISST-DFC size spectra, ranged from 10-420 μm, floc densities from 5-250 kg/m^3 and total volume concentrations from 1-3x10^3 ppm over the three surveys. Near-bed SSC was on the order of 100-300 mg/L and floc size distributions were unimodal, with median sizes ranging from 105-130 μm. Surface SSC was consistently lower throughout all surveys, with smaller median floc sizes and finer size distributions that concurrent bottom particles.

Table 5. Results summary.

	HSMD				**HSHD**				**LSMD**		
	FZ2	**FZ3**	**FZ4**		**FZ2**	**FZ3**	**FZ4**		**FZ2**	**FZ3**	**FZ4**
ds/dt **(Change in bottom salinity, psu/time)**	3.4	2.9	5.6		20.4	12.7	-		7.12	-	5.51
Max. *u* (m/s)	0.65	0.75	0.49		0.56	-0.62	-		0.75	-	0.53
Max. τ_b (Pa)	1.28	1.70	0.85		0.94	-1.15	-		1.79	-	0.92
Mean bottom SMD (μm)	92	91	97		104	92	-		36	-	40
Max. bottom D_{95} (μm)	808		810		750		-		458	-	552
Mean bottom ρ_e (kg/m^3)	9.1	13.8	13.5		8.8	14.8	-		57.3	-	36.2
Max. bottom C_V (Volumetric SSC from DFC-LISST, ppm)	2208	1387	1019		3839	2473	-		1899	-	1119
Max. bottom SSC (Gravimetric SSC from pumped samples, mg/L)	139	99	211		276	128	-		166	-	162

Patterns of floc size and density with near-bed stress, salinity and SSC on tidal timescales were relatively similar across all flow regimes (Fig. 18A-E). Larger, less-dense flocs were observed near-bed during times of moderate stress (0.2-1.0 Pa) and higher SSC (100-200 mg/L) at the initiation of and at peak flood (Fig. 18A, C, D, E).

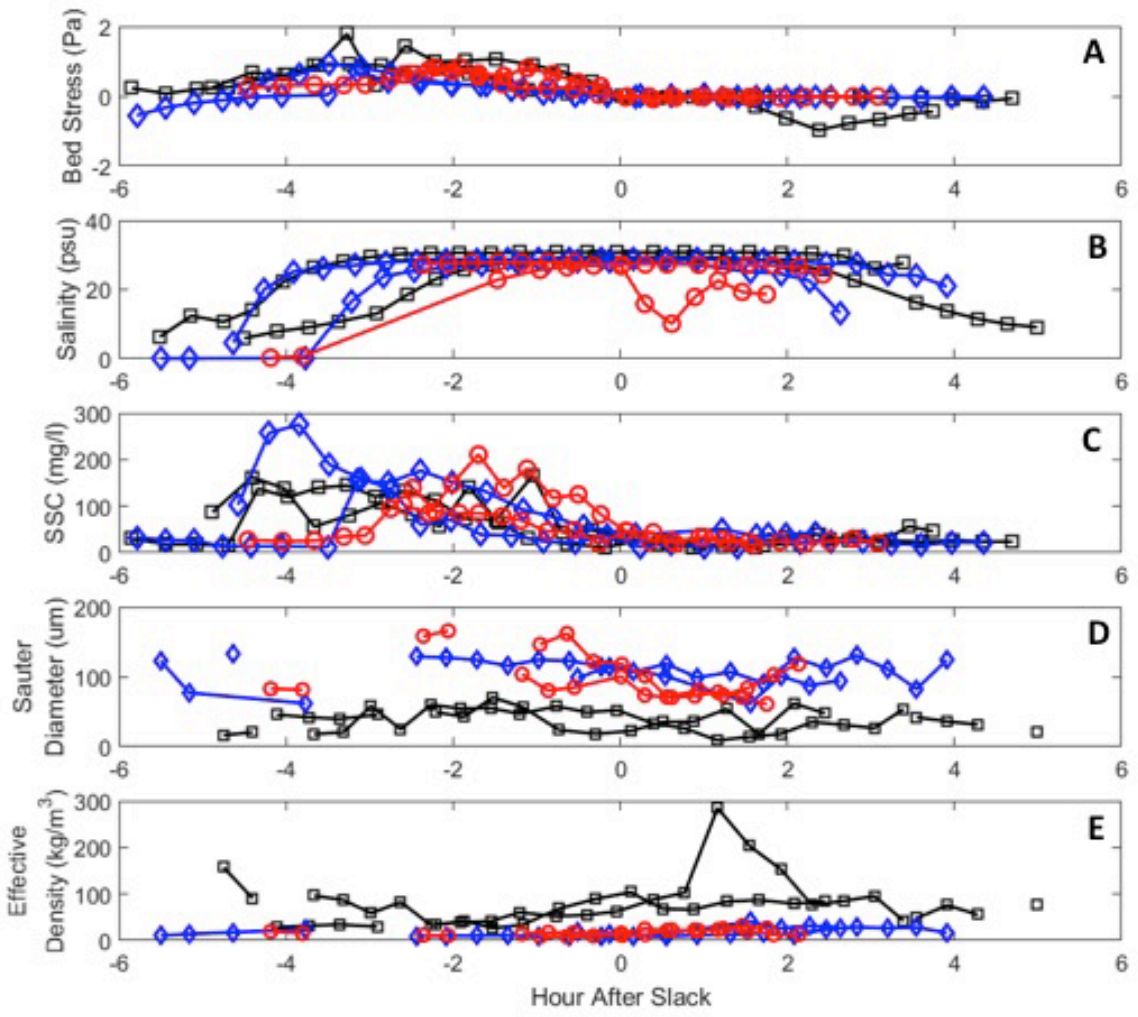

Figure 18. Near-bed timeseries of continuous anchor-station measurements [**A.**, bed stress (Pa), **B.** salinity (psu), **C.** *SSC* (mg/L), **D.** *SMD*, **E.** effective density (kg/m^3)] conducted over all three discharge regimes (red circles, HSMD; blue diamonds, HSHD; black squares, LSMD) relative to slackwater following flood tide. Slack is defined as when near-bed current velocity measured by the ADV equals 0.

4.3.1. Floc size, density and size distribution as a function of hydrologic conditions

Floc characteristics at 0.75 mab versus SSC and near-bed stress during the three survey periods are shown in Figures 19 and 20. The largest flocs observed during the project were found just above the bed in FZ4 during the HSMD period (Fig. 21; D_{95} = 808 μm; median *SMD* = 302 μm), with maximum C_V peaking at 2208 ppm. Near-bed flocs were generally loosely packed (median ρ_e = 11.7 kg/m^3). Bottom SSC reached a maximum of 211 mg/L in FZ4, concurrent with the observed maximum near-bed floc sizes. Peak SSC was observed throughout the estuary during HSHD sampling, with bottom concentrations reaching 275 mg/L and particle volume concentrations nearly double those of any other season (maximum C_V = 3839 ppm*)*. Flocs were the least dense observed over all three seasons, (median ρ_e =12.2 kg/m^3) and reached sizes of 750 μm. Mean near-bed flocs were 104 μm in diameter, the largest of any sampling period.

The most notable observation of this three-year study is the stark change in particle characteristics in LSMD (Fig. 21). The smallest, densest, most compact flocs were consistently observed during this survey (median *SMD* = 244 μm, ρ_e = 46.5 kg/m^3). Floc densities were on average double those of the previous two sampling periods, and an order of magnitude greater in near-bed aggregates. One-third of all particles observed in LSMD had ρ_e > 50 kg/m^3, compared to 4% in HSMD and 1% in HSHD. LSMD maximum C_V peaked at 1899 ppm, the lowest of the three surveys.

Full in-situ size distributions of near-bed particles observed in HSMD and HSHD are similar (Fig. 22-23). Unimodal at ~300 μm, the concentration of particles >100 μm nearly double that of LSMD. In-situ LSMD particles were on average unimodal at 200

μm and had higher concentrations of particles <100 μm (Fig. 22, Fig. 24). The surface in-situ distributions match the bottom, though with concentrations about one order of magnitude lower than the populations observed near the bed.

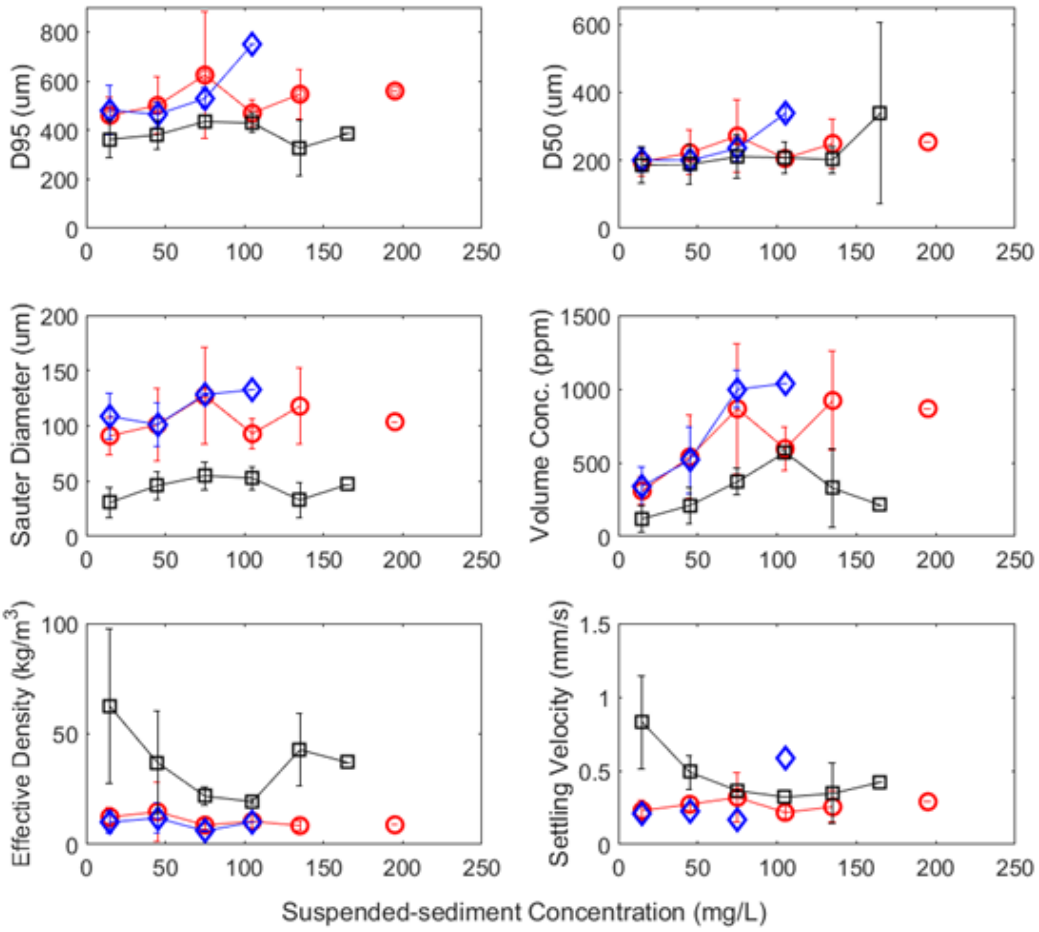

Figure 19. Near-bed particle characteristics during each regime bin-averaged by concurrently-observed near-bed SSC.

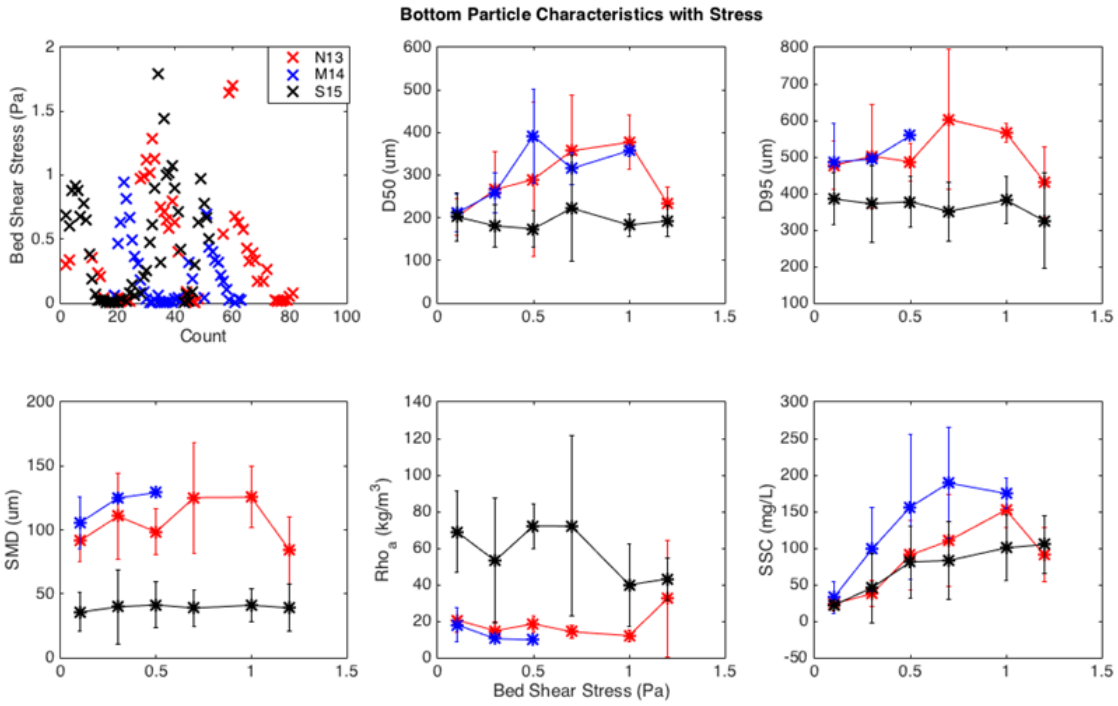

Figure 20. Mean near-bed suspended particle characteristics (D50, D95, SMD, apparent density and SSC) bin averaged by bed shear stress measured by the QSL over all three surveys.

4.3.2 Particle characteristics at fronts

The largest flocs were observed near the bed, typically concurrent with maximum SSC. Flocs reached 808 μm in FZ2 HSMD, with surface flocs typically on the order of 100 μm in median diameter during all surveys. In-situ size floc size distributions exhibited a tidal pattern, with the highest concentrations of larger particles observed during the flood, a decrease in concentration across all size classes during slack, and an increase with the initiation of the ebb, yet not reaching the size or concentration observed during flood for similar near-bed velocities and stresses (Fig. 23-25).

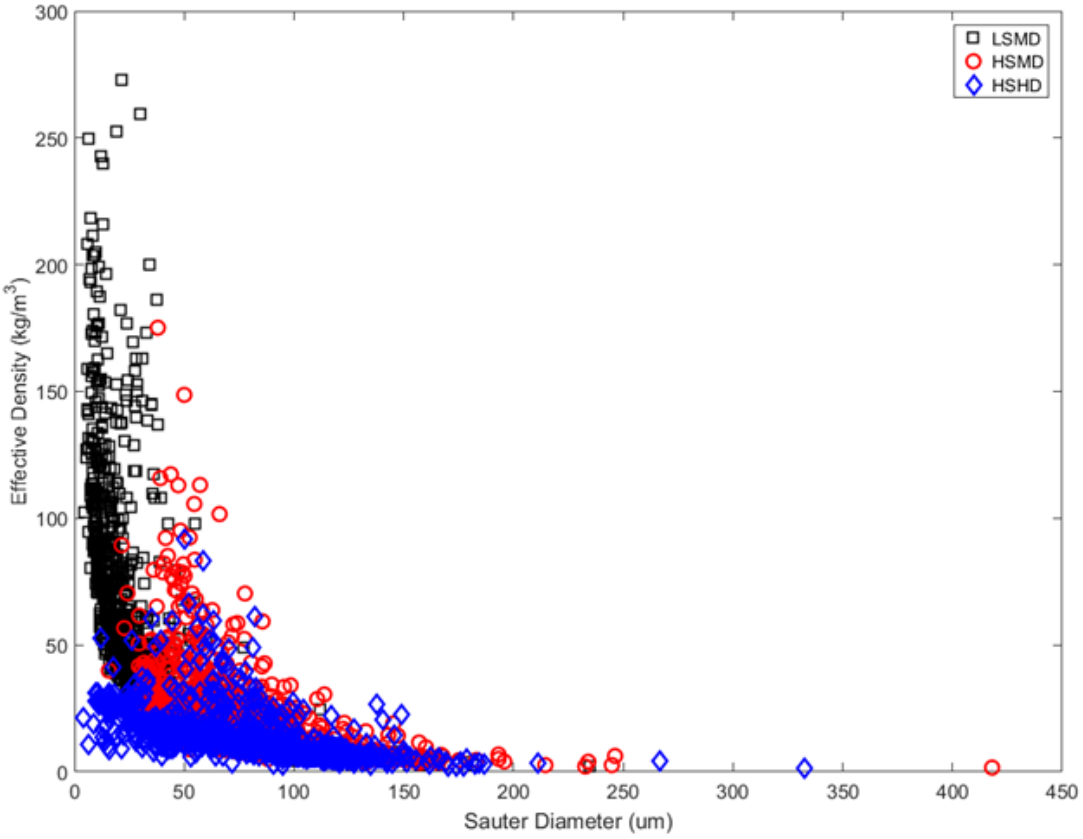

Figure 21. Sauter mean diameter (μm) and effective density (kg/m^3) as calculated in Eq. 1 and Eq. 3 respectively of particles observed throughout the water column and estuary over three hydrodynamic regimes. Higher-density, more compact aggregates dominate the suspended-sediment signal following an extended period of low-discharge during the LSMD regime (black squares). Low-density (<50 kg/m^3), loosely-packed flocs make up the majority of suspended-sediment during two high-sediment supply regimes (HSMD, red circles; HSHD, blue diamonds).

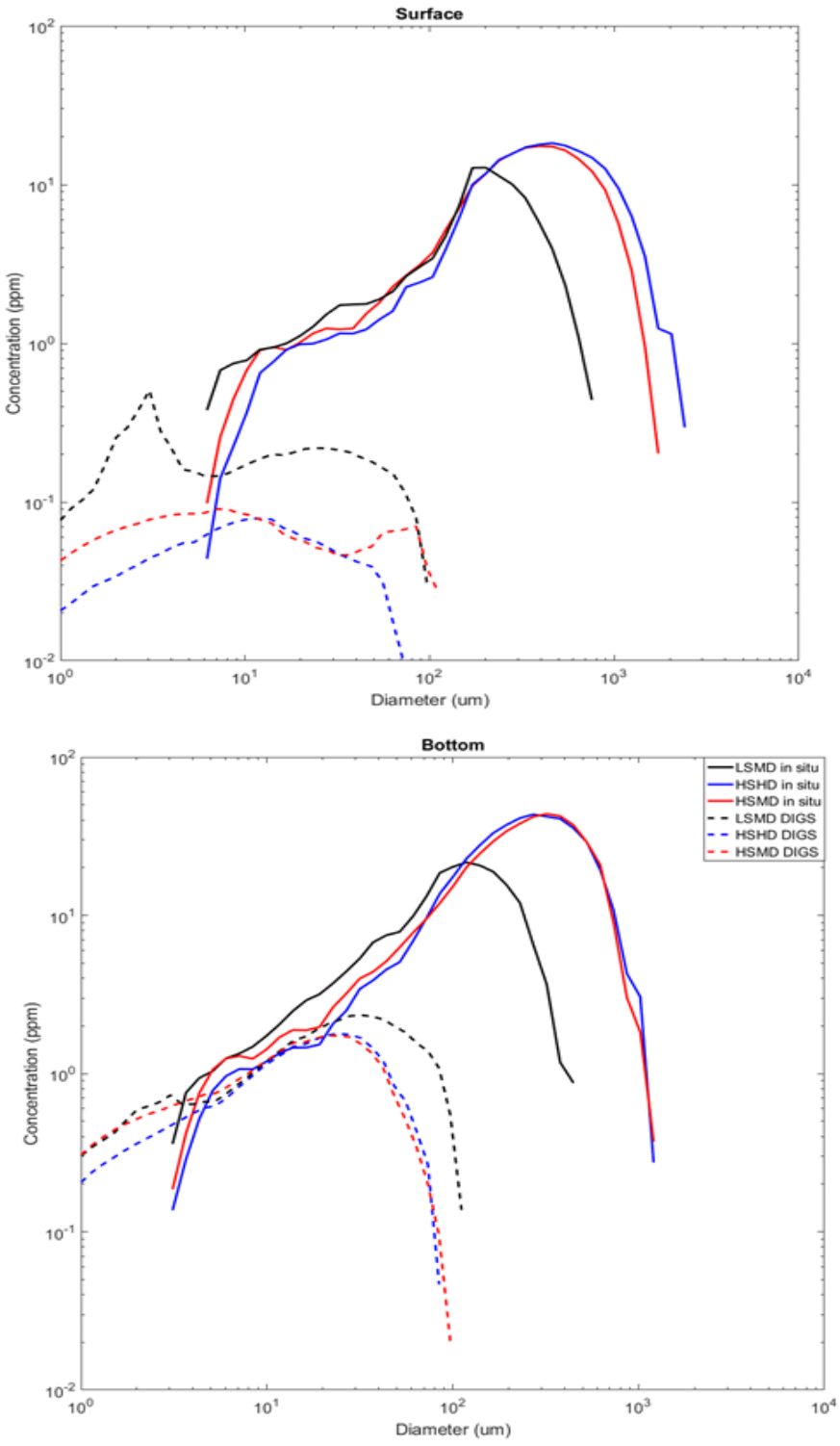

Figure 22. Full LISST-DFC merged in-situ size distributions (solid lines) and DIGS spectra (dashed lines) for surface (0.5-1.0m depth) and near-bed (0.5 mab) particles observed in HSMD, HSHD, LSMD.

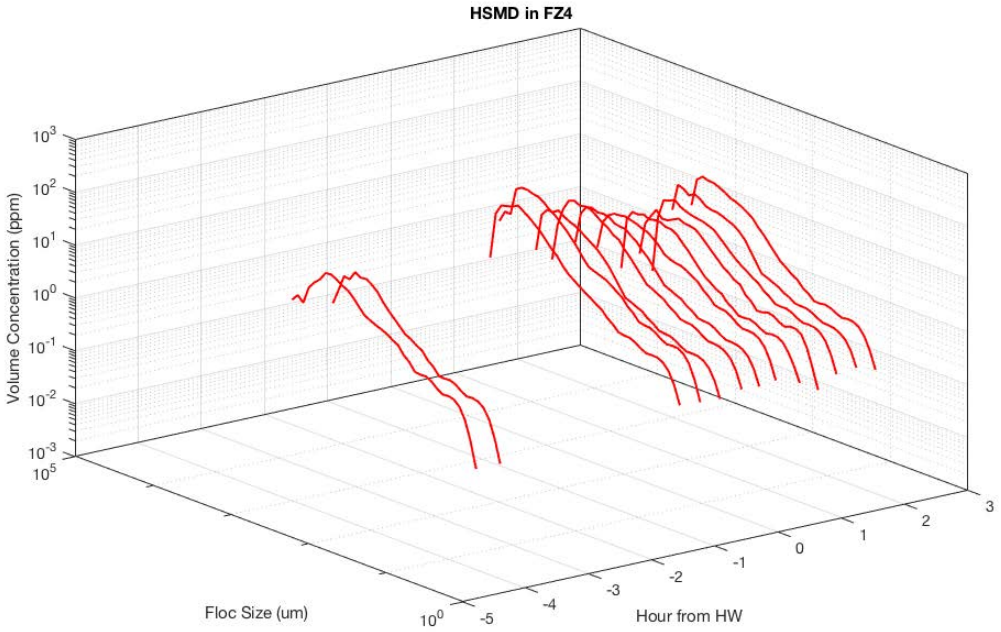

Figure 23. Timeseries of mean near-bed floc size distributions in FZ4 during HSMD on November 5, 2013 relative to high water (HW). The gap in data from 4 hours before HW to 0 is from LISST malfunction.

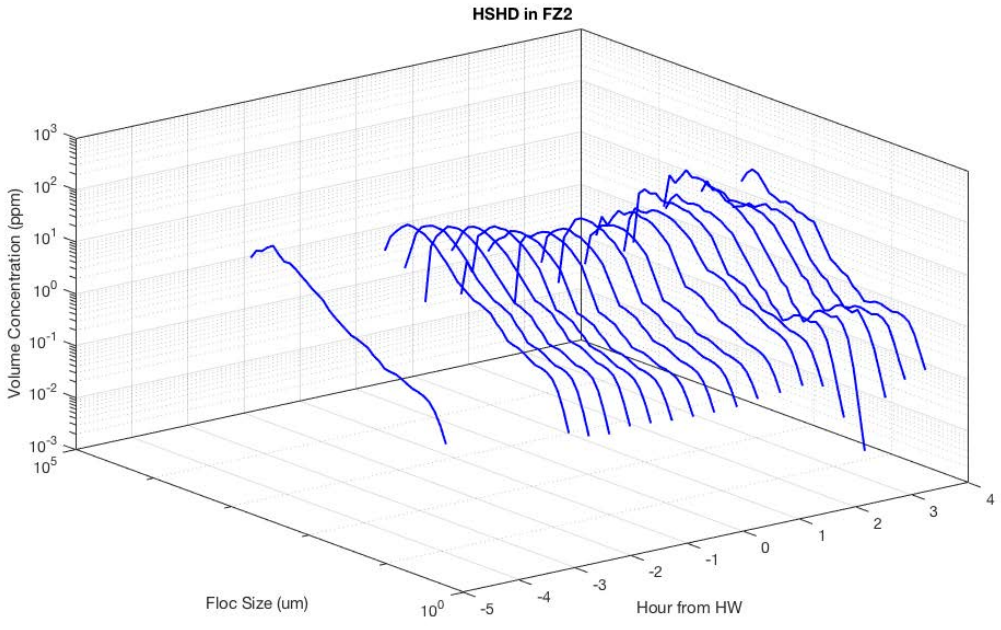

Figure 24. Timeseries of mean near-bed floc size distributions in FZ2 during HSHD on May 15, 2014 relative to high water (HW).

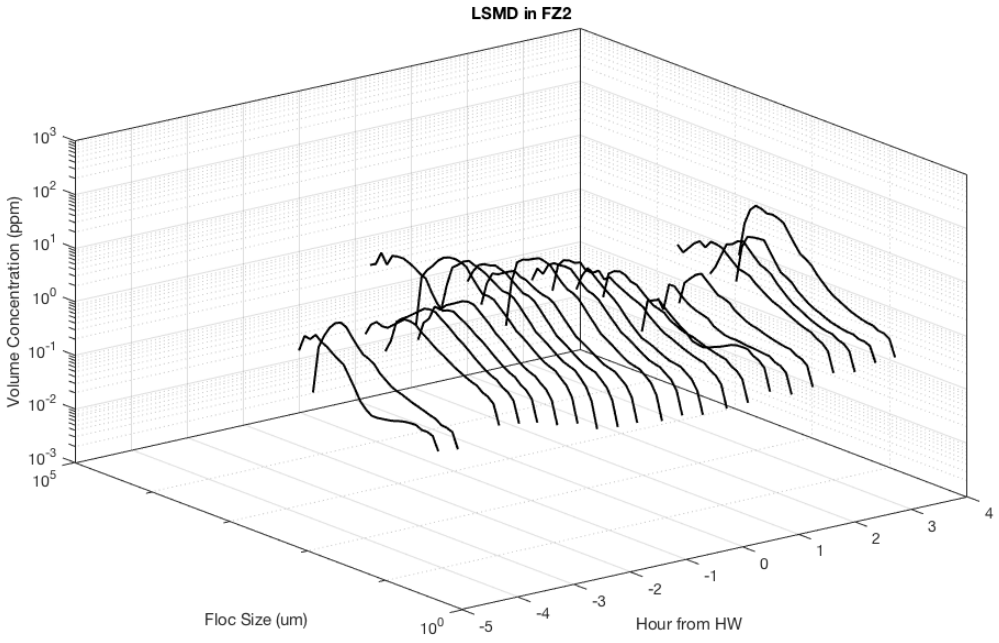

Figure 25. Timeseries of mean near-bed floc size distributions in FZ2 during LSMD on October 1, 2015 relative to high water (HW). Concentrations in the largest size classes (>300 μm) were one order of magnitude lower than the distributions observed in HSMD and HSHD.

4.3.2. Floc settling velocity

Least-squares linear regressions of Reynolds' turbulent diffusion (Eq. 7), led to bulk settling velocity estimates of 1.05 mm/s, 1.15 mm/s and 0.79 mm/s for mean near-bed particles observed in HSMD, HSHD, and LSMD respectively (Fig. 26).

The modified-Stokes settling using LISST-derived ρ_e (Eq. 8), enabled the calculation of settling velocity for each observed particle population from each DFC image. Settling rates ranged from 0.05 to 2.70 mm/s, and a weak positive relationship between w_s and floc size is observed ($r^2 = 0.003$; Fig 27). When bin-averaged by floc size, this relationship becomes stronger ($r^2 = 0.50$). The LSMD particles in all size classes had higher w_s than HSMD and HSHD particles. The expected (Van Leussuen, 1998; Safak et al., 2013) inverse relationship between ρ_e and floc size is observed ($\rho_e = -0.3\ D_{50} +83.9$, $r^2 = 0.26$), with the strongest negative correlation with the LSMD population ($r^2 = 0.51$, n = 1613). The size-binned regression is significantly correlated, $\rho_e = -0.3\ D_{50} +108.7$, $r^2 = 0.68$).

4.3.3. Disaggregated Inorganic Grain Size

The size distributions of component particles of in-situ flocs, or DIGS of the suspended-sediment from samples taken 0.5 mab, reach a maximum of 120 μm across all regimes, indicating that particles were packaged as flocs in-situ (Fig. 22). The average spectra of HSMD and HSHD are nearly identical, with median sizes of 15 μm and 17 μm respectively. LSMD DIGS were coarser than the previous two surveys, with bottom samples mean diameter ranging from 2 μm to 67 μm, and a median of 34 μm. The increased concentration of coarse (30-100 μm) grains and the lower SMD during the LSMD suggest that the LSMD aggregates were able to incorporate larger grains

compared to the HSMD and HSHD conditions.

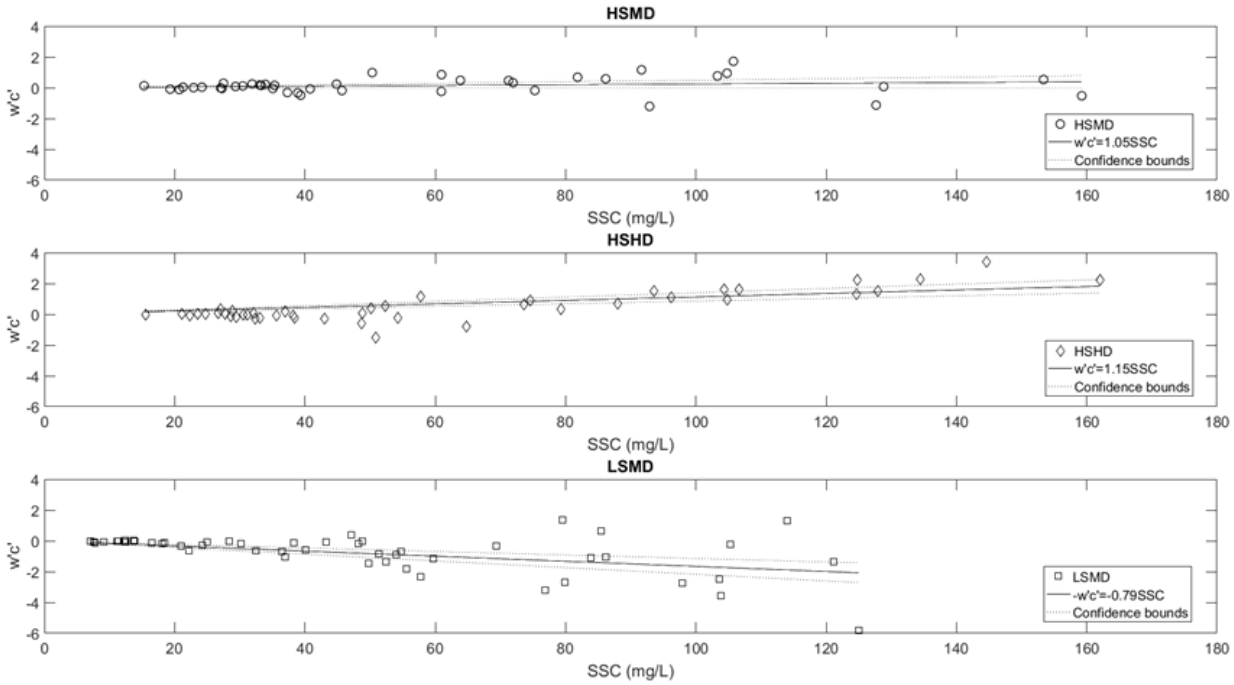

Figure 26. Best-fit linear regressions of Reynolds turbulent diffusion with adjusted ADV backscatter observed at 0.6 mab over each sampling period. The slope of each regression represents the bulk settling velocity of near-bed particles.

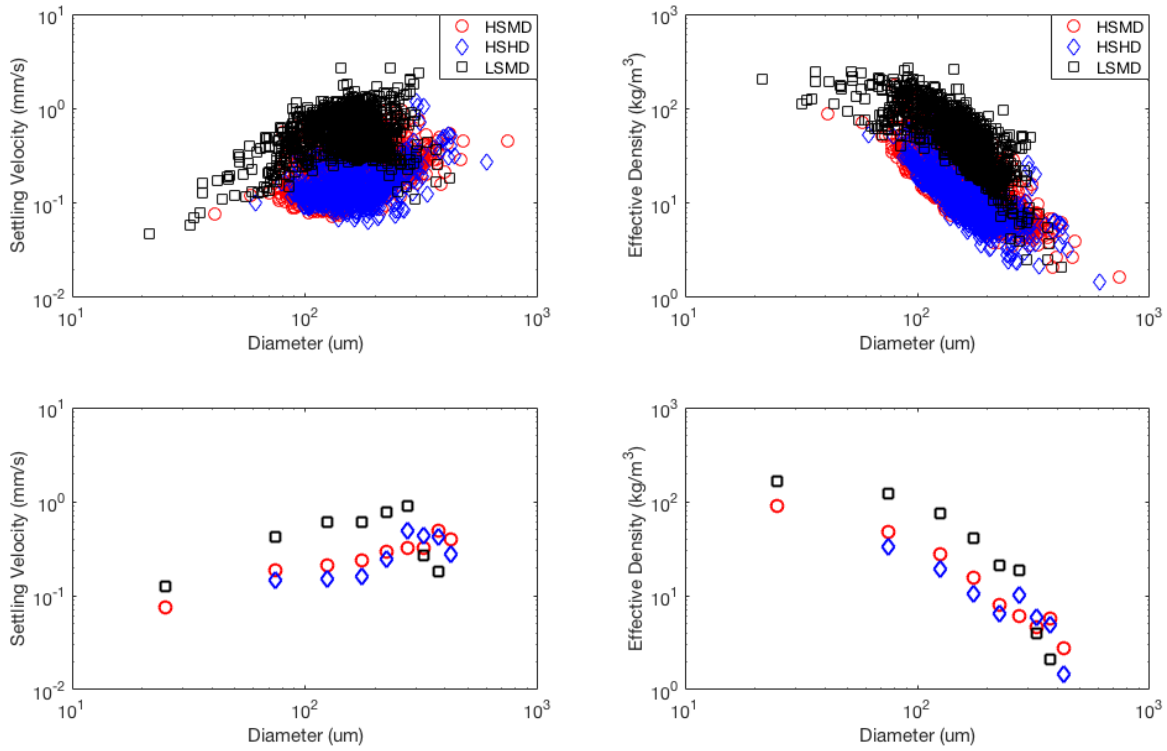

Figure 27. Floc size (D_{50}) versus floc settling velocity and floc effective density of all in-situ particles observed over HSMD, HSHD and LSMD throughout the Connecticut River estuary (n=4386, top). Bin-averaging the data into half-phi intervals resulted in relationships with strong correlation coefficients (r^2= 0.50 and 0.68 respectively).

5. DISCUSSION

The concurrent measurements of suspended-particle characteristics, currents, and water properties allow an evaluation of controls of floc size and suspended-sediment transport. Numerous relationships between floc characteristics and estuarine dyanmics were assessed in this study. For example, Winterwerp (1998) suggests a clear relationship between floc size and stress exists; as stress increases, so do inter-particle collisions resulting in the building of flocs up to a point, beyond which stresses become too strong and floc break-up occurs. A positive correlation between floc size and SSC, with higher concentrations enhancing flocculation has also been observed in previous studies (Winterwerp et al., 2004).

Additionally, due to the previously observed intense salinity fronts and stratified behavior of the system, my initial hypotheses focused on the influence of frontal trapping on flocculation processes. However, a simple correlation matrix for this study revealed that significant correlations between particle characteristics and estuarine properties measured varied under different discharge conditions. The only significant relationships observed under all hydrodynamic conditions were a positive correlation between τ_b and *SSC* and floc D_{50} and *SSC* (Table 6; Fig. 28). Patterns began to emerge when the entire dataset- regardless of location in the estuary or time within the tidal cycle- was considered in terms of prior hydrologic conditions, for example how long it had been since a significant discharge event. This suggests that hydrodynamic conditions have a major effect on suspended particle characteristics primarily through the input of suspended sediment to the system.

Table 6. Correlation matrix of Pearson correlation values (R) for all near-bed data collected over the entire project.

	τ_b	***ds/dt***	***SSC***	***Salinity***
D_{50}	**-0.193**	***0.241***	0.072	**-0.195**
D_{95}	**-0.195**	***0.230***	0.091	-0.152
SMD	-0.177	0.119	0.007	-0.135
ρ_a	0.086	-0.099	-0.094	0.184
SSC	***0.522***	0.120	-	-0.011
C_V	***0.239***	0.188	***0.470***	-0.124

Correlations in bold indicate significant relationships; italicized bold correlations are highly significant; N=142.

5.1. Flocs versus aggregates

The terminology within the body of cohesive sediment literature can be a bit ambiguous. In this study, the process of flocculation refers to the agglomeration of individual particles. Flocs are defined as recently coagulated and typically bound by organic molecules (Hill et al., 2009). Aggregates are defined as agglomerations of component particles that initially flocculated at a previous time, and through transport in turbulent eddies and cycles of resuspension, have achieved a higher degree of cohesion and are difficult to break up entirely (Milligan et al., 2001). Aggregates are typically resuspended and deposited from the bed, rather than formed in the water column during mixing and settling, as flocs do.

5.2. Effects of stratification on particle characteristics

5.2.1. Tidal patterns of suspended transport

Overall, the highest concentrations and largest flocs were most frequently observed just above the bed with the initiation (predominantly during LSMD) or passing

of the flood front (HSHD, HSMD; Fig. 15-17). Throughout the estuary in September 2015, maximum floc size and SSC often decreased after the initiation of the flood front, despite maintaining or increasing the level of bed stress, an indication of supply-limited resuspension. The floc growth with increasing bed stress observed during HSHD and HSMD suggest that sufficient material is available within the system for new flocculation to occur. During HSHD flocs build from 180 to 400 μm up to stresses of 1.0 Pa during the flood, and flocs grow from 200 to 415 μm over a 0.6 Pa increase in stress in HSMD (Fig. 28). The largest near-bed flocs observed 10 to 20 minutes following peak stress also suggests concentration-enabled flocculation is occurring (Fig. 18).

Similar to previous studies, the decrease in bottom stress during slack allows larger particles to settle through the water column and accumulate above the bed, seen as a clearing of the water column and near-bed following a drop in stress. This is in contrast with LSMD, where peak SSC and aggregate size occur at the initiation of the flood. As the strong flood front plows up-estuary, near-bed aggregates are resuspended and transported with the nose of the front. This is seen with recurring mid-water column maximums of floc density and the building horizontal salinity gradient in September 2015 (Fig. 17). Under all survey regimes, concentrations and floc sizes dropped during the transition from flood to ebb, mostly settling out of the water column. However, the water column clears faster under LSMD conditions, likely a manifestation of the denser aggregates with faster settling velocities and lack of new, organic-rich sediment available for new flocculation to occur.

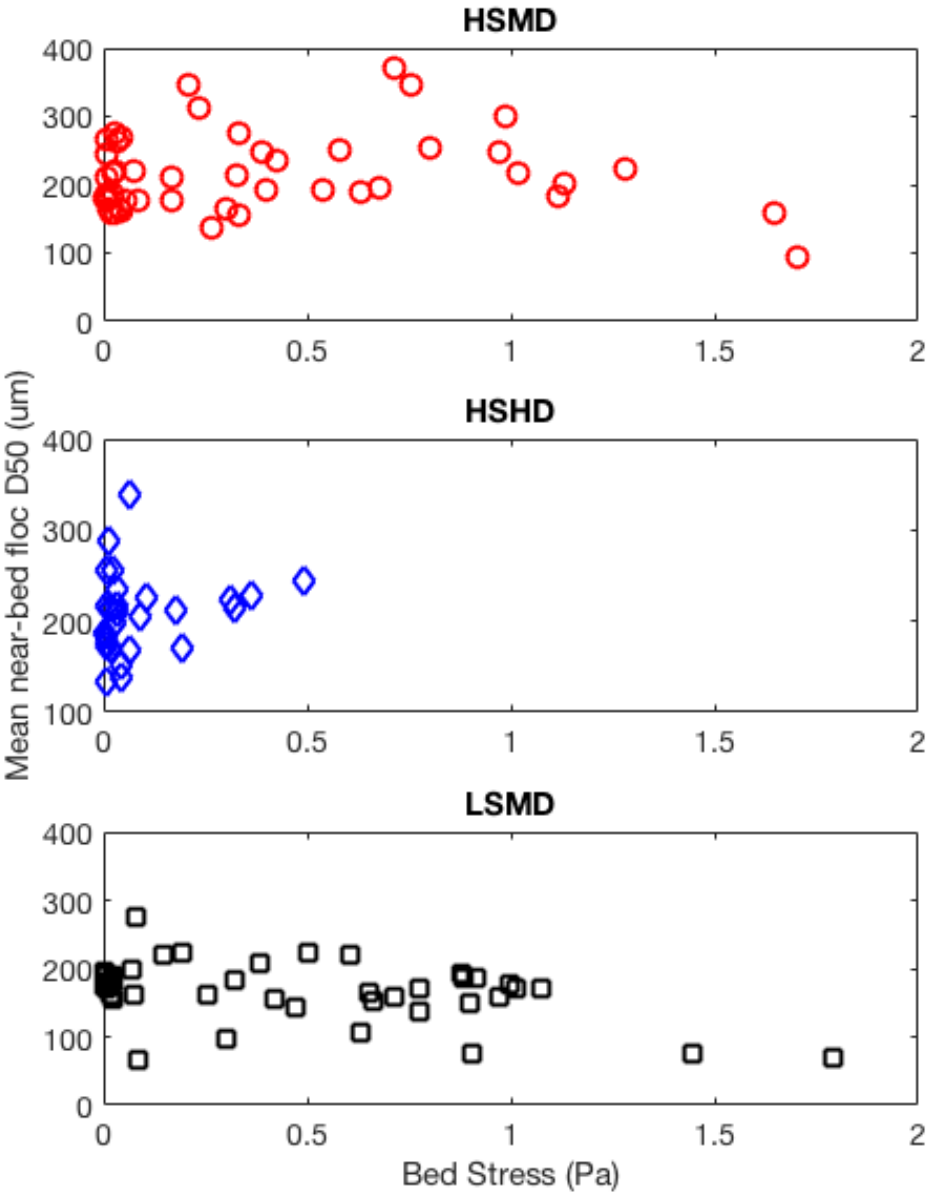

Figure 28. Near bed stress versus median floc size and mean full size spectra under each hydrologic regime.

5.2.2. Shearing of flocs through the pycnocline

During all seasons, once the pycnocline is established, the densest flocs are seen immediately above and below the region of strongest density gradient, with lighter flocs at the surface and bed. As the transition from flood to ebb tide continues, fresh water flows over the dense seawater, causing increased vertical stratification and receding bottom water until the pycnocline intersects the bed. The persistence of stratification all the way though the water column to the bed, the dense flocs settle to the bed, leaving only fluffy flocs above (Fig. 29). At times it appears that some light flocs, though large, become stranded just above the pycnocline (Fig. 30), as shown by maximum floc size observed mid-water column with a decrease below to the bed. However, LISST scattering off the pycnocline and schlieren corrupting DFC images make it difficult to fully describe this relationship.

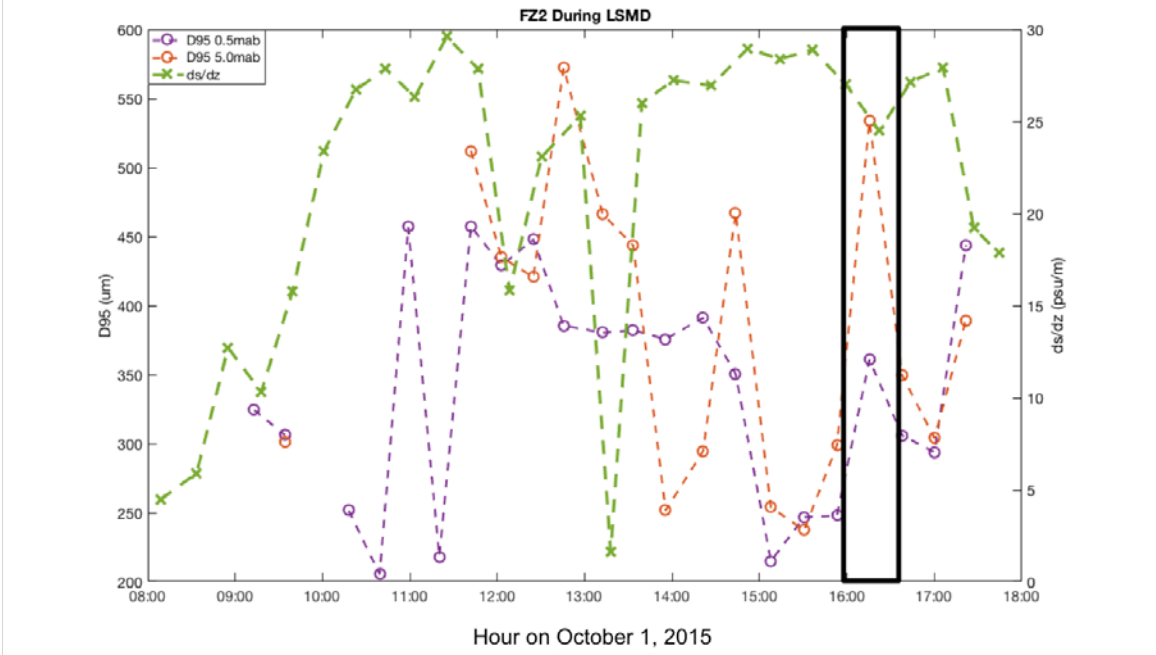

Figure 29. Timeseries of vertical salinity gradient, *ds/dz* (psu per meter depth, green x's), maximum floc size, D_{95} (in µm) 0.5 mab (purple circles) and 5.0 mab (orange circles) at an example anchor station located in FZ2 during LSMD on October 1, 2015. *Ds/dz* is high during both the flood (08:00 to 12:30) when the salt wedge flows under the fresh water, as well as during the early ebb (13:30-18:00). The black box highlights an example of floc properties affected by the steep *ds/dz*, or pycnocline.

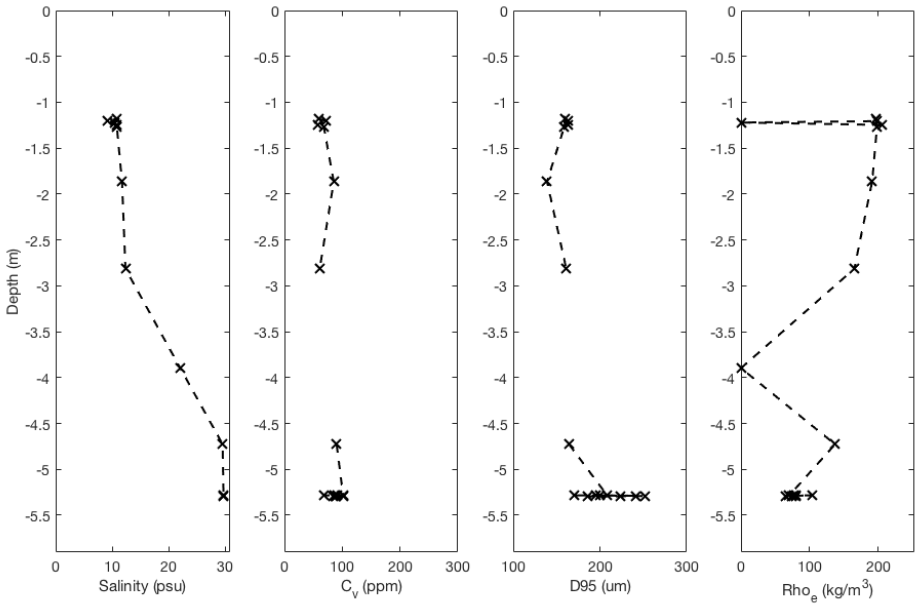

Figure 30. Salinity (psu), total volume concentration (C_v, ppm), maximum floc size (D_{95}, µm), and effective density (kg/m^3) with depth in FZ2 during LSMD on October 1, 2015, corresponding to the black box in Fig. 29. Dense flocs are stranded above the pycnocline at approximately 3 m depth.

5.3. Effects of discharge and sediment supply on particle characteristics

The clear presence of two separate suspended-particle populations in the estuary over the course of three hydrodynamic conditions, with major changes in floc density and size between low and high sediment-supply regimes implies the dominance of hydrologic conditions on sediment transport patterns (Fig. 21). Ultimately, sediment supply controls the rate of flocculation and thus the resulting particle characteristics of the suspension (Safak et al., 2013). During the HSMD survey, the elevated near-bed sediment concentrations support the building of large, loosely bound flocs; recently flocculated. Flocs appear to grow in size up to stresses of 0.6 Pa during this survey, above which the stress becomes too high for the loosely-bound flocs, and they are broken up. Similarly, the light, fluffy flocs observed during HSHD were likely able to form due to the increased sediment availability in the water column as well as additional organic material from riverine input during the high discharge spring freshet. The results from HSHD are most similar to the conclusions of Winterwerp and Van Kesteren (2004), suggesting a high sediment supply and limited stratification is best to satisfy the relationship of growing floc size with increasing stress to a maximum condition. This trend did not occur in LSMD period, when flocs of similar size (D_{50} =180 μm) were present in the water column at all levels of stress. This is likely because adequate fresh sediment was not available for new flocculation to occur to build flocs of larger sizes.

The ‘fresh’ supply of fine sediment during the high sediment supply regimes results in these fluffy flocs dominating the suspended-particle signal. The low concentrations observed in LSMD, following 22 weeks of below average discharge, limited the amount of new flocculation that could occur. Thus, the majority of particles in

suspension were small, dense aggregates. These compact aggregates likely initially flocculated at an earlier time, with higher water and sediment discharge, and have been deposited and suspended repeatedly with the landward migration of the salt wedge, becoming denser and more robust over time. As a result, the dense aggregates are able to incorporate and retain coarser silt particles within, as seen in the DIGS spectra (dashed black curves in Fig. 22).

A key observation on the two distinct floc populations needs to be made. The sediment supply to the estuary is controlled by hydrodynamic timescales longer than the five to seven days of each measurement period and the type of particle packing dominating each suspended-sediment population is driven by the timing of new sediment input. Although more sediment was observed throughout the water column in HSMD and maximum near-bed SSC was approximately 50 mg/L higher than that in LSMD, similar magnitude of near-bed SSC was observed at individual anchor stations across both regimes (Table 4). However, the extended period of low flow and lack of fluvial input preceding the LSMD sampling caused the dense aggregates to dominate the suspended-particle signal. Thus the near-bed SSC dominated by aggregates observed during LSMD is the result of tidal resuspension rather than flocculation and settling of fluvial-derived suspended-sediment in HSMD.

5.4. Exchange with Long Island Sound

Recent studies have described sediment transport and trapping within the Connecticut River estuary using different methods (Woodruff et al., 2013; Yellen et al., 2014; Yellen et al., 2017; Valentine et al., *in review*). Yellen et al. (2017) examined fine-sediment trapping within the estuary through the deployment of sediment traps and

collection of shallow cores in the off-river coves and channel margins. They found that fine sediment was accumulating within these off-channel locales and that the highest rates of sedimentation corresponded with the highest percentage of marine sediment signal. Preliminary results of Simans et al., (pers. com.) support these findings, suggesting that up-estuary directed residual bottom flow is the most important factor for the deposition of fines within the Connecticut River estuary.

The inter-annual changes driven by suspended-sediment input coupled with tidal front observations detailed in this study, reinforce the suspended-sediment transport pathways within the entire Connecticut River estuary-Long Island Sound system suggested by others. The system can be described as a 'conveyor belt' of fine suspended sediment; watershed inputs supply the estuary and nearby Sound with fine sediment, and tidal currents combined with the landward migration of the salt wedge transport recycled fines back into the estuary (Fig. 31). When the estuary is charged up with sufficient sediment inputs, such as during the spring freshet (HSHD) or following a water year with sufficient high flow and turbidity events (HSMD), SSC is high enough to enable new flocculation. These light flocs ("fluffies") form through inter-particle collisions as they settle during slack currents, some are trapped in stress refuges within the system, such as the off-river waterbodies and coves and channel margins (Woodruff et al., 2013). The remaining suspended load is discharged into Long Island Sound. In the energetic conditions of the Sound, the flocs are reworked, broken up and re-formed over and over, increasing in cohesion and density and carried back into the estuary by the mean, tidally-averaged up-estuary directed near-bed velocity. These aggregates ("toughies") are resuspended off the bed with the stronger stresses observed at the initiation of the flood

and fewer are resuspended during the stratified ebb conditions (Fig. 15). This results in net transport up the estuary until these recycled aggregates are also deposited along the banks or in the coves.

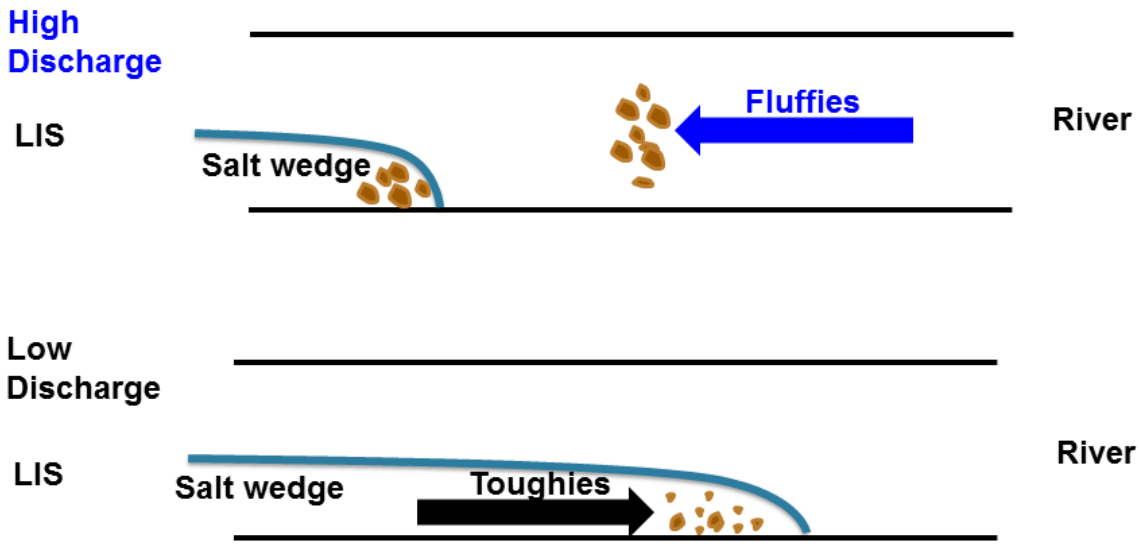

Figure 31. Conceptual diagram of a map view of the 'conveyor belt' of suspended-sediment transport in the Connecticut River estuary and Long Island Sound.

When the sediment supply is low and new flocculation is limited, the suspended-particle signal is dominated by these aggregates, as seen in LSHD. The composition of the aggregates and flocs appear to be the same source material, as indicated by matching DIGS spectra; but their strength and compact primary-particle packaging are a result of the degree of repeated resuspension and turbulence the flocs have been subjected to following initial flocculation, as observed in previous studies (Van Leussen, 1988; Winterwerp, 1998; Hill et al., 2009).

Bed-sediment grain-size data collected during the same sampling period support this model. Valentine et al., (*in review*) found the size spectra of DIGS from suspended-sediment from the water column, bank material, and 'mud drape', or a reoccurring surface layer of fine bed sediment, all appear to be a similar composition, shown by a unimodal distribution with a peak at 25 μm. Though bed-sediment sampling in Long Island Sound was beyond the scope of this project, data organized in the U.S.G.S. East-Coast Sediment Database had a core approximate 0.5 km from the estuary mouth, with a fine distribution slightly coarser than the observed suspended-sediment DIGS and up-estuary bed samples (Fig. 32). This suggests that some fraction of fine sediment delivered from the watershed to Long Island Sound (e.g. during HSMD and HSHD) is then reimported into the estuary over periods of low river discharge. This fine sediment is potentially resuspended with tidal currents forming denser aggregates that are transported back up estuary with the landward migration of the salt-wedge, and are ultimately deposited in the off-channel coves and channel margins.

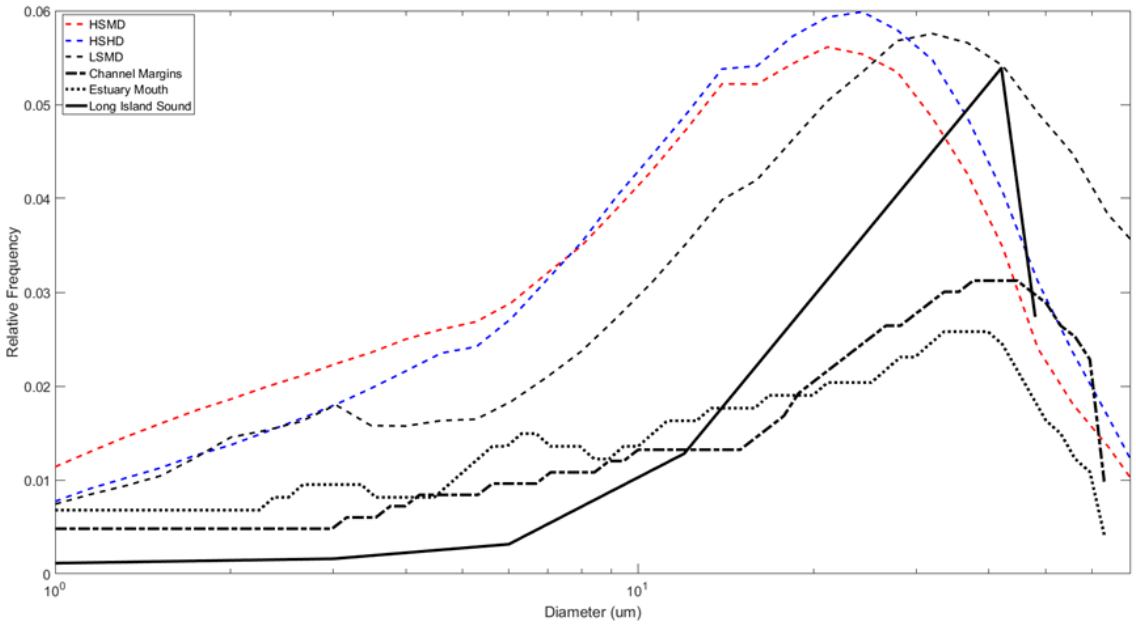

Figure 32. Grain size distribution of suspended-sediment (mean near-bed water-column DIGS across all three regimes, dashed curves), bed sediment from the channel margins (dash-dot curve) and estuary mouth (dotted curve) and distribution of fines (<45 μm) from Long Island Sound, approximately 0.5 km from the mouth of the estuary collected in 1996 as part of the USGS East-Coast Sediment Database (solid curve).

5.5. Comparison long-term floc dynamics studies

The observations of floc size, density and settling velocity from this study fall within previously determined ranges, despite using different methods of calculating effective density and settling velocity (Fig. 33, Fig. 34; Van Leussen, 1998; Manning and Bass, 2006; Markussen and Andersen, 2013). The method of Hurley et al. (2016) deriving effective density from apparent density has not been applied in many settings, and the resulting commonly observed inverse relationship between effective density and floc size confirms that this method can be reproduced under varied conditions.

Several long-term flocculation dynamics studies have been conducted under different hydrodynamic and estuarine settings and provide an interesting comparison to

our dataset. Fetteweis and Baeye (2015) conducted a field survey in the energetic (though wave-influenced) Belgian coastal area spanning over 700 days between 2006 and 2013. They found a clear seasonal trend in their data, with larger floc sizes and higher near-bed SSC in the summer and smaller flocs and lower yet more diffuse SSC in the winter. Unlike our dataset, no interannual trends emerged despite the long dataset, likely a consequence of abundant SSC (concentrations on the order of 1000 mg/L). Manning and Bass (2006) conducted surveys in the mesotidal, dendridic Tamar estuary in summer and fall 1998 and spring 2003. They were able to capture a high sediment supply regime as well as a diluted regime, and found that the spring-neap cycle was the most significant control on this shift in energy. The turbulent, highly concentrated spring flood tide conditions resulted in a bi-modal floc size distribution, with microflocs dominating the suspended signal. Whereas during the less-energetic neap ebb led to large settling fluxes to the bed. While interesting studies that display similar, well-documented relationships between sediment supply, bed stress, floc size and settling velocity similarly to this study, the inter-annual hydrologic variability that dominates the estuarine sediment supply and thus cohesive particle characteristics is unique to this study, as far as the author is aware.

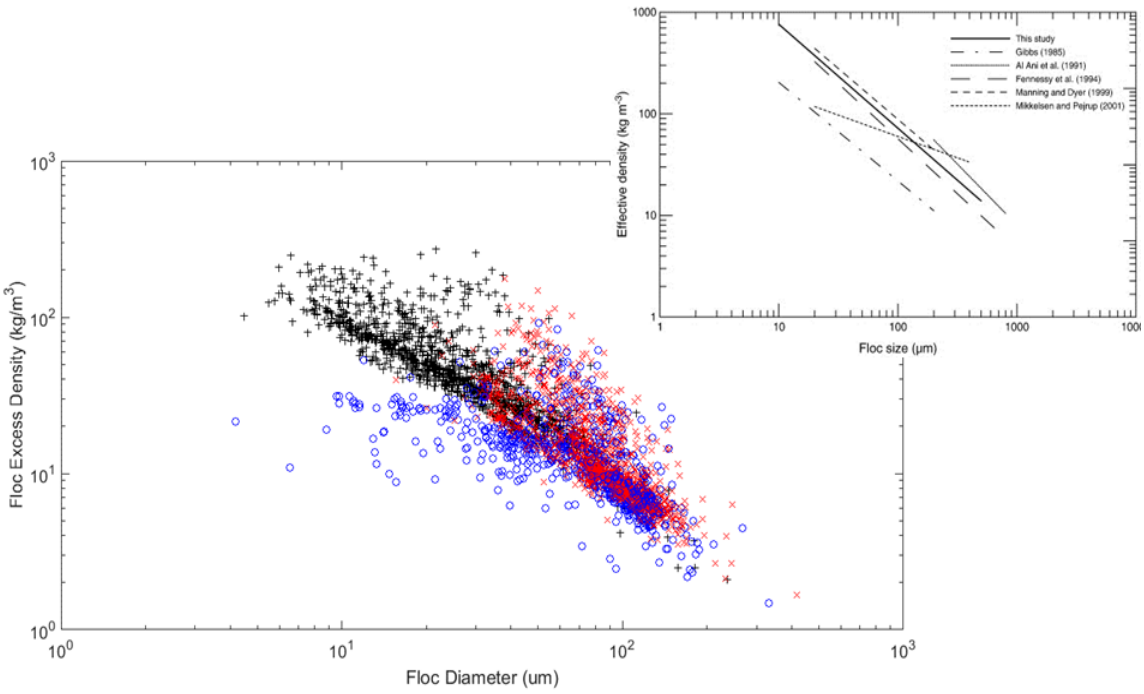

Figure 33. Floc size (SMD) versus floc excess density observed during this three-year study (left panel), compared with those collected by Markussen and Andersen (2013).

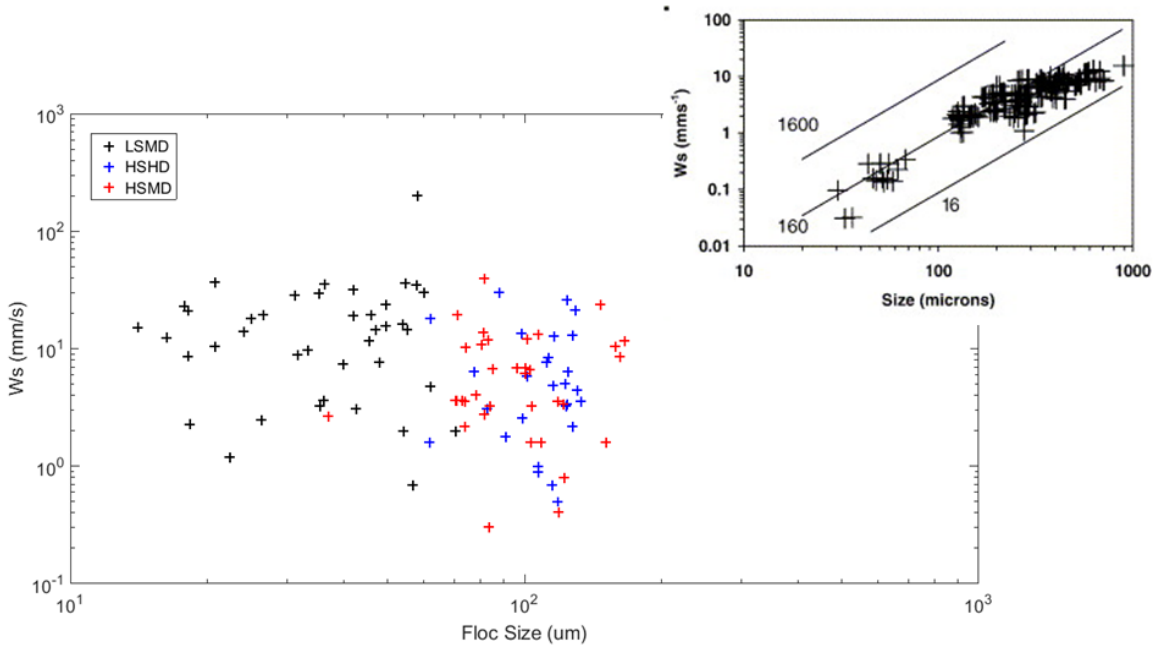

Figure 34. The observed relationship between floc size and settling velocity (calculated using a modified Fugate and Friedrichs method), in context with data from studies assembled by Manning and Bass (2006).

5.6. Future work

Calculating suspended-sediment fluxes and exchange with Long Island Sound is beyond the scope of this study, though the distinct populations we observe fit the pattern of export of fines under high discharge conditions and re-import of the same material into the estuary under periods of low flow. Analyses are currently underway to quantify suspended-sediment flux within the estuary using acoustic backscatterance sensors and comprehensively characterize grain size at the estuary mouth and near Sound.

To provide further context of the inter-annual seasonal hydrodynamic patterns, additional surveys should be conducted to confirm the significance of the count of large events preceding the time of observations and to better quantify the time it takes for the estuary system to become 'charged' or depleted. Additionally, capturing extended timeseries of particle characteristics near the mouth of the estuary would be beneficial to confirm that landward import from Long Island Sound is the source of aggregates observed during LSMD regimes.

The influence of the pycnocline on cohesive suspended-sediment dynamics is under-studied in coastal sediment transport literature. Density gradients are such an integral component of estuarine dynamics, however difficulties using the LISST through these density gradients can be problematic. Using image-only in-situ methods would allow a more robust study of the interaction between flocculation and the pycnocline.

6. SUMMARY

Two distinct suspended particle populations were observed over the three years of this study provide insight on the suspended-sediment transport pathways in the Connecticut River estuary. High sediment supply driven by seasonal discharge patterns, enables the formation of new, large, fragile flocs. Following periods of low discharge without sufficient new sediment supply to build new flocs, the fluffy flocs are reworked, broken up and re-flocculated, eventually re-packaged into more compact aggregates. Similar grain size distributions of suspended particles and fine bottom-sediments along channel margins and outside the estuary mouth suggest that the observed changes in particle populations are controlled by changes in cohesive particle packaging rather than changes in supply material.

The water and sediment discharge forcings outlined in this study suggest that seasonality must be viewed on inter-annual timescales in order to correctly capture the suspended-sediment transport and deposition patterns within the estuary. For systems like the Connecticut River watershed which historically experiences a fairly even distribution of precipitation throughout the year, the confirmation that multiple years affect fine-sediment transport patterns could be important in the future, as the frequency and magnitude of large storm events could change with a warming climate.

7. REFERENCES

Agrawal, Y. C., and Mikkelsen O. A., 2009, Shaped focal plane detectors for particle concentration and mean size observations, Optics Express, v. 17, n. 25, p. 23066-23077.

Agrawal, Y. C., and Pottsmith, H. C., 2000, Instruments for particle size and settling velocity observations in sediment transport, Marine Geology, v. 168, p. 89-114.

Blake, A.C., Kineke, G.C., Milligan, T.G. and Alexander, C.R., 2001, Sediment trapping and transport in the ACE Basin, South Carolina, Estuaries, v. 24, p. 721-733.

Burban, P. Y., Lick, W., and Lick, J., 1989, The flocculation of fine-grained sediments in estuarine waters, Journal of Geophysical Research, v. 94, p. 8323-8330.

Curran, K. J., Hill, P. S., Milligan, T. G., Mikkelsen, O. A., Law, B. A., Durrieu de Madron, X., and Bourrin, F., 2007, Settling velocity, effective density, and mass composition of suspended sediment in a coastal bottom boundary layer, Gulf of Lions, France, Continental Shelf Research, v. 27, p. 1408-1421.

Davies, E. J., Nimmo-Smith, A. M., Agrawal, Y. C., and Souza, A. J., 2012, LISST-100 response to large particles, Marine Geology, v. 307-310, p. 117-122.

Dyer, K. R., 1997, Estuaries: A Physical Introduction, 2nd ed., West Sussex, England, John Wiley & Sons, pp. 140.

Dyer, K. R., 1995, Sediment transport processes in estuaries, *in* Perillo, G. M. E., ed., Geomorphology and Sedimentology of Estuaries, Amsterdam, Netherlands, Elsevier Science, Developments in Sedimentology 53, p. 423-447.

Dyer, K. R., 1989, Sediment processes in estuaries: future research questions, Journal of Geophysical Research, v. 94, n. 10, p. 14327-14339.

Eisma, D., 1986, Flocculation and de-flocculation of suspended matter in estuaries, Netherlands Journal of Sea Research, v. 20, p. 183-199.

Fettweis, M., and Baeye, M., 2015, Seasonal variation in concentration, size, and settling velocity of muddy marine flocs in the benthic boundary layer, Journal of Geophysical Research: Oceans, v. 120, p. 5648-5667.

Filippa, L., Trento, A., and Alvarez, A. M., 2012, Sauter mean diameter determination for the fine fraction of suspended sediments using a LISST-25X diffractometer, Measurement, v. 45, p. 364-368.

Fox, J. M., 2003, Flocculation on the Po River Delta, Master's thesis, Dalhousie University.

Fugate, D. C., and Friedrichs, C.T., 2003, Controls on suspended aggregate size in partially mixed estuaries, Estuarine, Coastal and Shelf Science, v. 58, p. 389-404.

Fugate, D. C., and Friedrichs, C. T., 2002, Determining concentration and fall velocity of estuarine particle populations using ADV, OBS and LISST, Continental Shelf Research, v. 22, p. 1867-1886.

Garvine, R. W., 1974, Physical features of the Connecticut River outflow during high discharge, Journal of Geophysical Research, v. 79, p. 831-846.

Garvine, 1975, Distribution of salinity and temperature in the Connecticut River estuary, Journal of Geophysical Research, v. 80, n. 9, p. 1176-1183.

Geyer, W. R., Lavery, A. C., Scully, M. E., and Trowbridge, J. H., 2010, Mixing by shear instability at high Reynolds number, Geophysical Research Letters, v. 37, p.1-5.

Geyer, W. R., 1993, The importance of suppression of turbulence by stratification on the estuarine turbidity maximum, Estuaries, v. 16, p. 113-125.

Geyer, W. R. and Farmer. D.M., 1989, Tide-induced variation of the dynamics of a salt wedge estuary, Journal of Physical Oceanography, v. 19, p. 1060-1072.

Harris, C. K., and Wiberg, P., 2002, Across-shelf sediment transport: interactions between suspended sediment and bed sediment, Journal of Geophysical Research, v. 107, p. 805-819.

Hill, P. S., Fox, J. M., Crockett, J. S., Curran, K. J., Friedrichs, C. T., Geyer, W. R., Milligan, T. G., Ogston, A. S., Puig, P., Scully, M. E., Traykovski, P. A., and Wheatcroft, R. A., 2009, Sediment delivery to the seabed on continental margins,

Hill, P. S., Milligan, T. G., and Geyer, W. R., 2000, Controls of effective settling velocity of suspended sediment in the Eel River flood plume, Continental Shelf Research, v. 20, p. 2095-2111.

Horne, G. S. and Patton, P. C., 1989, Bedload-sediment transport through the Connecticut River estuary, Geological Society of America Bulletin, v. 101, p. 805-819.

Hurley, A., Hill, P. S., Milligan, T. G., and Law, B. A., 2016, Optical methods for estimating apparent density of sediment in suspension, Methods in Oceanography, v. 17, p. 153-168.

Kim, S. C., Friedrichs, C. T., Maa, J. P. Y. and L. D. Wright. 2000. Estimating bottom stress in tidal boundary layer from acoustic doppler velocimeter data, Journal of Hydraulic Engineering, v. 126, n. 6, p. 399-406.

Kineke, G. C. and Geyer, W.R., 1997, Time variation of suspended sediments in the Lower Hudson River estuary, unpublished manuscript.

Kranck, K., 1973, Flocculation of suspended sediment in the sea, Nature, v. 246, p. 348-350.

Kranck, K., 1980, Experiments on the significance of flocculation in the settling of fine-grained sediment in still water, Canadian Journal of Earth Science, v. 17, p. 1517-1526.

Kranck, K., and Milligan, T. G., 1992, Characteristics of suspended particles at an 11-hour anchor station in San Francisco Bay, California, Journal of Geophysical Research, v. 97, p. 11373-11382.

Manning, A., J., and Bass, S. J., 2006, Variability in cohesive sediment settling fluxes: observations under different estuarine tidal conditions, Marine Geology, v. 235, p. 177-192.

Manning, A. J., and Schoellhamer, D. H., 2013, Factors controlling floc settling velocity along a longitudinal estuarine transect, Marine Geology, v. 345, p. 266-280.

Markussen, T. N., and Andersen, T. J., 2013, A simple method for calculating in situ floc settling velocities based on effective density functions, Marine Geology, v. 344, p. 10-18.

McCave, I. N., 2005, Deposition from suspension, *in* Selley, Cocks and Malone eds., Encyclopedia of Geology, Elsevier, Oxford, p. 8-17.

Meade, R. H., 1966, Salinity variations in the Connecticut River, Water Resources Research, v. 2, n. 3, p. 567-579.

Mehta, A. J., 1989, On estuarine cohesive sediment suspension behavior, Journal of Geophysical Research, v. 94, p. 14303-14314.

Mikkelsen, O. A., Milligan, T. G., Hill, P. S., Chant, R. J., Jago, C. F., Jones, S. E., Kristov, V., and Mitchelson-Jacob, G., 2008, The influence of schlieren on in situ optical measurements used for particle characterization, Limnology and Oceanography: Methods, v. 6, p. 133-143.

Mikkelsen, O. A., Hill, P. S., and Milligan, T. G., 2006, Single-grain, microfloc and macrofloc volume variations observed with a LISST-100 and a digital floc camera, Journal of Sea Research, v. 55, n. 2, p. 87-102.

Mikkelsen, O. A., Hill, P. S., Milligan, T. G., and Chant, R. J., 2005, In situ particle size distributions and volume concentrations from a LISST-100 laser particle sizer and a digital floc camera, Continental Shelf Research, v. 25, p. 1959-1978.

Milligan, T. G., Hill, P. S., and Law, B. A., 2007, Flocculation and the loss of sediment from the Po River plume, Continental Shelf Research, v. 27, p. 309-321.

Milligan, T. G., Kineke, G. C., Blake, A. C., Alexander, C. R. and Hill, P.S., 2001, Flocculation and sedimentation in the ACE Basin, South Carolina, Estuaries, v. 24, p. 734-744.

Milligan, T. G., and Loring, D H., 1997, The effect of flocculation on the size distributions of bottom sediment in coastal inlets: implications for contaminant transport, Water, Air and Soil Pollution, v. 99, p. 33-42.

Open University, 1999, Waves, Tides and Shallow-Water Processes, Elsevier Science, 227 pp.

Patton, P. C., and Horne, G. S., 1992, Response of the Connecticut River estuary to late Holocene sea level rise, Geomorphology, v. 5, p. 391-417.

Ralston, D. K., Cowles, G. W., Geyer, W. R., and Holleman, R. C., 2017, Turbulent and numerical mixing in a salt wedge estuary: Dependence on grid resolution, bottom roughness, and turbulence closure, Journal of Geophysical Research: Oceans, v. 122, n.1, p. 692-712.

Ralston, D. K., Geyer, W. R., and Warner, J. C., 2012, Bathymetric controls on sediment transport in the Hudson River estuary: lateral asymmetry and frontal trapping, Journal of Geophysical Research: Oceans, v. 117, n. C10013.

Safak, I., Allison, M. A., and Sheremet, A., 2013, Floc variability under changing turbulent stresses and sediment availability on a wave energetic muddy shelf, Continental Shelf Research, v. 53, p. 1-10.

Schneider, C. A., Rasband, W. S., and Eliceiri, K. W., 2012, NIH Image to ImageJ: 25 years of image analysis, Nature Methods, v. 9, p. 671-675.

Sheldon, R.W., 1972, Size separation of marine seston by membrane and glass-fiber filters, Limnology and Oceanography, v. 17, p. 464-498.

Smith, S. J., and Friedrichs, C. T., 2015, Image processing methods for in situ estimation of cohesive sediment floc size, settling velocity, and density, Limnology and Oceanography: Methods, v. 13, p. 250-264.

Sternberg, R. W., Kineke, G. C., and Johnson, R., 1991, An instrument system for profiling suspended sediment, fluid, and flow conditions in shallow marine environments, Continental Shelf Research, v. 11, n. 2, p. 109-122.

Sternberg, R. W., 1972, Predicting initial motion and bedload transport of sediment particles in the shallow marine environment, *in* Swift, Duane, and Pilkey, eds., Shelf Sediment Transport, Stroudsburg, PA, p. 61-82.

Traykovski, P., Geyer, W. R., and Sommerfield, C., 2004, Rapid sediment deposition and fine-scale strata formation in the Hudson estuary, Journal of Geophysical Research, v. 109, F02004.

Uncles, R. J., Stephens, J. A., and Law, D. J., 2006, Turbidity maximum in the microtidal, highly turbid Humber Estuary, UK: flocs, fluid mud, stationary suspensions and tidal bores, Estuarine, Coastal and Shelf Science, v. 67, p. 30-52.

U.S. Geological Survey, 2000, East-Coast Sediment Analysis: Procedures, Database, and Georeferenced Displays. Poppe, L. J., and Polloni, C. F., eds. U.S. Geological Survey Open-File Report 00-358.

Valentine, K., Kineke, G. C., Ralston, D. K., Sherwood, C. R., and Geyer, W. R., 2017, Response of sediment grain size and bedforms to changing flow conditions in a shallow, energetic estuary, *submitted to* Journal of Geophysical Research.

Valentine, K., 2015, Characterization of the Bed, Critical Boundary Shear Stress, Roughness, and Bedload Transport in the Connecticut River Estuary, Master's thesis, Boston College.

Van Leussen, W., 1998, The variability of settling velocities of suspended fine-grained sediment in the Ems estuary, Journal of Sea Research, v. 41, p. 109-118.

Van Leussen, W., 1988, Aggregation of particles, settling velocity of mud flocs; a review, *in* Dronkers and van Leussen, eds., Physical Processes in Estuaries, Springer-Verlag, Berlin, p. 347-403.

Winterwerp, J. C., 2002, On the flocculation and settling velocity of estuarine mud, Continental Shelf Research, v. 22, p. 1339-1360.

Winterwerp, J. C., 1998, A simple model for turbulence induced flocculation of cohesive sediment, Journal of Hydraulic Research, v. 36, p. 309-326.

Winterwerp, J. C., and van Kesteren, W. G. M., 2004, Physics of Cohesive Sediment in the Marine Environment, Amsterdam, Netherlands, Elsevier Science, Developments in Sedimentology 56, pp. 576.

Woodruff, J. D., Geyer, W. R., Sommerfield, C. K., and Driscoll, N. W., 2001, Seasonal variation of sediment deposition in the Hudson River estuary, Marine Geology, v. 179, p. 105-119.

Woodruff, J. D., Martini, A. P., Elzidani, E. Z. H., Naughton, T. J., Kekacs, D. J. and MacDonald, D.G., 2013, Off-river waterbodies on tidal rivers: human impact on rates of infilling and the accumulation of pollutants, Geomorphology, v. 184, p. 38-50.

Wright, J., Colling, A. and Park, D., 1989, Waves, tides and shallow-water processes, Oxford, Butterworth Heinemann, p. 149-176.

Xia, X. M., Li, Y., Yang, H., Wu, C. Y., Sing, T. H., and Pong, H. K., 2004, Observations on the size and settling velocity distributions of suspended sediment in the Pearl River Estuary, China, Continental Shelf Research, v. 24, p. 1809-1826.

Yang, Y., Wang, Y. P., Li, C., Gao, S., Shi, B., Zhou, L., Wang, D., Li, G., and Dai, C., 2016, On the variability of near-bed floc size due to complex interactions between turbulence, SSC, settling velocity, effective density and the fractal dimension of flocs, Geo-Marine Letters, v. 36, p. 135-149.

Yellen, B., Woodruff, J. D., Ralston, D. K., MacDonald, D. G., and Jones, D. S., 2017, Salt wedge dynamics lead to enhanced sediment trapping within side embayments in high-energy estuaries, Journal of Geophysical Research: Oceans, v. 122, no. 3, p. 2226-2242.

Yellen, B., Woodruff, J. D., Kratz, L. N., Mabee, S. B., Morrison, J., and Martini, A. M., 2014, Source, conveyance and fate of suspended sediments following Hurricane Irene. New England, USA, Geomorphology, v. 226, p. 124-134.

Appendix I. Locations of anchor stations

Year	Month	Day	FZ	Lat Deg	Lat Min	Lon Deg	Lon Min	Casts
2013	11	5	4	41	20.355	72	21.648	26
2013	11	6	2	41	17.022	72	20.907	7
2013	11	6	4	41	20.048	72	21.503	15
2013	11	7	1.5	41	16.464	72	20.462	9
2013	11	7	3	41	18.596	72	20.959	5
2013	11	7	4.3	41	20.294	72	21.468	4
2013	11	7	4.35	41	20.563	72	22.199	3
2013	11	7	3.5	41	19.406	72	20.806	3
2013	11	8	4	41	20.345	72	21.614	9
2013	11	8	3	41	18.572	72	20.968	10
2014	5	14	3	41	18.915	72	20.837	18
2014	5	15	2	41	17.111	72	20.93	25
2014	5	17	2.3	41	17.523	72	20.918	16
2014	5	17	3.3	41	18.57	72	20.984	4
2015	9	28	4	41	20.334	72	21.682	26
2015	9	29	3	41	18.075	72	21.213	25
2015	10	1	2	41	17.273	72	20.967	26

Appendix II. Drag coefficient error analysis

Valentine (2015) calculated a drag coefficient (C_D) at 1 mab at each anchor station during the HSMD and HSHD surveys using three methods: a Reynolds stress, Turbulent Kinetic Energy (TKE), and the 'ID method'. The C_D estimates ranged from 10^{-5} to 10^{-2}, though no significant difference in resulting bed-stress calculations were determined (see Valentine (2015), Fig. 43).

An independent check was conducted by using the Law of the Wall (Eq. 10) to back calculate a stress at the theoretical 1 mab and compare to the estimate of stress at 0.75 mab using the generic 3.1 x 10^{-3} value for C_D. The results are shown in Figures AII.1 and AII.2 below. ADV data from Frontal Zone 4 on September 28, 2015 was used to test the accuracy of using the generic C_D. First, an roughness length, z_0 was estimated by rearranging Eq. 10. Then, a new estimate of shear velocity (u_*) was made using the roughness length estimate. Using the Quadratic Stress Law (Eq. 9), a new estimate of C_D was made using the previously observed bed stress and this new estimate of shear velocity. It appears that using the value of 3.1 x 10^{-3} for C_D slightly underestimates bed stress. However, the error on this check was not significant.

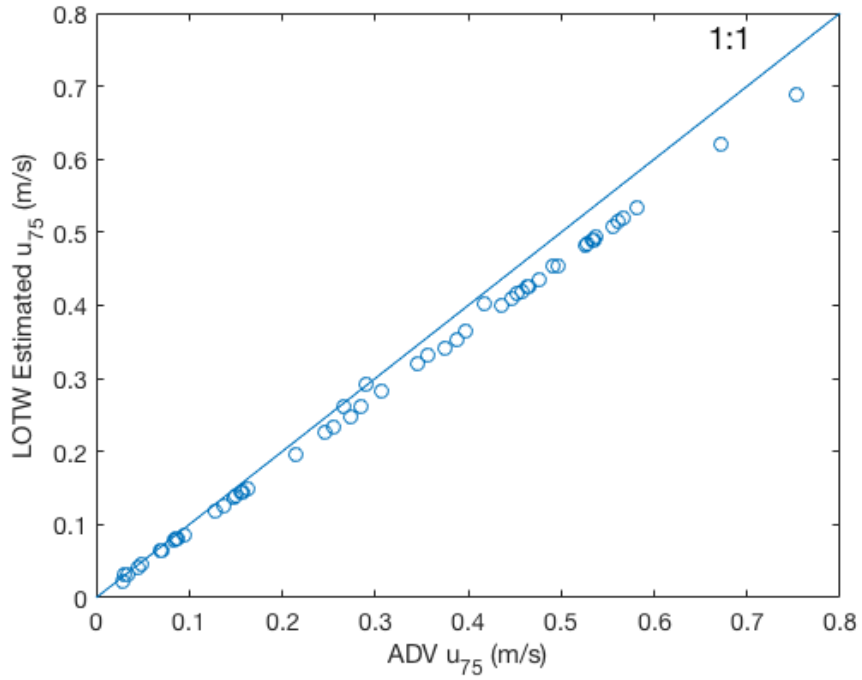

Figure AII.1. Estimated u_{75} based on a Law of the Wall calculation of a C_{75} using observed near-bed velocity from the ADV. The line shows a 1:1 relationship.

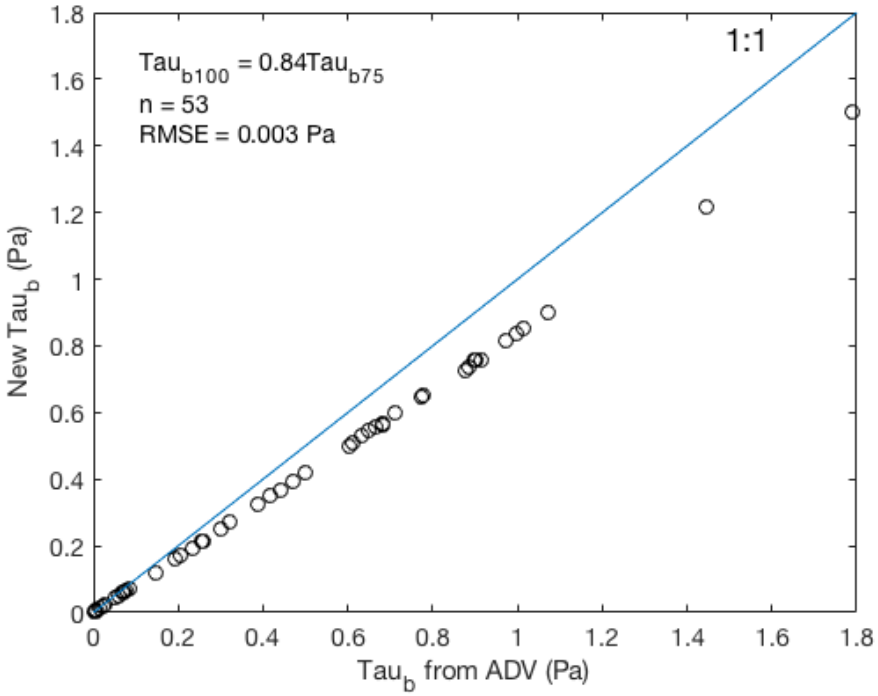

Figure AII.2. Estimated bed stress using an estimated roughness length.

Appendix III. Full near-bed volumetric size distributions from merged LISST-DFC data

Size classes ranging from 3-72 μm

Datenum	3.11	3.67	4.33	5.11	6.03	7.11	8.39	9.9	11.69	13.79	16.27	19.2	22.66	26.74	31.56	37.24	43.95	51.86	61.2	72.22
735543.3806	0.11	0.32	0.74	1.22	1.53	1.62	1.58	1.85	2.32	2.64	2.6	2.7	3.77	4.64	6.53	7.45	8.86	9.9	10.89	12.18
735543.3965	0.11	0.29	0.61	0.92	1.12	1.18	1.15	1.33	1.61	1.78	1.74	1.79	2.43	2.95	4.08	4.66	5.58	6.29	8.08	10.39
735543.4937	NaN	NaN	NaN	NaN	NaN	NaN	NaN	NaN	NaN	NaN	NaN	NaN	NaN	NaN	NaN	NaN	NaN	NaN	NaN	NaN
735543.5149	0.24	0.52	0.88	1.17	1.33	1.36	1.34	1.51	1.79	2.01	2.04	2.14	2.73	3.29	4.32	5.03	5.97	6.94	8.29	9.92
735543.5278	0.23	0.55	1	1.41	1.64	1.68	1.64	1.85	2.24	2.54	2.59	2.75	3.65	4.47	6.04	7.14	8.63	10.09	11.01	12.07
735543.5417	0.22	0.43	0.68	0.87	0.97	0.99	0.98	1.1	1.31	1.47	1.49	1.55	1.92	2.21	2.74	3.03	3.42	3.77	5.45	7.87
735543.5558	0.27	0.54	0.84	1.06	1.19	1.23	1.25	1.44	1.73	1.95	1.99	2.08	2.58	3	3.77	4.26	4.87	5.44	7.34	9.92
735543.5674	0.25	0.5	0.78	0.97	1.08	1.11	1.12	1.28	1.54	1.74	1.76	1.83	2.24	2.58	3.19	3.53	3.98	4.41	6.02	8.23
735543.5784	0.28	0.6	1	1.33	1.52	1.57	1.57	1.8	2.21	2.54	2.62	2.78	3.64	4.4	5.83	6.71	7.86	8.84	9.14	9.88
735543.5943	0.2	0.38	0.62	0.89	1.04	1.06	1.01	1.12	1.31	1.42	1.38	1.39	1.75	2.05	2.73	3.05	3.68	4.36	5.74	7.64
735543.606	0.12	0.3	0.64	1.05	1.23	1.25	1.14	1.27	1.5	1.6	1.47	1.45	1.98	2.38	3.41	3.8	4.7	5.53	7.08	9.07
735543.6183	0.21	0.44	0.74	0.97	1.11	1.14	1.12	1.24	1.45	1.59	1.58	1.62	2.02	2.35	3.02	3.47	4.16	4.87	5.88	7.32
735543.631	0.23	0.43	0.64	0.78	0.88	0.91	0.93	1.04	1.21	1.33	1.34	1.37	1.61	1.8	2.15	2.37	2.67	2.93	4.37	6.5
735543.6438	0.17	0.36	0.62	0.85	0.97	1	0.96	1.06	1.21	1.29	1.25	1.26	1.58	1.85	2.44	2.79	3.43	4.08	5.4	7.23
735543.6559	NaN	NaN	NaN	NaN	NaN	NaN	NaN	NaN	NaN	NaN	NaN	NaN	NaN	NaN	NaN	NaN	NaN	NaN	NaN	NaN
735544.3454	0.2	0.52	1.03	1.5	1.77	1.81	1.75	2.01	2.45	2.77	2.8	2.99	4.15	5.26	7.45	8.92	11	12.99	13.9	14.88
735544.3595	0.21	0.54	1.06	1.55	1.85	1.92	1.89	2.18	2.67	3.07	3.17	3.44	4.76	6.06	8.57	10.41	12.89	15.33	15.52	15.71
735544.3711	0.19	0.49	0.94	1.34	1.58	1.63	1.62	1.89	2.34	2.73	2.86	3.15	4.41	5.67	8.03	9.72	11.87	13.67	14.05	14.44
735544.3826	0.21	0.52	0.96	1.35	1.58	1.62	1.6	1.87	2.32	2.72	2.87	3.16	4.38	5.59	7.81	9.41	11.4	13.03	13.87	14.78
735544.3954	0.2	0.49	0.91	1.28	1.49	1.53	1.51	1.75	2.17	2.54	2.68	2.95	4.1	5.24	7.33	8.84	10.77	12.42	13.7	15.12
735544.4077	0.24	0.6	1.11	1.58	1.9	1.98	2	2.33	2.9	3.41	3.65	4.04	5.56	7.11	9.89	12.13	14.85	17.36	18.15	19.03
735544.4195	0.21	0.52	0.98	1.39	1.66	1.72	1.72	2.01	2.52	2.96	3.13	3.45	4.82	6.19	8.69	10.48	12.72	14.58	15.34	16.15
735544.4549	0.18	0.47	0.92	1.35	1.61	1.68	1.65	1.95	2.34	2.61	2.61	2.76	3.9	4.96	7.02	8.18	9.85	11.4	12.93	14.66
735544.4674	0.14	0.4	0.88	1.35	1.63	1.67	1.59	1.78	2.09	2.28	2.23	2.31	3.18	3.98	5.61	6.65	8.32	10.13	10.42	10.8
735544.479	NaN	NaN	NaN	NaN	NaN	NaN	NaN	NaN	NaN	NaN	NaN	NaN	NaN	NaN	NaN	NaN	NaN	NaN	NaN	NaN
735544.4922	NaN	NaN	NaN	NaN	NaN	NaN	NaN	NaN	NaN	NaN	NaN	NaN	NaN	NaN	NaN	NaN	NaN	NaN	NaN	NaN
735544.5047	0.3	0.73	1.38	1.97	2.32	2.4	2.38	2.76	3.41	3.88	3.9	4.08	5.36	6.42	8.53	9.77	11.64	13.41	14.04	14.69
735544.5178	0.23	0.53	0.95	1.29	1.48	1.53	1.53	1.79	2.22	2.56	2.63	2.8	3.7	4.45	5.83	6.55	7.49	8.15	9.65	11.43
735544.5307	0.25	0.62	1.16	1.64	1.92	1.99	1.98	2.32	2.89	3.35	3.43	3.65	4.9	5.98	8.07	9.34	11.06	12.52	13.94	15.54
735544.5542	0.23	0.54	0.97	1.33	1.53	1.59	1.58	1.87	2.3	2.61	2.6	2.71	3.63	4.39	5.89	6.66	7.84	8.91	10.64	12.73
735544.5657	0.3	0.65	1.07	1.38	1.6	1.68	1.72	2.06	2.53	2.89	2.93	3.06	4	4.75	6.19	6.96	7.94	8.73	10.19	11.93
735544.5793	0.26	0.53	0.82	1.03	1.17	1.22	1.25	1.49	1.83	2.12	2.2	2.34	3.01	3.58	4.56	5.14	5.79	6.29	7.49	9.2
735544.5908	0.19	0.4	0.65	0.84	0.95	0.98	0.97	1.14	1.37	1.53	1.51	1.54	1.94	2.21	2.72	2.91	3.22	3.48	5.09	7.45
735544.6025	0.18	0.37	0.63	0.85	0.96	0.99	0.95	1.1	1.31	1.42	1.37	1.38	1.81	2.17	2.97	3.19	3.24	3.04	4.56	6.9
735544.6144	0.15	0.34	0.65	1.01	1.22	1.26	1.2	1.37	1.65	1.82	1.76	1.82	2.46	3.01	4.19	4.79	5.8	6.77	7.42	8.46
735544.6266	0.22	0.43	0.68	0.86	0.94	0.97	0.97	1.13	1.37	1.54	1.54	1.59	1.98	2.26	2.79	2.99	3.34	3.64	5.12	7.22
735544.6356	0.17	0.37	0.65	0.87	0.94	0.95	0.92	1.04	1.23	1.35	1.31	1.33	1.69	1.96	2.51	2.71	3.13	3.52	4.91	6.85
735544.6444	0.01	0.05	0.19	0.46	1	1.4	0.76	0.81	0.98	0.75	0.37	0.28	0.52	0.73	2.48	2.37	4.13	5.54	5.46	5.52
735544.6522	0.06	0.13	0.32	0.69	0.9	0.85	0.61	0.63	0.67	0.57	0.4	0.35	0.43	0.48	0.68	0.74	1.07	1.64	2.48	3.77
735544.6575	0.13	0.27	0.51	0.73	0.81	0.81	0.74	0.81	0.91	0.94	0.87	0.84	1.04	1.18	1.52	1.65	1.97	2.33	3.32	4.75
735544.6799	0.14	0.32	0.63	0.91	1.02	1.03	0.97	1.09	1.31	1.45	1.44	1.5	2.03	2.48	3.41	3.87	4.65	5.3	6.56	8.3
735544.6902	0.06	0.13	0.32	0.61	0.84	0.95	0.8	0.85	0.95	0.92	0.73	0.66	1	1.29	2.3	2.65	3.79	4.96	5.51	6.42
735544.6948	0.04	0.15	0.49	0.92	1.08	1.09	0.97	1.11	1.35	1.45	1.29	1.25	1.82	2.2	3.22	3.39	4.04	4.53	5.83	7.49
735545.4331	0.27	0.67	1.18	1.6	1.89	1.97	1.97	2.3	2.81	3.23	3.39	3.69	5.09	6.46	4.84	3.63	2.72	4.61	7.94	10.86
735545.4632	0.3	0.67	1.1	1.42	1.67	1.75	1.78	2.08	2.5	2.87	3.01	3.28	4.4	5.51	4.22	3.24	2.5	4.38	7.29	10.28
735545.4742	0.33	0.78	1.39	1.89	2.19	2.26	2.23	2.59	3.17	3.61	3.67	3.92	5.28	6.55	4.55	3.17	2.21	3.66	5.5	6.98
735545.4866	0.28	0.62	0.99	1.26	1.45	1.51	1.52	1.77	2.16	2.48	2.62	2.86	3.79	4.71	3.89	3.22	2.66	4.76	8	11.53
735545.4998	NaN	NaN	NaN	NaN	NaN	NaN	NaN	NaN	NaN	NaN	NaN	NaN	NaN	NaN	NaN	NaN	NaN	NaN	NaN	NaN
735545.5115	0.22	0.5	0.84	1.08	1.22	1.25	1.23	1.42	1.7	1.9	1.93	2.06	2.77	3.45	3.07	2.74	2.45	4.32	7.13	10.41
735545.5377	0.23	0.55	0.97	1.29	1.49	1.53	1.51	1.75	2.11	2.38	2.42	2.58	3.51	4.38	3.7	3.13	2.65	4.83	7.91	10.89
735545.5508	0.23	0.53	0.92	1.22	1.39	1.41	1.38	1.57	1.87	2.08	2.09	2.21	2.94	3.62	3.17	2.78	2.43	4.16	6.88	9.27
735545.5625	0.24	0.52	0.87	1.14	1.3	1.33	1.3	1.48	1.75	1.94	1.95	2.06	2.68	3.26	2.97	2.72	2.49	4.34	6.99	9.27
735545.5742	0.23	0.49	0.77	0.96	1.07	1.08	1.05	1.18	1.39	1.53	1.55	1.62	2.08	2.49	2.41	2.34	2.27	3.94	6.23	8.49
735545.5826	0.21	0.46	0.76	0.95	1.06	1.07	1.03	1.16	1.34	1.46	1.46	1.53	1.98	2.4	2.33	2.25	2.19	3.63	5.89	7.6
735545.5951	0.22	0.46	0.72	0.9	0.99	0.99	0.96	1.07	1.23	1.34	1.32	1.36	1.71	2.02	2.02	2.02	2.02	3.47	5.34	6.93
735545.6083	0.18	0.4	0.69	0.99	1.16	1.17	1.08	1.2	1.37	1.44	1.36	1.36	1.74	2.05	2.06	2.09	2.16	3.7	5.5	7.03
735545.6538	0.24	0.47	0.7	0.85	0.93	0.94	0.92	1.03	1.2	1.33	1.36	1.42	1.73	2	2.13	2.27	2.41	4.07	6.02	7.52
735545.6646	0.23	0.43	0.62	0.75	0.81	0.82	0.81	0.89	1.03	1.14	1.16	1.21	1.46	1.67	1.89	2.15	2.44	4.1	6.43	8.16

735545.6754	0.18	0.36	0.62	0.83	0.91	0.9	0.84	0.93	1.08	1.16	1.13	1.15	1.44	1.68	1.86	2.08	2.33	4.03	6.61	8.23
735546.3137	0.17	0.38	0.7	0.95	1.08	1.1	1.06	1.18	1.39	1.51	1.44	1.44	1.84	2.09	2.71	2.95	3.49	4	5.77	8.32
735546.3249	0	0.02	0.17	0.61	0.95	1.03	0.79	0.77	0.78	0.66	0.44	0.36	0.58	0.8	1.6	2.04	3.36	4.99	6.73	9.09
735546.3355	0	0	0.06	0.36	0.77	0.98	0.76	0.73	0.72	0.57	0.35	0.27	0.48	0.69	1.58	2.07	3.67	5.77	6.88	8.2
735546.346	0.11	0.24	0.41	0.55	0.6	0.61	0.58	0.65	0.73	0.77	0.73	0.72	0.92	1.06	1.4	1.55	1.88	2.18	3.61	5.99
735546.3566	0.09	0.2	0.4	0.56	0.62	0.62	0.58	0.63	0.71	0.74	0.67	0.65	0.84	0.97	1.3	1.43	1.77	2.1	3.46	5.7
735546.3681	0.05	0.13	0.34	0.64	0.78	0.79	0.68	0.72	0.79	0.77	0.63	0.57	0.78	0.92	1.38	1.55	2.08	2.66	4.03	6.16
735546.3792	0.03	0.11	0.33	0.65	0.83	0.86	0.74	0.8	0.89	0.86	0.7	0.62	0.85	0.99	1.46	1.59	2.08	2.61	3.74	5.38
735546.3906	0.11	0.26	0.47	0.64	0.71	0.73	0.71	0.8	0.93	0.99	0.93	0.91	1.15	1.31	1.7	1.83	2.12	2.38	3.56	5.37
735546.4119	0.31	0.64	1.09	1.53	1.83	2.01	2.11	2.4	2.75	3.04	3.12	3.26	4.17	4.88	6.25	6.98	7.76	8.28	9.92	11.91
735546.4236	NaN	NaN	NaN	NaN	NaN	NaN	NaN	NaN	NaN	NaN	NaN	NaN	NaN	NaN	NaN	NaN	NaN	NaN	NaN	NaN
735546.4384	NaN	NaN	NaN	NaN	NaN	NaN	NaN	NaN	NaN	NaN	NaN	NaN	NaN	NaN	NaN	NaN	NaN	NaN	NaN	NaN
735546.4505	NaN	NaN	NaN	NaN	NaN	NaN	NaN	NaN	NaN	NaN	NaN	NaN	NaN	NaN	NaN	NaN	NaN	NaN	NaN	NaN
735546.4628	NaN	NaN	NaN	NaN	NaN	NaN	NaN	NaN	NaN	NaN	NaN	NaN	NaN	NaN	NaN	NaN	NaN	NaN	NaN	NaN
735546.475	NaN	NaN	NaN	NaN	NaN	NaN	NaN	NaN	NaN	NaN	NaN	NaN	NaN	NaN	NaN	NaN	NaN	NaN	NaN	NaN
735546.4874	0.16	0.4	0.84	1.31	1.62	1.79	1.84	2.14	2.55	2.95	3.13	3.44	4.92	6.2	8.66	9.86	11.23	11.84	14.3	17.32
735546.4995	0.11	0.3	0.66	1.07	1.32	1.46	1.48	1.71	2.04	2.33	2.42	2.62	3.78	4.79	6.84	7.81	9.04	9.72	12.13	15.15
735546.5129	0.1	0.26	0.57	0.92	1.12	1.23	1.25	1.43	1.68	1.89	1.94	2.07	2.95	3.68	5.19	5.85	6.73	7.22	9.64	12.88
735546.5261	0.12	0.28	0.57	0.86	1.02	1.12	1.15	1.33	1.58	1.79	1.85	1.99	2.81	3.49	4.88	5.44	6.18	6.56	8.94	12.23
735546.5375	0.11	0.24	0.42	0.59	0.69	0.75	0.78	0.89	1.03	1.16	1.2	1.27	1.72	2.07	2.75	3.07	3.41	3.57	5.96	9.97
735734.3542	0.1	0.2	0.35	0.47	0.54	0.58	0.59	0.67	0.77	0.85	0.87	0.92	1.22	1.46	1.93	2.14	2.4	2.52	4.33	7.45
735734.3694	0.1	0.19	0.31	0.42	0.47	0.51	0.52	0.59	0.67	0.74	0.75	0.78	1.03	1.22	1.62	1.79	2.03	2.18	3.9	7.02
735734.3843	0.1	0.19	0.32	0.43	0.49	0.53	0.55	0.62	0.72	0.8	0.82	0.86	1.14	1.36	1.79	1.99	2.23	2.36	3.94	6.62
735734.3989	0.1	0.19	0.31	0.42	0.48	0.51	0.52	0.59	0.67	0.74	0.76	0.79	1.04	1.22	1.59	1.76	2	2.14	3.73	6.51
735734.4147	0.12	0.21	0.32	0.41	0.46	0.49	0.51	0.57	0.66	0.73	0.75	0.79	1.02	1.2	1.54	1.68	1.86	1.96	3.48	6.22
735734.4297	0.12	0.24	0.37	0.49	0.56	0.6	0.64	0.73	0.85	0.97	1.03	1.11	1.48	1.77	2.31	2.58	2.81	2.89	4.75	8.06
735734.4449	0.14	0.3	0.53	0.74	0.88	0.97	1.03	1.2	1.43	1.64	1.75	1.88	2.52	3.02	3.93	4.33	4.72	4.79	6.56	9.41
735734.4597	0.11	0.22	0.41	0.59	0.68	0.74	0.75	0.86	1.01	1.13	1.14	1.2	1.64	1.96	2.61	2.81	3.13	3.3	5.28	8.46
735734.4749	0.02	0.06	0.2	0.5	0.79	0.98	0.89	0.95	1	0.91	0.7	0.61	0.87	1.04	1.67	1.94	2.84	4.1	5.85	8.48
735734.4902	0	0.02	0.13	0.45	0.79	1.02	0.91	0.97	1.01	0.88	0.6	0.47	0.72	0.9	1.65	1.96	3.02	4.33	6.22	8.98
735734.5061	0.04	0.1	0.25	0.5	0.79	1.13	0.92	0.99	1.07	0.93	0.7	0.63	0.91	1.09	1.83	2.07	3.08	4.31	6.05	8.56
735734.5214	0.07	0.13	0.28	0.54	0.7	0.77	0.7	0.74	0.79	0.77	0.65	0.62	0.85	1.02	1.52	1.72	2.28	2.92	4.58	7.25
735734.5372	0.08	0.17	0.34	0.54	0.64	0.68	0.64	0.7	0.76	0.76	0.68	0.66	0.89	1.05	1.51	1.68	2.07	2.45	3.85	6.1
735734.5529	0.11	0.26	0.52	0.78	0.91	0.98	0.99	1.12	1.3	1.45	1.47	1.53	2.06	2.44	3.24	3.51	3.89	4.11	6.25	9.51
735734.5692	0.06	0.22	0.33	0.48	0.73	0.78	0.89	0.98	1.06	1.2	1.39	1.5	1.68	1.97	2.22	3.02	3.13	3.16	4.95	7.74
735734.585	0.16	0.3	0.42	0.54	0.63	0.69	0.73	0.83	0.94	1.06	1.12	1.18	1.41	1.56	1.79	1.88	1.85	1.76	2.94	4.95
735734.6015	NaN	NaN	NaN	NaN	NaN	NaN	NaN	NaN	NaN	NaN	NaN	NaN	NaN	NaN	NaN	NaN	NaN	NaN	NaN	NaN
735734.6182	NaN	NaN	NaN	NaN	NaN	NaN	NaN	NaN	NaN	NaN	NaN	NaN	NaN	NaN	NaN	NaN	NaN	NaN	NaN	NaN
735734.6335	NaN	NaN	NaN	NaN	NaN	NaN	NaN	NaN	NaN	NaN	NaN	NaN	NaN	NaN	NaN	NaN	NaN	NaN	NaN	NaN
735734.6492	NaN	NaN	NaN	NaN	NaN	NaN	NaN	NaN	NaN	NaN	NaN	NaN	NaN	NaN	NaN	NaN	NaN	NaN	NaN	NaN
735734.6646	NaN	NaN	NaN	NaN	NaN	NaN	NaN	NaN	NaN	NaN	NaN	NaN	NaN	NaN	NaN	NaN	NaN	NaN	NaN	NaN
735734.68	NaN	NaN	NaN	NaN	NaN	NaN	NaN	NaN	NaN	NaN	NaN	NaN	NaN	NaN	NaN	NaN	NaN	NaN	NaN	NaN
735734.6945	NaN	NaN	NaN	NaN	NaN	NaN	NaN	NaN	NaN	NaN	NaN	NaN	NaN	NaN	NaN	NaN	NaN	NaN	NaN	NaN
735734.7098	0.44	0.85	1.33	1.74	2.01	2.15	2.23	2.49	2.84	3.21	3.44	3.78	5	6.11	8.03	9.31	10.66	11.61	12.75	14.04
735736.3634	0.37	0.69	1.08	1.42	1.62	1.74	1.8	2	2.27	2.52	2.63	2.81	3.63	4.29	5.49	6.14	6.96	7.59	9.54	12.01
735736.3779	0.3	0.55	0.8	1.03	1.18	1.26	1.3	1.43	1.59	1.76	1.85	1.97	2.49	2.9	3.6	4.03	4.5	4.84	7.1	10.43
735736.4358	0.25	0.49	0.81	1.11	1.29	1.34	1.34	1.44	1.56	1.67	1.7	1.78	2.26	2.67	3.44	3.97	4.53	4.96	6.75	9.29
735736.4583	0.27	0.52	0.87	1.24	1.45	1.54	1.49	1.58	1.73	1.82	1.8	1.87	2.5	3.06	4.26	5.02	6.2	7.22	9.01	11.29
735736.4746	0.01	0.05	0.26	0.77	1.15	1.31	1.15	1.23	1.34	1.28	1.01	0.9	1.41	1.78	3.04	3.45	4.63	5.74	7.25	9.16
735736.4906	0.01	0.05	0.25	0.74	1.15	1.35	1.19	1.26	1.36	1.31	1.07	0.99	1.64	2.21	4	4.81	6.74	8.56	9.98	11.72
735736.5058	NaN	NaN	NaN	NaN	NaN	NaN	NaN	NaN	NaN	NaN	NaN	NaN	NaN	NaN	NaN	NaN	NaN	NaN	NaN	NaN
735736.5231	0.78	1.55	1.77	1.89	2.35	2.64	3.08	3.65	4.31	5.15	6.02	6.58	7.37	8.71	10.23	13.36	14.98	15.81	22.95	33.34
735736.5408	0.66	1.28	1.43	1.49	1.81	1.98	2.25	2.59	2.98	3.51	4.11	4.58	5.23	6.35	7.63	10.2	11.65	12.4	19.63	31.13
735736.5564	0.7	1.39	1.58	1.68	2.08	2.36	2.84	3.55	4.48	5.65	6.67	7.06	7.57	8.47	9.45	11.71	12.38	12.45	20.21	32.83
735736.5714	0.65	1.32	1.53	1.64	2.05	2.33	2.78	3.42	4.24	5.36	6.55	7.37	8.5	10.13	11.9	15.21	16.35	16.27	24.97	38.46
735736.5868	NaN	NaN	NaN	NaN	NaN	NaN	NaN	NaN	NaN	NaN	NaN	NaN	NaN	NaN	NaN	NaN	NaN	NaN	NaN	NaN
735736.6139	0.38	0.83	1.02	1.11	1.33	1.44	1.63	1.94	2.34	2.92	3.63	4.31	5.43	6.89	8.58	11.1	12.28	12.54	18.08	26.15
735736.6573	0.3	0.64	0.77	0.8	0.94	0.99	1.08	1.25	1.47	1.79	2.17	2.51	3.06	3.82	4.72	6.18	6.98	7.38	10.62	15.32
735736.6727	0.27	0.59	0.73	0.77	0.87	0.88	0.92	1.01	1.14	1.34	1.6	1.9	2.46	3.3	4.44	6.25	7.79	9.11	13.02	18.64
735736.6869	0.22	0.49	0.6	0.64	0.73	0.72	0.74	0.76	0.8	0.88	1.01	1.12	1.3	1.64	2.1	3.03	3.93	4.92	7.22	10.6
735736.702	0.21	0.46	0.53	0.54	0.61	0.59	0.59	0.59	0.6	0.63	0.68	0.71	0.74	0.85	0.96	1.27	1.47	1.69	2.28	3.09
736235.363	0.21	0.47	0.53	0.53	0.6	0.57	0.56	0.55	0.55	0.57	0.61	0.63	0.65	0.71	0.76	0.95	1.02	1.08	1.41	1.87
736235.3792	0.23	0.51	0.63	0.67	0.79	0.79	0.82	0.86	0.92	1.01	1.1	1.15	1.25	1.38	1.51	1.82	1.93	2.01	2.87	4.13
736235.3955	0.23	0.51	0.59	0.61	0.71	0.69	0.7	0.71	0.73	0.78	0.84	0.86	0.9	0.99	1.09	1.38	1.56	1.74	3.12	6.15

736235.4104	0.26	0.58	0.69	0.71	0.82	0.82	0.83	0.86	0.89	0.93	0.98	0.97	0.98	1.05	1.11	1.37	1.49	1.6	3.08	6.2
736235.4293	0.29	0.61	0.69	0.7	0.8	0.79	0.82	0.85	0.88	0.93	0.99	0.99	0.97	1.02	1.04	1.2	1.22	1.24	2.88	7.76
736235.4442	0.28	0.56	0.62	0.61	0.68	0.68	0.7	0.74	0.78	0.86	0.94	0.95	0.96	1.03	1.1	1.36	1.5	1.67	2.14	2.79
736235.4587	0.1	0.32	0.66	1.03	1.39	1.58	1.69	2.05	2.6	3.18	3.37	3.35	4.03	4.7	6.12	7.71	9.53	11.51	12.04	13.46
736235.4726	0.11	0.3	0.54	0.7	0.8	0.85	0.91	1.16	1.6	2.09	2.17	1.92	1.96	1.96	2.38	2.89	3.68	4.89	6.28	8.05
736235.487	NaN	NaN	NaN	NaN	NaN	NaN	NaN	NaN	NaN	NaN	NaN	NaN	NaN	NaN	NaN	NaN	NaN	NaN	NaN	NaN
736235.502	0.5	0.8	0.84	0.81	0.92	1.04	1.31	1.84	2.76	4.06	5.06	5.13	5.13	5.26	5.8	6.99	7.91	9	12.29	16.78
736235.5198	0.71	1.05	1.08	1.02	1.11	1.26	1.53	2.08	2.99	4.15	4.74	4.3	3.75	3.4	3.46	3.99	4.8	6.37	6.74	7.2
736235.5382	0.85	1.2	1.12	1.02	1.12	1.26	1.54	2.04	2.84	3.94	4.69	4.48	4	3.73	3.75	4.34	5.03	6.34	9.31	13.69
736235.5558	NaN	NaN	NaN	NaN	NaN	NaN	NaN	NaN	NaN	NaN	NaN	NaN	NaN	NaN	NaN	NaN	NaN	NaN	NaN	NaN
736235.5717	0.8	1	0.86	0.72	0.75	0.81	0.97	1.26	1.74	2.41	2.94	2.86	2.49	2.23	2.14	2.42	2.82	3.64	5.86	9.44
736235.5871	0.43	0.9	1.05	1.14	1.41	1.55	1.76	2.01	2.28	2.63	3.01	3.31	3.77	4.46	5.21	6.75	7.67	8.42	12.25	18.27
736235.6035	0.4	0.85	1.02	1.1	1.33	1.44	1.6	1.82	2.07	2.4	2.78	3.1	3.63	4.44	5.43	7.27	8.57	9.64	14.17	21.76
736235.6197	0.38	0.84	1.06	1.17	1.39	1.47	1.59	1.78	1.99	2.29	2.64	2.99	3.67	4.61	5.85	7.87	9.42	10.72	15.12	21.36
736235.6372	0.36	0.94	1.37	1.64	1.99	2.12	2.27	2.57	2.94	3.41	3.91	4.45	5.7	7.31	9.64	13.03	15.92	18.25	24.21	32.18
736235.6526	0.35	0.93	1.34	1.59	1.96	2.09	2.27	2.61	3.03	3.6	4.25	4.94	6.37	8.15	10.47	13.71	15.56	16.19	22.19	30.5
736235.6677	0.32	0.76	0.98	1.08	1.29	1.36	1.47	1.64	1.83	2.1	2.43	2.75	3.32	4.09	4.97	6.42	7.03	7.17	10.45	15.3
736235.6985	0.28	0.67	0.89	1	1.21	1.27	1.37	1.52	1.71	1.96	2.25	2.54	3.11	3.87	4.8	6.29	7.08	7.44	10.82	15.74
736235.7135	0.25	0.6	0.77	0.86	1.03	1.07	1.14	1.26	1.39	1.56	1.76	1.95	2.32	2.84	3.48	4.6	5.26	5.65	7.89	11.05
736235.7288	0.22	0.54	0.7	0.78	0.92	0.95	1.01	1.1	1.2	1.35	1.51	1.66	1.98	2.42	2.97	3.95	4.63	5.18	7.06	9.85
736235.7438	0.19	0.46	0.56	0.61	0.73	0.75	0.79	0.84	0.89	0.97	1.05	1.11	1.24	1.46	1.7	2.23	2.51	2.66	3.73	5.28
736235.7586	0.18	0.43	0.53	0.58	0.7	0.71	0.76	0.82	0.88	0.96	1.04	1.07	1.16	1.32	1.47	1.88	2.02	2.05	2.77	3.9
736236.3624	0.22	0.52	0.66	0.74	0.91	0.97	1.06	1.17	1.29	1.43	1.56	1.62	1.81	2.06	2.34	2.88	3.18	3.33	3.36	3.49
736236.3829	0.31	0.85	1.16	1.39	1.8	1.97	2.23	2.57	2.91	3.32	3.73	3.97	4.55	5.35	6.28	8.12	9.18	9.82	6.3	4.14
736236.3971	0.18	0.45	0.55	0.6	0.72	0.74	0.82	0.92	1.04	1.16	1.23	1.26	1.34	1.49	1.64	2.05	2.06	2	1.97	2.07
736236.4128	0.13	0.33	0.4	0.42	0.48	0.47	0.49	0.53	0.57	0.61	0.62	0.59	0.57	0.59	0.6	0.72	0.75	0.77	1.18	2.1
736236.4278	0.11	0.27	0.37	0.48	0.57	0.53	0.5	0.52	0.54	0.54	0.51	0.49	0.53	0.59	0.7	0.88	1.05	1.22	1.43	1.76
736236.4438	0.17	0.38	0.47	0.51	0.59	0.6	0.63	0.68	0.74	0.82	0.93	1.02	1.18	1.42	1.71	2.27	2.63	2.89	3.73	4.82
736236.458	0.26	0.6	0.76	0.84	1	1.08	1.19	1.38	1.58	1.84	2.09	2.3	2.7	3.17	3.71	4.56	5.02	5.26	8.88	15.37
736236.4737	0.27	0.55	0.63	0.65	0.75	0.78	0.84	0.94	1.06	1.21	1.39	1.55	1.82	2.24	2.73	3.61	4.21	4.61	6.31	8.73
736236.4882	0.3	0.6	0.69	0.72	0.85	0.89	0.97	1.09	1.23	1.44	1.72	2	2.42	3.04	3.79	5.13	6.02	6.63	8.34	10.53
736236.5032	0.44	0.72	0.75	0.73	0.83	0.88	0.97	1.1	1.27	1.51	1.83	2.16	2.67	3.41	4.31	5.74	6.89	7.8	10.04	12.99
736236.5179	NaN	NaN	NaN	NaN	NaN	NaN	NaN	NaN	NaN	NaN	NaN	NaN	NaN	NaN	NaN	NaN	NaN	NaN	NaN	NaN
736236.5324	NaN	NaN	NaN	NaN	NaN	NaN	NaN	NaN	NaN	NaN	NaN	NaN	NaN	NaN	NaN	NaN	NaN	NaN	NaN	NaN
736236.5485	0.42	0.75	0.81	0.81	0.91	0.9	0.87	0.82	0.75	0.71	0.69	0.66	0.66	0.79	1.02	1.62	2.47	3.75	4.31	5.09
736236.5683	0.38	0.73	0.81	0.83	0.98	1.05	1.14	1.24	1.33	1.45	1.61	1.73	1.92	2.33	2.79	3.76	4.34	4.77	6.19	8.36
736236.5829	NaN	NaN	NaN	NaN	NaN	NaN	NaN	NaN	NaN	NaN	NaN	NaN	NaN	NaN	NaN	NaN	NaN	NaN	NaN	NaN
736236.5976	0.72	1.65	2.05	2.26	2.77	2.98	3.31	3.74	4.22	4.92	5.8	6.58	7.84	9.47	11.1	13.95	14.74	14.59	11.8	9.54
736236.6285	0.64	1.56	2.05	2.33	2.9	3.2	3.65	4.35	5.22	6.43	7.85	9.16	11.31	13.7	16.11	19.57	20.16	19.04	15.49	12.61
736236.6447	0.56	1.41	1.88	2.17	2.74	3.05	3.52	4.22	5.1	6.28	7.61	8.76	10.68	12.62	14.34	16.76	16.26	14.62	18.39	27.21
736236.6604	0.41	1.1	1.6	1.91	2.37	2.6	2.92	3.51	4.29	5.35	6.53	7.72	10.02	12.48	15.31	18.77	19.4	18.17	15.58	13.4
736236.6753	0.36	1.03	1.56	1.94	2.45	2.68	2.97	3.52	4.23	5.15	6.18	7.2	9.42	11.91	15.03	18.87	20.39	19.95	26.29	35.77
736236.6904	0.24	0.72	1.22	1.62	2.08	2.26	2.45	2.87	3.43	4.14	4.87	5.67	7.69	10.02	13.31	17.06	19.02	19.19	22.3	26.08
736238.3513	0.21	0.61	0.98	1.24	1.55	1.67	1.8	2.09	2.46	2.93	3.43	3.99	5.36	7	9.33	12.2	13.9	14.26	17.02	20.55
736238.3678	0.21	0.58	0.88	1.08	1.32	1.41	1.52	1.75	2.05	2.41	2.78	3.19	4.17	5.39	7.12	9.36	10.71	11.11	12.18	13.78
736238.3839	0.18	0.5	0.78	0.96	1.16	1.23	1.3	1.5	1.77	2.1	2.45	2.84	3.79	4.95	6.65	8.78	10.28	11.06	13.52	17.36
736238.3987	0.19	0.5	0.73	0.87	1.05	1.11	1.19	1.37	1.61	1.9	2.2	2.51	3.24	4.11	5.34	6.94	8.05	8.58	10.5	13.06
736238.4137	0.16	0.41	0.61	0.73	0.88	0.92	0.95	1.06	1.19	1.35	1.48	1.6	1.99	2.48	3.23	4.3	5.4	6.41	7.74	9.47
736238.4291	0.17	0.43	0.57	0.66	0.81	0.85	0.91	1	1.1	1.23	1.37	1.49	1.73	2.09	2.52	3.31	3.72	4.08	4.58	5.17
736238.4439	0.17	0.43	0.56	0.64	0.78	0.82	0.87	0.94	1.01	1.1	1.2	1.24	1.33	1.51	1.68	2.1	2.28	2.44	2.95	3.61
736238.4575	0.23	0.57	0.72	0.8	0.97	0.98	0.96	0.89	0.78	0.69	0.62	0.56	0.51	0.53	0.56	0.73	0.84	1.02	1.23	1.51
736238.4723	0.16	0.38	0.46	0.5	0.59	0.6	0.62	0.63	0.64	0.66	0.68	0.68	0.7	0.78	0.86	1.09	1.17	1.24	1.38	1.6
736238.4874	0.18	0.42	0.51	0.55	0.64	0.66	0.69	0.73	0.77	0.84	0.91	0.96	1.05	1.21	1.38	1.76	1.92	2.02	2.5	3.11
736238.5019	0.27	0.64	0.82	0.9	1.09	1.16	1.26	1.41	1.58	1.8	2.02	2.2	2.57	3.04	3.58	4.46	4.86	5.06	6.2	7.66
736238.5171	0.23	0.52	0.65	0.7	0.82	0.84	0.89	0.97	1.07	1.23	1.4	1.58	1.9	2.36	2.94	3.93	4.55	4.98	6.28	8
736238.5316	0.28	0.53	0.59	0.59	0.67	0.67	0.7	0.74	0.79	0.87	0.97	1.06	1.21	1.44	1.72	2.26	2.61	2.93	4.2	6.08
736238.5502	0.3	0.6	0.69	0.71	0.81	0.83	0.88	0.95	1.04	1.18	1.34	1.51	1.82	2.29	2.9	3.94	4.71	5.34	7.46	10.61

Size classes ranging from 85-1205 μm

Datenum	85.22	100.57	118.68	140.04	165.26	195.02	230.14	271.58	320.48	378.19	446.29	526.65	621.48	733.39	865.45	1021.3	1205.2
735543.3806	13.86	18.34	24.56	31.28	35.15	41.56	47.55	46.28	32.15	25.65	18.8	8.87	11.26	8.39	0	0	0
735543.3965	13.36	17.84	25.43	31.54	37.22	36	41.62	27.98	29.21	14.45	7.54	0	0	0	0	0	0
735543.4937	NaN	NaN	NaN	NaN	NaN	NaN	NaN	NaN	NaN	NaN	NaN	NaN	NaN	NaN	NaN	NaN	NaN

735543.5149	11.88	15.46	21.6	26.83	35.79	47.67	58.81	73.16	86.54	103.21	89.63	84.28	78.35	50.93	6.81	0	0
735543.5278	13.3	17.72	25.37	34.03	45.13	56.51	72.28	84.38	105.13	123.74	128.85	140.31	140.32	120.63	37.1	37.56	23
735543.5417	11.37	14.89	19.15	23	27.02	32.41	37.91	41.53	47.12	56.67	47.94	48.08	35.87	7.04	0	0	0
735543.5558	13.45	17.27	24.17	27.05	34.17	39.04	46.92	56.39	60.09	56.3	64.12	58.29	37.28	17.15	3.43	0	0
735543.5674	11.25	14.07	18.7	22.01	27.09	27.68	29.18	35.31	36.77	35.79	39.57	37.63	26.03	6.76	0	0	0
735543.5784	11.18	14.99	18.45	22.21	23.81	26.78	28.59	30.61	29.37	28.69	24.6	16.73	5.04	0	0	0	0
735543.5943	10.29	13.09	17.17	19.85	20.16	22.84	22.8	21.56	24.26	22.11	22.58	14.91	1.62	0	0	0	0
735543.606	11.61	14.82	18.3	19.44	19.91	22.2	19.62	17.2	16.96	22.71	15.67	10.49	2.56	0	0	0	0
735543.6183	9.38	11.91	14.93	16.57	18.05	18.71	19.66	21.22	23.73	29.28	25.84	24.06	10.6	0.92	0	0	0
735543.631	9.68	12.48	15.11	16.66	18.61	20.24	20.51	22.07	27.25	30.95	26.93	32.53	35.43	10.93	0	0	0
735543.6438	9.79	12.42	16.89	20.14	23.52	26.26	28.4	33.5	37.78	41.96	42.82	46.3	37.08	11.05	0	0	0
735543.6559	NaN	NaN	NaN	NaN	NaN	NaN	NaN	NaN	NaN	NaN	NaN	NaN	NaN	NaN	NaN	NaN	NaN
735544.3454	15.93	21.29	30.74	41.07	53.57	66.74	77.33	95.22	102.87	98.88	90.07	78.68	66.08	13.42	0	0	0
735544.3595	15.91	24.02	32.26	46.34	60.31	88.32	98.17	140.23	145.52	176.31	163.06	134.59	148.09	32.02	0	0	0
735544.3711	14.85	18.81	25.31	32.09	37.01	42.96	47.66	56.83	40.99	36.28	27.82	26.39	9.12	0	0	0	0
735544.3826	15.76	22.87	31.43	41.14	49.46	55.02	66.9	64.52	70.82	73.47	47.41	46.33	27.74	3.84	0	0	0
735544.3954	16.68	21.98	32.53	39.96	47.2	58.57	59.5	73.11	72.06	59.08	72.42	52.74	22.64	0	0	0	0
735544.4077	20.03	27.67	39.99	53.28	66.61	81.59	90.78	97.37	88.51	79.25	60.95	37.59	15.26	6.31	0	0	0
735544.4195	17.01	23.33	32.74	42.52	54.63	64.43	71.28	80.08	93.84	75.3	66.96	42.53	46.62	8.17	0	0	0
735544.4549	16.62	20.26	26.66	35.85	45.03	50.59	61.46	80.98	106.68	105.5	132.58	96.44	107.82	84.77	59.89	52.92	0
735544.4674	11.28	14.18	19.62	23.27	32.42	42.16	52.97	76.92	84.52	112.12	122.46	137.07	130.7	107.54	78.43	22.78	0
735544.479	NaN	NaN	NaN	NaN	NaN	NaN	NaN	NaN	NaN	NaN	NaN	NaN	NaN	NaN	NaN	NaN	NaN
735544.4922	NaN	NaN	NaN	NaN	NaN	NaN	NaN	NaN	NaN	NaN	NaN	NaN	NaN	NaN	NaN	NaN	NaN
735544.5047	15.37	20.57	27.55	32.02	46.19	57.14	72.57	81.19	106.94	116.08	77.67	42.87	39.36	18.4	0	0	0
735544.5178	13.54	19.01	23.66	26.4	30.03	29.98	42.36	39.57	37.19	43.12	32.85	16.36	0	0	0	0	0
735544.5307	17.34	21.16	30.03	37.58	44.59	54.06	59.19	55.75	59.84	45.66	26.28	22.96	20.8	0	0	0	0
735544.5542	15.27	19.55	25.9	31.69	40.97	45.91	52.57	57.24	59.59	54.64	49.27	36.27	23.6	17.4	1.74	0	0
735544.5657	14.02	17.2	22.84	27.11	31.7	36.38	37.89	38.35	41.69	36.83	26.48	17.4	10.64	0	0	0	0
735544.5793	11.62	14.5	18.25	19.23	22.22	23.05	25.58	25.07	19.92	18.98	18.05	12.33	1.94	0	0	0	0
735544.5908	10.92	12.8	14.9	17.83	18.34	21.03	19.92	17.29	18.07	17.08	12.23	9.55	1.01	0	0	0	0
735544.6025	10.56	12.89	15.58	17.71	17.79	18.83	19.68	18.11	18.38	21.3	19.58	11.85	4.53	0	0	0	0
735544.6144	10.04	12.62	15.09	16.34	17.43	18.2	17.87	15.12	15.35	13.76	16.43	13.65	5.78	0	0	0	0
735544.6266	10.25	11.87	14.74	17.03	16.22	17.69	17.78	14.78	10.11	11.09	3.65	2.46	0	0	0	0	0
735544.6356	9.56	11.61	13.93	16.45	17.26	18.84	17.96	19.73	19.45	21.75	13.26	6.79	0	0	0	0	0
735544.6444	5.76	6.21	6.84	6.31	5.56	6.51	5.53	7.1	3.97	0.56	0.44	0	0	0	0	0	0
735544.6522	5.72	6.52	7.19	7.54	7.7	7.89	9.29	9.38	9.28	10.09	7.33	0	0	0	0	0	0
735544.6575	6.82	8.11	9.89	10.12	9.6	11.59	11.04	9.94	11.95	14.8	18.6	11.48	0	0	0	0	0
735544.6799	10.73	11.89	14.29	15.38	15.29	14.74	10.46	11.77	5.9	2.84	1.32	0	0	0	0	0	0
735544.6902	7.85	8.94	10.68	11.62	13.48	12.3	11.27	9.99	9.86	4.09	0	0	0	0	0	0	0
735544.6948	9.64	13.61	16.93	20.92	24.13	27.02	29.17	44.34	41.52	41.12	39.26	20.02	10.59	0	0	0	0
735545.4331	15.61	20.88	27.67	33.91	40.71	47.39	50.69	55.95	66.1	41.89	19.27	17.05	0	0	0	0	0
735545.4632	14.42	19.91	27.41	33.69	41.34	47.16	48.58	53.49	45.22	35.54	18.81	8.06	3.37	0	0	0	0
735545.4742	9.01	10.88	13.53	14.33	17.95	17.13	15.11	15.89	13.49	10.09	3.77	0	0	0	0	0	0
735545.4866	16.71	22.87	31.01	40.35	46.82	55.31	59.44	63.6	61.28	40.4	31.52	17.86	5.59	0	0	0	0
735545.4998	NaN	NaN	NaN	NaN	NaN	NaN	NaN	NaN	NaN	NaN	NaN	NaN	NaN	NaN	NaN	NaN	NaN
735545.5115	15.26	21.09	29.76	37.42	46.4	57.2	63.79	69.2	62.11	51.59	33.02	21.17	5.65	0	0	0	0
735545.5377	15.08	20.46	27.59	35.51	44.04	54.4	60.29	69.93	78.52	79.93	67.07	53.34	28.71	6.07	0	0	0
735545.5508	12.9	17.04	22.26	28.18	35.84	43.36	53.13	51.92	64.64	60.79	49.31	33.94	24.05	8.84	0	0	0
735545.5625	12.9	16.4	21.96	27.66	34.14	40.54	48.14	48.74	51.02	43.67	35.4	24.54	17.01	0	0	0	0
735545.5742	11.16	15.15	19.94	23.89	31.05	36.13	47.57	51.87	56.76	57.86	48.41	29	7.06	0	0	0	0
735545.5826	10.28	13.58	17.4	22.59	29.18	35.55	45.11	53.68	58.37	59.96	48.96	33.24	18.13	4.84	0	0	0
735545.5951	9.45	11.66	15.88	19.32	25.96	32.99	40.83	50.16	57.04	56.35	63.61	38.61	38.44	9.55	0	0	0
735545.6083	9.42	11.63	14.88	19.3	21.27	25.44	31.04	33.63	29.68	34.56	25.19	21.09	11.78	3.56	0	0	0
735545.6538	9.46	11.47	14.28	16.57	18.21	19.23	20.49	22.65	21.88	24.03	17.13	2.95	0	0	0	0	0
735545.6646	10.66	13.1	16.86	18.74	19.53	19.84	18.04	14.68	11.48	7.23	3.4	0.94	0	0	0	0	0
735545.6754	10.76	12.99	17.36	19.12	18.69	18.33	18.14	16.39	12.94	9.78	3.7	0.74	0	0	0	0	0
735546.3137	12.01	13.72	17.43	22.6	25.8	22.97	24.98	20.86	27.19	26.65	34.8	39.74	16.21	0	0	0	0
735546.3249	12.28	15.51	19.81	22.63	26.96	27.75	26.93	26.53	16.7	13.08	5.74	0	0	0	0	0	0
735546.3355	9.78	11.46	14.36	16.66	23.42	24.45	23.7	25.35	26.48	14.54	15.68	13.1	0	0	0	0	0
735546.346	9.94	11.63	13.88	16.86	16.46	21.22	22.9	25.58	21.02	15.28	17.06	2.76	0	0	0	0	0
735546.3566	9.4	10.71	12.38	16.53	20.44	19.34	21.13	23.67	21.62	16.9	11.97	7.71	0	0	0	0	0
735546.3681	9.47	11.53	14.16	16.44	19.23	22.97	20.6	23.26	12.49	12.85	12.49	6.99	0	0	0	0	0
735546.3792	7.73	8.92	10.46	12.47	14.19	16.54	19.68	19.64	21.76	22.92	19.7	12.9	3.42	0	0	0	0
735546.3906	8.14	8.95	11.32	11.85	12.84	17.66	17.51	17.1	24.08	15.03	16.94	10.94	0	0	0	0	0

735546.4119	14.32	17.84	24.66	29.45	34.62	42.96	51.7	63.79	74.45	73.48	92.53	123.15	104.04	81.12	75.32	50.29	0
735546.4236	NaN	NaN	NaN	NaN	NaN	NaN	NaN	NaN	NaN	NaN	NaN	NaN	NaN	NaN	NaN	NaN	NaN
735546.4384	NaN	NaN	NaN	NaN	NaN	NaN	NaN	NaN	NaN	NaN	NaN	NaN	NaN	NaN	NaN	NaN	NaN
735546.4505	NaN	NaN	NaN	NaN	NaN	NaN	NaN	NaN	NaN	NaN	NaN	NaN	NaN	NaN	NaN	NaN	NaN
735546.4628	NaN	NaN	NaN	NaN	NaN	NaN	NaN	NaN	NaN	NaN	NaN	NaN	NaN	NaN	NaN	NaN	NaN
735546.475	NaN	NaN	NaN	NaN	NaN	NaN	NaN	NaN	NaN	NaN	NaN	NaN	NaN	NaN	NaN	NaN	NaN
735546.4874	21.07	29.79	41.02	52.81	71.19	84.05	101.08	107.29	116	115.49	93.44	70.93	51.17	25.32	0	0	0
735546.4995	18.94	26.84	37.77	49.88	64.42	78.48	96.18	97.27	99.44	90.08	78.26	53.16	22.06	9.57	0	0	0
735546.5129	17.24	23.12	31.74	41.54	52.31	62.74	71.77	77.81	75.96	72.11	52.89	39.07	22.41	1.76	0	0	0
735546.5261	16.79	22.41	30.88	37.83	45.96	53.12	60.47	64.72	64.11	57.74	42.26	24.55	15.34	0	0	0	0
735546.5375	16.71	21.78	28.66	36.12	41.71	49.05	55.03	53.13	53.47	45.25	33.81	26.4	4.85	7.22	1.52	0	0
735734.3542	12.82	16.51	21.24	25.37	30.82	32.7	34.31	36.06	34.97	32.46	22.95	19.05	14.52	9.12	0	0	0
735734.3694	12.68	16.62	21.57	25.75	28.63	30.93	32.86	30.35	26.18	20.7	19.61	12.81	0.82	0	0	0	0
735734.3843	11.16	14.61	18.58	21.62	25.47	26.26	29.96	28.79	25.03	20.76	15.21	4.4	0	0	0	0	0
735734.3989	11.38	14.44	19.65	22.34	27.91	29.63	33.14	33.72	33.56	28.66	17.47	10.97	1.31	0	0	0	0
735734.4147	11.19	14.23	17.9	21.06	23.73	24.15	23.99	21.75	19.85	14.15	10.67	2.71	0	0	0	0	0
735734.4297	14.03	17.89	22.41	27.39	29.99	30.31	33.99	31.47	26.07	28.03	19.34	12.28	16.53	6.49	0	0	0
735734.4449	14.05	17.21	20.39	24.59	27.08	28.48	29.46	27.93	22.61	21.75	23.27	13.47	2.85	0	0	0	0
735734.4597	13.6	16.78	21.01	23.26	27.75	27.9	29.78	31.3	29.09	29.55	36.65	33.38	36.74	27.92	2.88	0	0
735734.4749	12.48	14.49	17.84	19.88	22.24	21.61	25.08	24.85	22.96	24.17	28.8	21.67	12.63	0	10.44	0	0
735734.4902	13.05	15.63	20.1	23.92	26.84	28.59	36.6	40.45	40.96	48.37	48.8	45.77	57.59	38.94	27.05	34.87	7.94
735734.5061	12.24	14.21	17.07	17.81	19.17	19.15	18.94	18.82	17.92	22.51	23.45	21.48	29.01	16.61	0	3.21	0
735734.5214	11.55	13.06	14.39	15.44	14.17	16.45	14.21	11.96	12.93	10.38	9.37	8.27	0	0	0	0	0
735734.5372	9.67	10	11.48	11.7	14.16	14.93	13.43	15.43	16.75	23.72	32.7	36.28	28.52	17.67	0	0	0
735734.5529	14.5	19.09	25.88	34.38	41.21	49.69	57.67	60.52	59.39	52.44	41.57	32.72	13.13	10.94	4.53	0	0
735734.5692	12.13	14.47	17.54	21.99	24.93	27	28.01	27.66	23.82	17.27	9.06	3.87	0	0	0	0	0
735734.585	8.34	9.71	11.03	12.37	13.08	13.93	13	10.75	9.48	5.02	0.69	0	0	0	0	0	0
735734.6015	NaN	NaN	NaN	NaN	NaN	NaN	NaN	NaN	NaN	NaN	NaN	NaN	NaN	NaN	NaN	NaN	NaN
735734.6182	NaN	NaN	NaN	NaN	NaN	NaN	NaN	NaN	NaN	NaN	NaN	NaN	NaN	NaN	NaN	NaN	NaN
735734.6335	NaN	NaN	NaN	NaN	NaN	NaN	NaN	NaN	NaN	NaN	NaN	NaN	NaN	NaN	NaN	NaN	NaN
735734.6492	NaN	NaN	NaN	NaN	NaN	NaN	NaN	NaN	NaN	NaN	NaN	NaN	NaN	NaN	NaN	NaN	NaN
735734.6646	NaN	NaN	NaN	NaN	NaN	NaN	NaN	NaN	NaN	NaN	NaN	NaN	NaN	NaN	NaN	NaN	NaN
735734.68	NaN	NaN	NaN	NaN	NaN	NaN	NaN	NaN	NaN	NaN	NaN	NaN	NaN	NaN	NaN	NaN	NaN
735734.6945	NaN	NaN	NaN	NaN	NaN	NaN	NaN	NaN	NaN	NaN	NaN	NaN	NaN	NaN	NaN	NaN	NaN
735734.7098	15.51	21.71	29.55	39	48.78	60.95	65.87	75.78	71.76	74.4	68.51	67.03	43.71	33.04	2.32	0	0
735736.3634	15.12	20.89	28.48	36.37	45.09	55.77	62.51	72.1	77.29	89.53	82.65	57.01	45.23	11.07	0	0	0
735736.3779	15.34	20.48	28.35	34.47	40.62	48.42	49.78	55.54	48.7	46.21	36.92	20.57	10.33	0	0	0	0
735736.4358	12.96	15.31	18.88	22.11	23.78	24.44	21.15	23.15	19.66	15.94	7.45	4.3	0	0	0	0	0
735736.4583	14.19	18.47	23.96	29.8	37.26	42.14	45.7	53.93	52.69	57.13	51.96	43.56	29.6	16.48	0	0	0
735736.4746	11.57	14.47	18.22	18.97	25.15	24.04	24.13	24.02	20.07	19.06	15.17	17.82	0	0	0	0	0
735736.4906	13.87	18.17	23.04	27.92	33.45	34.61	35.23	38.64	25.9	27.11	15.8	14.44	0	0	0	0	0
735736.5058	NaN	NaN	NaN	NaN	NaN	NaN	NaN	NaN	NaN	NaN	NaN	NaN	NaN	NaN	NaN	NaN	NaN
735736.5231	48.43	57.42	68.96	70.32	67.1	58.05	37.34	28.14	16.39	0	0	0	0	0	0	0	0
735736.5408	49.47	55.83	56.08	54.78	40.88	34.07	19.29	10.04	0	0	0	0	0	0	0	0	0
735736.5564	53.41	58.71	58.66	54.74	41.3	25.86	19.88	8.2	0	0	0	0	0	0	0	0	0
735736.5714	59.49	70.3	64.74	65.25	45.58	37.06	21.13	9.94	0	0	0	0	0	0	0	0	0
735736.5868	NaN	NaN	NaN	NaN	NaN	NaN	NaN	NaN	NaN	NaN	NaN	NaN	NaN	NaN	NaN	NaN	NaN
735736.6139	37.95	38.26	36.67	30.15	24.82	15.98	12.88	1.58	0	0	0	0	0	0	0	0	0
735736.6573	22.17	23.54	20.92	16.18	13.04	8.02	4.2	0.62	0	0	0	0	0	0	0	0	0
735736.6727	26.77	31.51	32.92	31.03	28.98	24.05	17.64	8.51	6.48	0	0	0	0	0	0	0	0
735736.6869	15.58	18.7	21.61	20.71	21.01	18.88	17.01	7.28	0	0	0	0	0	0	0	0	0
735736.702	4.22	6	5.81	7.1	7.99	4.8	2.31	0	0	0	0	0	0	0	0	0	0
736235.363	2.51	3.21	3.84	4.16	4.94	4.87	1.42	0	0	0	0	0	0	0	0	0	0
736235.3792	5.97	5.64	7.2	6.81	5.67	2.04	0	0	0	0	0	0	0	0	0	0	0
736235.3955	13.31	11.88	13.42	12.15	13.61	8.65	6.24	4.12	0	0	0	0	0	0	0	0	0
736235.4104	12.94	14.05	16.02	18.05	17.61	12.38	6.19	4.24	0	0	0	0	0	0	0	0	0
736235.4293	23.2	25.38	27.27	29.18	28.04	32.81	26.45	22.32	21.49	8.46	5.47	0	0	0	0	0	0
736235.4442	3.7	4	4.9	5.32	6.79	4.56	1.41	0	0	0	0	0	0	0	0	0	0
736235.4587	16.45	19.92	20.9	22.96	26.78	25.03	17.29	12.56	1.12	0	0	0	0	0	0	0	0
736235.4726	10.34	11.63	13.52	10.66	9.7	6.79	2.12	0	0	0	0	0	0	0	0	0	0
736235.487	NaN	NaN	NaN	NaN	NaN	NaN	NaN	NaN	NaN	NaN	NaN	NaN	NaN	NaN	NaN	NaN	NaN
736235.502	22.91	20.52	30.14	20.79	20.15	16.71	19.63	4.46	0	0	0	0	0	0	0	0	0
736235.5198	7.78	10.71	11.49	14.98	19.93	19.73	31.63	23.45	12.69	0	0	0	0	0	0	0	0
736235.5382	20.11	24.28	30.52	23.99	33.1	30.51	24.2	13.01	0	0	0	0	0	0	0	0	0

736235.5558	NaN	NaN	NaN	NaN	NaN	NaN	NaN	NaN	NaN	NaN	NaN	NaN	NaN	NaN	NaN	NaN	NaN
736235.5717	15.21	14.14	17.29	20.95	11.55	8.35	12.43	0	4.8	0	0	0	0	0	0	0	0
736235.5871	27.85	33.59	36.12	38.94	34.75	32.13	25.23	16.59	7.42	0	0	0	0	0	0	0	0
736235.6035	34.68	44.93	54	65.66	66.36	64.42	42.72	33.81	24.15	11.67	0	0	0	0	0	0	0
736235.6197	30.21	35.84	39.07	37.8	35.01	25.56	16.16	6.01	2.87	0	0	0	0	0	0	0	0
736235.6372	42.83	48.04	52.39	53.89	51.51	42.18	26.28	15.99	5.93	0	0	0	0	0	0	0	0
736235.6526	42.01	49.13	57.04	56.71	54.62	48.89	30.54	23.87	15.76	6.33	0	0	0	0	0	0	0
736235.6677	22.49	22.79	21.46	17.91	15.75	10.71	4.73	1.03	0	0	0	0	0	0	0	0	0
736235.6985	22.94	27.57	26.86	26.46	24.7	20.21	12.45	9.28	0.96	0	0	0	0	0	0	0	0
736235.7135	15.52	17.37	16.06	17.01	13.86	7.79	2.62	0	0	0	0	0	0	0	0	0	0
736235.7288	14.04	14.78	16.29	12.92	11.67	10.25	5.42	1.4	1.16	0	0	0	0	0	0	0	0
736235.7438	7.51	8.08	8.87	8.18	7.41	6.09	3.18	0.56	0	0	0	0	0	0	0	0	0
736235.7586	5.75	5.72	7.41	6.66	7.47	3.69	1.68	0	0	0	0	0	0	0	0	0	0
736236.3624	3.72	4.65	4.56	3.66	2.35	3.06	0	0	0	0	0	0	0	0	0	0	0
736236.3829	2.8	2.58	3.26	3.58	4.12	0.58	0	0	0	0	0	0	0	0	0	0	0
736236.3971	2.31	2.84	2.64	2.59	1.72	0.42	0	0	0	0	0	0	0	0	0	0	0
736236.4128	4.5	5.38	4.71	3.99	4.37	4.12	2.38	3.32	3.45	0	0	0	0	0	0	0	0
736236.4278	2.24	2.68	2.16	2.04	1.4	0.75	0	0	0	0	0	0	0	0	0	0	0
736236.4438	6.26	6.5	6.65	9.29	7.45	4.79	0.67	0	0	0	0	0	0	0	0	0	0
736236.458	27.16	31.99	33.93	38.09	33.82	30.08	26.94	19.47	7.28	0	0	0	0	0	0	0	0
736236.4737	12.19	12.31	12.19	11.41	11.39	5.08	3.73	0.58	0	0	0	0	0	0	0	0	0
736236.4882	13.33	14.56	14.82	17.28	13.33	11.03	7.4	2.54	0	0	0	0	0	0	0	0	0
736236.5032	16.89	18.34	17.94	16.26	14.59	9.27	8.26	2.03	0	0	0	0	0	0	0	0	0
736236.5179	NaN	NaN	NaN	NaN	NaN	NaN	NaN	NaN	NaN	NaN	NaN	NaN	NaN	NaN	NaN	NaN	NaN
736236.5324	NaN	NaN	NaN	NaN	NaN	NaN	NaN	NaN	NaN	NaN	NaN	NaN	NaN	NaN	NaN	NaN	NaN
736236.5485	6.16	6.89	8.55	6.48	6.76	3.33	0	0	0	0	0	0	0	0	0	0	0
736236.5683	11.67	13.09	11.69	8.78	5.67	3.16	0.41	0	0	0	0	0	0	0	0	0	0
736236.5829	NaN	NaN	NaN	NaN	NaN	NaN	NaN	NaN	NaN	NaN	NaN	NaN	NaN	NaN	NaN	NaN	NaN
736236.5976	7.72	7.52	8.27	6.73	4.08	0	0	0	0	0	0	0	0	0	0	0	0
736236.6285	10.26	8.61	6.86	2.77	1.62	0	0	0	0	0	0	0	0	0	0	0	0
736236.6447	44.12	49.29	58.13	65.92	72.65	72.05	68.19	42.62	64.83	36.48	32.05	0	0	0	0	0	0
736236.6604	11.56	8.8	9.16	5	3.8	1.66	0	0	0	0	0	0	0	0	0	0	0
736236.6753	50.04	55.5	58.16	56.51	51.34	41.54	30.08	23.02	15.54	1.73	0	0	0	0	0	0	0
736236.6904	30.66	34.12	36.71	40.43	36.01	28.35	23.23	9.82	3.11	0	0	0	0	0	0	0	0
736238.3513	25.09	27.53	29.81	27.32	26.44	23.09	16.12	9.46	0	4.05	0	0	0	0	0	0	0
736238.3678	16.02	16.6	19.66	17.37	14.96	12.9	12.23	7.29	2.66	0	0	0	0	0	0	0	0
736238.3839	23.08	25.2	26.63	23.82	20.83	19.13	15.58	6.24	0.85	0	0	0	0	0	0	0	0
736238.3987	16.48	16.82	16.29	16.21	13.83	8.53	9.83	5.41	0	0	0	0	0	0	0	0	0
736238.4137	11.73	11.74	15.02	13.48	13.65	12.56	9.17	2.84	0	0	0	0	0	0	0	0	0
736238.4291	5.84	6.93	5.77	7.68	6.41	7.07	4.68	2.38	0	0	0	0	0	0	0	0	0
736238.4439	4.48	4.68	5.66	6.04	5.58	4.59	1.52	0	0	0	0	0	0	0	0	0	0
736238.4575	1.89	1.69	1.49	0.37	0	0	0	0	0	0	0	0	0	0	0	0	0
736238.4723	1.96	2.51	2.49	0.78	1.15	0	0	0	0	0	0	0	0	0	0	0	0
736238.4874	3.86	3.35	2.62	1.99	0.75	0	0	0	0	0	0	0	0	0	0	0	0
736238.5019	9.57	10.18	10.43	7.49	8.87	7.4	5.54	4.19	5.34	0	0	0	0	0	0	0	0
736238.5171	10.28	9.47	7.64	6.91	3.93	2.21	1.48	0	0	0	0	0	0	0	0	0	0
736238.5316	8.9	8.71	8.38	7.82	4.59	0.96	0	0	0	0	0	0	0	0	0	0	0
736238.5502	15.46	17.33	18.51	17.74	19.84	20.59	15.81	8.06	1.87	0	0	0	0	0	0	0	0

Appendix IV. DIGS dataset

Filter	Year	Month	Day	Hour	Minutes	Cast	FZ	Bag (0=surf)	SSC (mg/L)	D50	D75	D25	D5	D95
2008499	2013	11	6	8	59	30	2	1	150	15	28	6	2	57
2012104	2013	11	6	8	6	27	2	1	105	22	36	12	3	64
2012107	2013	11	6	8	25	28	2	0	7	8	17	4	1	45
2012108	2013	11	6	8	25	28	2	1	132	18	32	7	2	60
2012111	2013	11	6	8	43	29	2	1	161	23	39	10	2	69
2013107	2013	11	6	9	17	31	2	1	98	22	43	10	2	76
2013111	2013	11	6	9	34	32	2	0	25	35	67	11	2	99
2013112	2013	11	6	9	34	32	2	1	100	24	48	10	2	84
2013115	2013	11	6	9	52	33	2	1	85	24	44	11	2	72
2013121	2013	11	6	10	43	34	4	3	145	13	23	5	2	41
2013122	2013	11	6	11	1	35	4	0	13	11	30	5	2	80
2013123	2013	11	6	11	1	35	4	1	86	13	26	5	1	49
2013124	2013	11	6	11	1	35	4	2	86	17	32	8	2	59
2013127	2013	11	6	11	18	36	4	1	97	15	27	7	2	45
2013128	2013	11	6	11	18	36	4	3	199	13	25	5	2	43
2013129	2013	11	6	11	37	37	4	0	9	9	16	4	1	40
2013131	2013	11	6	11	37	37	4	1	222	16	28	8	2	49
2013133	2013	11	6	11	55	38	4	1	234	15	25	7	2	42
2013136	2013	11	6	11	37	37	4	3	485	15	26	7	2	42
2013137	2013	11	6	11	55	38	4	0	81	8	15	4	1	33
2013139	2013	11	6	12	12	39	4	1	238	18	29	8	2	46
2013209	2013	11	5	11	7	8	4	3	92	15	25	7	2	44
2013212	2013	11	5	11	25	9	4	3	88	15	27	7	2	52
2013214	2013	11	5	11	39	10	4	1	96	14	25	7	2	43
2013237	2013	11	5	10	35	6	4	3	158	14	25	6	2	44
2013239	2013	11	5	10	51	7	4	1	144	15	26	6	2	44
2013293	2013	11	6	12	30	40	4	0	10	10	22	4	1	58
2013295	2013	11	6	12	30	40	4	2	143	14	24	7	2	39
2013296	2013	11	6	12	30	40	4	1	125	17	29	8	2	57
2013299	2013	11	6	12	48	41	4	1	128	16	26	8	2	49
2013301	2013	11	6	12	48	41	4	3	147	14	24	7	2	40
2013304	2013	11	6	13	4	42	4	2	93	13	23	6	2	39
2013305	2013	11	6	13	4	42	4	1	89	15	26	8	2	45
2013308	2013	11	6	13	22	43	4	1	47	15	28	7	2	53
2013315	2013	11	6	13	42	44	4	3	29	14	25	6	2	51
2008496	2013	11	6	8	43	29	2	2	188	5.4	12	2.5	1	26.4
2008498	2013	11	6	8	59	30	2	0	8	3.48	6.2	2	1	13.7
2012103	2013	11	6	8	6	27	2	0	2	4.14	7.3	2.2	1	15
2012106	2013	11	6	8	6	27	2	3	71	7.89	15	3.3	1	30.2
2012110	2013	11	6	8	43	29	2	0	11	5.44	9.8	2.7	1	23.3
2013113	2013	11	6	9	34	32	2	3	116	7.45	14	3.3	1	26.4
2013114	2013	11	6	9	52	33	2	0	23	3.66	6.7	2	1	16.4
2013117	2013	11	6	9	52	33	2	3	159	4.35	8.3	2.3	1	19.5
2013138	2013	11	6	12	12	39	4	0	123	4.7	8.4	2.4	1	18.5

2013238	2013	11	5	10	51	7	4	0	3.38	4.66	8.6	2.3	1	16.6
2013302	2013	11	6	13	4	42	4	0	12	5.08	9	2.5	1	19.5
2013351	2013	11	7	9	16	54	1.5	0	7.41	3.48	7	1.9	1	19.3
2013357	2013	11	7	9	33	55	1.5	0	6.43	3.85	8.3	2	1	22.5
2013427	2013	11	8	7	14	74	4	0	7.37	4.74	9.7	2.3	1	24.9
2013459	2013	11	8	12	41	91	3	0	6.2	3.65	7	2	1	16.4
2013460	2013	11	8	12	41	91	3	2	61.08	7.11	16	3	1	32.6
2013532	2013	11	8	9	10	81	4	3	13.6	3.74	6.7	2	1	15.1
2013534	2013	11	8	9	10	81	4	0	2.2	3.38	6.7	1.8	1	15.1
2014002	2014	5	15	8	44	19	2	3	247	15	27	7	2	48
2014003	2014	5	15	9	11	20	2	0	6	10	22	4	1	49
2014004	2014	5	15	9	0	20	2	1	218	16	27	7	2	48
2014006	2014	5	15	9	6	20	2	3	334	16	28	7	2	51
2014007	2014	5	15	9	32	21	2	0	8	10	21	5	2	44
2014009	2014	5	15	9	22	21	2	2	289	17	30	8	2	57
2014014	2014	5	15	9	44	22	2	2	209	16	28	7	2	49
2014018	2014	5	15	10	7	23	2	2	174	18	30	8	2	51
2014020	2014	5	15	10	38	24	2	0	6	8	19	4	1	65
2014022	2014	5	15	10	25	24	2	1	144	20	35	9	2	59
2014026	2014	5	15	10	55	25	2	3	86	18	31	8	2	53
2014028	2014	5	15	11	10	26	2	1	74	19	33	9	2	56
2014030	2014	5	15	11	43	27	2	0	8	7	13	3	1	47
2014032	2014	5	15	11	38	27	2	3	39	16	31	7	2	57
2014035	2014	5	15	12	28	29	2	0	8	7	16	3	1	47
2014036	2014	5	15	12	23	29	2	3	24	15	31	6	2	59
2014068	2014	5	17	8	41	44	2.3	0	9	11	20	5	2	43
2014069	2014	5	17	8	30	44	2.3	1	31	15	29	6	2	53
2014079	2014	5	17	10	0	48	2.3	0	10	9	18	4	1	36
2014080	2014	5	17	9	53	48	2.3	2	14	13	25	6	2	51
2014083	2014	5	17	10	21	49	2.3	3	14	13	23	6	2	44
2014084	2014	5	17	10	55	50	2.3	0	8	8	16	4	1	36
2014085	2014	5	17	10	48	50	2.3	2	13	14	26	7	2	57
2014089	2014	5	17	11	15	51	2.3	3	180	17	28	8	2	47
2014107	2014	5	17	11	32	52	2.3	2	176	16	28	8	2	49
2014110	2014	5	17	11	54	53	2.3	1	199	18	30	8	2	53
2014114	2014	5	17	12	16	54	2.3	1	171	19	31	9	2	56
2014116	2014	5	17	12	29	54	2.3	0	8	11	22	5	2	47
2014118	2014	5	17	12	41	55	2.3	1	141	18	31	9	2	54
2014121	2014	5	17	13	7	56	2.3	1	98	17	31	8	2	58
2014125	2014	5	17	13	28	57	2.3	1	90	17	29	8	2	50
2014128	2014	5	17	13	50	58	2.3	1	56	16	28	8	2	54
2014130	2014	5	17	14	40	59	2.3	0	18	13	31	5	2	61
2014131	2014	5	17	14	35	59	2.3	3	39	13	27	6	2	59
2012198	2014	5	15	8	50	19	2	0	11	9	17	4	1	37
2012199	2014	5	15	8	37	19	2	1	30	12	23	6	2	45
2013466	2014	5	14	10	32	2	3	0	9	8	16	4	1	40
2013467	2014	5	14	10	21	2	3	1	14	12	22	5	2	49
2013470	2014	5	14	10	48	3	3	1	142	15	27	7	2	50

2013473	2014	5	14	11	11	4	3	1	89	16	29	7	2	54
2013476	2014	5	14	11	35	5	3	1	65	14	25	7	2	51
2013479	2014	5	14	11	58	6	3	1	44	12	21	5	2	45
2011337	2015	10	1	17	27	79	2	0	15	5	15	3	1	44
2011339	2015	10	1	17	29	79	2	1	72	22	42	9	2	74
2011342	2015	10	1	17	45	80	2	0	14	5	16	3	1	46
2011343	2015	10	1	17	46	80	2	1	53	18	35	7	2	68
2014150	2015	9	28	16	5	21	4	0	17	4	15	2	1	49
2014151	2015	9	28	16	7	21	4	4	34	16	37	4	2	95
2014180	2015	10	1	11	54	64	2	2	117	36	62	15	2	92
2014182	2015	10	1	11	47	64	2	0	23	6	27	3	1	71
2014183	2015	10	1	11	37	63	2	3	154	29	51	13	3	84
2014186	2015	10	1	11	26	63	2	0	38	14	28	4	2	64
2014189	2015	10	1	11	10	62	2	2	131	27	47	12	2	75
2014190	2015	10	1	11	5	62	2	1	151	28	46	12	2	79
2014191	2015	10	1	11	3	62	2	0	20	5	19	3	1	55
2014192	2015	10	1	10	56	61	2	3	143	25	42	11	2	70
2014193	2015	10	1	10	50	61	2	2	136	23	39	9	2	66
2014195	2015	10	1	10	44	61	2	0	19	5	21	3	1	52
2014199	2015	10	1	10	25	60	2	1	125	18	30	8	2	53
2014200	2015	10	1	10	23	60	2	0	18	4	10	3	1	45
2015304	2015	9	28	17	55	26	4	0	13	4	12	2	1	41
2015305	2015	9	28	17	57	26	4	1	27	4	15	3	1	54
2015322	2015	9	29	10	0	31	3	0	17	10	26	3	1	55
2015323	2015	9	29	10	2	31	3	4	92	22	39	9	2	69
2015324	2015	9	29	10	12	31	3	3	249	23	40	10	2	73
2015325	2015	9	29	10	22	32	3	0	17	9	31	3	2	71
2015328	2015	9	29	10	34	32	3	3	118	21	38	9	2	70
2015329	2015	9	29	10	45	33	3	0	56	19	38	8	2	81
2015333	2015	9	29	10	57	33	3	3	110	27	50	11	2	84
2015362	2015	9	29	14	51	44	3	4	54	15	33	6	2	57
2015374	2015	9	29	16	31	48	3	3	81	26	49	10	2	80
2015382	2015	9	28	11	24	9	4	0	25	14	30	5	2	70
2015383	2015	9	28	11	26	9	4	4	142	27	50	14	3	88
2015400	2015	9	29	16	42	49	3	0	19	18	38	5	2	68
2015401	2015	9	29	16	43	49	3	1	123	27	49	11	2	80
2015425	2015	9	28	8	23	1	4	1	80	11	22	4	2	42
2015426	2015	9	28	8	28	1	4	2	93	12	25	4	1	60
2015427	2015	9	28	8	33	1	4	3	88	14	29	5	2	84
2015428	2015	9	28	8	48	2	4	0	15	3	6	2	1	31
2015429	2015	9	28	8	50	2	4	1	162	14	27	6	2	55
2015430	2015	9	28	8	55	2	4	2	248	22	41	10	2	75
2015431	2015	9	28	9	0	2	4	3	76	14	30	4	2	61
2015432	2015	9	28	9	11	3	4	0	14	3	11	2	1	62
2015435	2015	9	28	9	18	3	4	2	215	27	48	13	2	87
2015436	2015	9	28	9	23	3	4	3	117	19	35	8	2	67
2015441	2015	9	28	9	58	5	4	0	20	4	18	3	1	59
2015445	2015	9	28	10	10	5	4	3	132	25	49	9	2	91

2015446	2015	9	28	10	22	6	4	0	16	4	18	3	1	53
2015448	2015	9	28	10	28	6	4	2	118	21	38	9	2	72
2015449	2015	9	28	10	34	6	4	3	112	23	39	10	2	76

Appendix V. Matched PCP and tripod data

iPC	iGaf	Cruise	SSC	Tb	ds/dt	Sal.	D95	D50	SMD	RHOA	VC	RHOW	RHOE	Ws
1	2	1	24.56	0.30	NaN	0.3	418.12	164.43	82.96	19.80	447.17	-0.05	12.33	0.17
2	3	1	25.88	0.33	NaN	0.7	339.30	155.74	81.52	15.31	340.31	0.23	9.53	0.12
3	11	1	78.18	0.35	NaN	22.9	NaN	NaN	NaN	NaN	NaN	17.17	NaN	NaN
4	13	1	45.82	0.23	NaN	25.7	641.64	313.42	146.50	9.02	853.94	19.28	5.55	0.27
5	14	1	48.76	0.21	NaN	26.5	740.94	346.32	161.96	8.54	1288.72	19.86	5.26	0.32
6	15	1	19.82	0.04	NaN	26.9	570.93	267.89	122.01	10.09	492.66	20.17	6.20	0.22
7	16	1	46.07	0.01	NaN	27.3	577.39	264.62	118.00	11.22	612.10	20.41	6.90	0.24
8	17	1	24.88	0.01	NaN	27.3	558.16	244.74	101.29	12.98	416.24	20.45	7.98	0.24
9	18	1	25.24	0.01	NaN	27.3	452.67	176.07	71.06	21.62	357.41	20.44	13.29	0.21
10	19	1	33.22	0.01	NaN	27.2	455.75	184.88	80.91	21.19	276.29	20.39	13.03	0.22
11	20	1	22.30	0.04	NaN	26.8	433.23	162.38	73.95	25.67	262.53	20.09	15.79	0.21
12	21	1	16.88	0.01	NaN	27.2	505.70	211.60	83.92	19.82	291.35	20.34	12.19	0.28
13	22	1	23.72	0.03	NaN	27.0	596.76	263.84	102.74	12.75	335.12	20.20	7.84	0.28
14	23	1	18.81	0.03	NaN	26.6	579.94	275.67	118.38	13.00	427.85	19.95	8.00	0.31
15	24	1	24.42	0.02	NaN	24.4	NaN	NaN	NaN	NaN	NaN	18.29	NaN	NaN
16	28	1	137.57	0.97	2.45	24.0	542.68	246.94	121.49	13.33	952.13	17.92	8.21	0.25
17	29	1	138.89	0.99	1.69	26.4	595.05	301.06	151.25	8.43	1418.05	19.75	5.18	0.24
18	30	1	132.50	1.12	0.69	28.3	473.89	184.56	83.26	18.98	518.84	21.17	11.67	0.20
19	31	1	90.93	1.02	0.26	29.2	522.56	215.91	102.93	13.32	717.89	21.78	8.18	0.19
20	32	1	107.86	1.28	0.50	29.4	506.26	223.36	107.24	12.51	725.61	21.90	7.68	0.19
21	33	1	120.66	1.13	1.00	30.0	457.64	201.45	100.41	14.14	895.16	22.33	8.69	0.18
23	35	1	83.77	0.75	3.72	5.4	807.70	347.17	158.47	11.62	1177.15	3.88	7.22	0.44
24	36	1	148.00	0.71	5.64	8.9	727.75	370.21	165.97	10.90	1145.96	6.49	6.76	0.47
25	37	1	211.00	0.65	3.50	14.5	NaN	NaN	NaN	NaN	NaN	10.75	NaN	NaN
26	38	1	139.47	0.59	2.80	18.8	NaN	NaN	NaN	NaN	NaN	14.05	NaN	NaN
27	39	1	180.53	0.80	2.29	21.5	559.53	254.24	103.71	14.43	867.42	16.10	8.89	0.29
28	40	1	117.47	0.63	1.66	23.9	434.76	190.74	80.40	17.57	431.01	17.83	10.82	0.20
29	41	1	125.24	0.40	0.84	25.7	481.77	192.96	84.97	17.31	601.92	19.20	10.65	0.20
30	43	1	46.89	0.03	0.36	27.3	535.41	221.27	100.37	15.99	612.24	20.31	9.84	0.24
31	44	1	43.78	0.08	0.11	27.6	439.93	175.98	73.75	24.66	441.30	20.54	15.16	0.24
32	45	1	19.09	0.04	0.15	27.8	445.63	163.61	70.51	22.82	292.28	20.69	14.03	0.19
33	46	1	33.91	0.01	0.08	27.9	419.06	165.00	72.69	22.44	232.17	20.78	13.80	0.19
34	47	1	28.28	0.00	0.19	27.9	457.57	180.38	78.11	23.27	246.32	20.81	14.31	0.23
35	48	1	23.67	0.03	1.00	27.9	473.26	158.53	70.61	31.44	244.94	20.81	19.33	0.25
44	57	1	106.96	0.54	1.00	29.7	415.32	192.84	81.31	24.75	508.42	22.01	15.20	0.29
45	59	1	40.83	1.65	0.97	24.2	357.40	159.85	74.06	41.27	461.49	17.97	25.42	0.33
46	60	1	52.19	1.70	1.16	25.1	272.64	94.31	36.87	93.47	207.31	18.63	57.54	0.26
47	61	1	60.91	0.68	1.28	26.5	441.22	196.09	96.12	16.73	555.05	19.68	10.30	0.20
48	62	1	38.59	0.63	0.53	27.2	NaN	NaN	NaN	NaN	NaN	20.17	NaN	NaN
50	64	1	46.38	0.58	3.21	18.6	529.06	250.59	118.95	14.74	700.89	13.79	9.10	0.29

51	65	1	34.75	0.43	2.53	21.8	519.72	233.89	108.34	17.24	558.47	16.18	10.63	0.29
52	66	1	32.90	0.33	1.10	23.1	485.72	215.37	100.32	18.11	472.89	17.09	11.16	0.26
54	67	1	24.30	0.39	NaN	21.5	517.44	248.42	117.84	13.98	491.76	15.94	8.62	0.27
55	68	1	32.90	0.33	1.22	22.8	545.26	274.52	128.76	12.76	507.12	16.88	7.86	0.30
56	69	1	34.24	0.17	0.76	23.8	487.26	212.14	91.98	25.93	331.35	17.67	15.97	0.36
57	71	1	25.60	0.17	0.15	28.4	409.38	176.96	74.64	19.61	238.16	21.06	12.06	0.19
58	72	1	23.89	0.26	0.28	28.2	328.13	137.88	65.52	20.82	193.00	20.88	12.80	0.12
60	75	1	15.94	0.03	1.75	20.1	523.97	217.04	96.85	16.33	348.59	15.00	10.07	0.24
61	76	1	14.18	0.02	3.52	14.2	347.22	157.22	95.00	33.42	249.68	10.57	20.67	0.26
62	77	1	10.40	0.01	1.24	13.6	448.57	184.61	106.93	34.25	253.88	10.11	21.19	0.36
63	78	1	9.15	0.03	0.95	12.2	412.00	187.03	96.90	12.65	219.92	9.09	7.83	0.14
64	79	1	25.45	0.02	0.34	9.9	421.85	186.92	98.91	13.78	215.87	7.28	8.54	0.15
65	80	1	6.20	0.05	0.63	8.9	410.89	177.03	93.11	24.19	208.95	6.57	15.00	0.24
66	81	1	10.00	0.08	0.87	7.6	469.35	220.07	99.69	26.25	216.47	5.57	16.29	0.40
1	19	2	103.06	0.06	20.49	4.7	750.35	337.96	132.68	16.39	1038.25	2.76	10.19	0.59
2	20	2	257.43	0.47	3.16	20.1	NaN	NaN	NaN	NaN	NaN	15.08	NaN	NaN
3	21	2	275.78	0.63	0.53	25.3	NaN	NaN	NaN	NaN	NaN	19.33	NaN	NaN
4	22	2	189.96	0.94	1.76	26.3	NaN	NaN	NaN	NaN	NaN	20.14	NaN	NaN
5	23	2	159.58	0.82	1.07	27.1	NaN	NaN	NaN	NaN	NaN	20.80	NaN	NaN
6	24	2	136.21	0.66	0.52	27.9	NaN	NaN	NaN	NaN	NaN	21.45	NaN	NaN
7	25	2	60.31	0.49	0.18	28.3	558.34	243.18	129.12	9.74	1087.21	21.78	5.98	0.18
8	26	2	70.57	0.36	0.13	28.5	499.61	227.91	127.69	10.05	909.16	21.94	6.17	0.16
9	27	2	38.95	0.31	0.00	28.6	498.98	222.70	124.16	10.37	711.11	22.06	6.37	0.16
10	28	2	37.33	0.18	0.10	28.8	474.71	211.03	115.99	10.74	600.42	22.17	6.60	0.15
11	29	2	24.49	0.09	0.20	28.8	457.52	204.86	124.38	8.34	516.41	22.18	5.12	0.11
12	30	2	20.97	0.03	0.17	28.8	486.01	208.60	123.12	8.49	373.27	22.22	5.21	0.11
13	31	2	37.50	0.00	0.24	28.9	428.22	186.37	115.00	7.96	306.42	22.31	4.89	0.09
14	32	2	12.35	0.01	0.06	28.9	400.37	183.36	107.06	10.03	269.76	22.31	6.16	0.10
15	33	2	18.90	0.03	0.17	28.9	427.12	199.10	118.41	8.48	310.32	22.26	5.21	0.10
16	34	2	11.64	0.06	0.31	28.8	379.00	169.03	99.04	11.35	230.43	22.19	6.97	0.10
17	35	2	10.28	0.01	0.13	28.5	449.64	177.59	107.11	12.84	350.65	21.97	7.89	0.13
18	36	2	40.63	0.01	1.84	28.4	441.57	173.27	90.99	15.91	324.97	21.85	9.77	0.15
19	37	2	22.50	0.01	1.48	28.3	631.23	256.01	127.43	10.72	425.68	21.80	6.59	0.22
20	38	2	22.90	0.02	0.86	27.5	595.81	214.77	112.60	24.25	313.55	21.08	14.91	0.35
21	39	2	24.12	0.01	2.16	27.4	529.80	217.29	130.70	28.82	590.52	21.00	17.72	0.42
22	40	2	19.71	0.03	1.80	24.3	634.31	235.42	111.63	26.76	307.57	18.50	16.47	0.46
23	41	2	17.09	0.04	0.96	24.1	424.77	152.41	82.67	28.27	181.13	18.31	17.41	0.20
24	42	2	22.35	0.01	4.25	20.9	632.08	287.25	124.14	16.91	282.76	15.70	10.43	0.43
25	45	2	27.43	0.32	0.00	0.1	484.07	215.09	122.93	10.91	564.14	-1.03	6.80	0.16
26	46	2	25.84	0.19	0.00	0.1	381.04	169.30	77.23	14.00	266.03	-1.05	8.72	0.13
27	50	2	12.59	0.05	18.58	0.1	313.14	137.30	61.98	23.95	134.30	-1.00	14.92	0.14
28	51	2	155.36	0.70	3.66	16.5	NaN	NaN	NaN	NaN	NaN	12.11	NaN	NaN
29	52	2	150.96	0.44	3.01	23.9	NaN	NaN	NaN	NaN	NaN	18.07	NaN	NaN
30	53	2	176.31	0.40	1.26	25.3	NaN	NaN	NaN	NaN	NaN	19.22	NaN	NaN
31	54	2	152.54	0.33	0.82	26.4	NaN	NaN	NaN	NaN	NaN	20.04	NaN	NaN
32	55	2	131.24	0.32	0.44	27.2	NaN	NaN	NaN	NaN	NaN	20.73	NaN	NaN
33	56	2	92.83	0.22	0.10	27.8	NaN	NaN	NaN	NaN	NaN	21.27	NaN	NaN
34	57	2	77.39	0.17	0.11	27.9	NaN	NaN	NaN	NaN	NaN	21.37	NaN	NaN

35	58	2	56.05	0.11	0.25	28.1	534.04	226.29	98.44	18.60	822.27	21.53	11.43	0.30
36	59	2	38.71	0.02	1.00	28.3	457.88	255.47	115.20	13.06	775.97	21.62	8.02	0.26
38	61	2	36.40	0.01	7.24	25.1	360.39	133.15	61.86	40.90	262.04	19.04	25.17	0.23
39	62	2	39.05	0.03	5.06	24.6	518.95	216.35	101.01	26.30	581.78	18.60	16.19	0.38
40	63	2	42.62	0.02	1.00	22.5	462.48	170.46	87.97	32.01	279.62	16.91	19.73	0.29
1	2	3	162.01	0.68	0.39	5.9	NaN	NaN	NaN	NaN	NaN	2.58	NaN	NaN
2	3	3	139.13	0.60	1.54	7.9	497.50	219.42	45.82	28.44	626.37	4.11	17.66	0.43
3	4	3	55.98	0.88	0.96	9.1	409.93	193.53	41.93	32.12	459.99	5.06	19.94	0.38
4	5	3	80.74	0.92	2.58	10.7	404.98	185.04	39.78	34.42	482.34	6.28	21.35	0.37
5	6	3	106.73	0.88	2.73	13.1	400.75	185.73	45.53	29.88	560.31	8.11	18.52	0.32
6	7	3	82.18	0.68	5.51	18.5	NaN	NaN	NaN	NaN	NaN	12.24	NaN	NaN
7	8	3	56.45	0.78	4.34	23.1	380.99	169.84	49.56	34.51	324.08	15.77	21.28	0.31
8	9	3	141.75	0.65	2.01	25.8	350.04	164.95	42.47	42.12	183.01	17.84	25.94	0.36
9	10	3	65.35	0.39	1.50	27.2	458.82	207.83	70.48	26.66	285.85	18.91	16.41	0.36
10	11	3	30.39	0.19	0.87	28.4	448.58	224.08	56.58	34.00	185.73	19.78	20.92	0.53
11	12	3	18.71	0.07	0.74	29.3	374.08	198.41	24.10	68.45	59.03	20.42	42.09	0.84
12	13	3	11.45	0.02	0.25	29.6	362.51	188.24	18.29	89.50	41.40	20.64	55.03	0.98
13	14	3	25.19	0.02	0.05	29.3	308.64	154.95	22.41	103.85	60.96	20.49	63.86	0.77
14	15	3	24.46	0.02	0.24	29.5	368.82	181.02	35.34	67.95	109.86	20.61	41.78	0.69
15	16	3	17.73	0.00	0.14	29.4	348.58	190.16	36.04	66.83	129.37	20.57	41.10	0.75
16	17	3	15.35	0.01	0.25	29.1	406.16	191.36	53.99	83.70	279.17	20.33	51.47	0.95
17	18	3	16.60	0.02	0.47	28.7	357.35	182.29	18.16	87.27	53.85	20.02	53.68	0.90
18	19	3	19.00	0.00	1.21	27.3	440.47	196.27	61.94	79.49	253.55	18.91	48.93	0.95
19	20	3	28.52	0.01	1.55	25.8	354.98	169.47	47.91	84.17	110.09	17.81	51.84	0.75
20	21	3	34.09	0.03	3.30	22.6	NaN	NaN	NaN	NaN	NaN	15.32	NaN	NaN
21	23	3	23.50	0.02	2.26	16.3	430.13	181.05	41.94	48.04	251.98	10.43	29.72	0.49
22	24	3	27.10	0.08	2.84	13.8	552.04	276.05	36.22	76.01	221.65	8.54	47.08	1.81
23	25	3	24.03	0.15	2.87	11.5	457.70	220.58	31.56	55.76	282.98	6.79	34.57	0.85
24	26	3	23.57	0.06	0.64	10.0	NaN	NaN	NaN	NaN	NaN	5.58	NaN	NaN
47	28	3	17.87	0.08	1.56	6.3	NaN	NaN	NaN	NaN	NaN	2.89	NaN	NaN
48	29	3	17.79	0.21	6.58	12.4	NaN	NaN	NaN	NaN	NaN	7.47	NaN	NaN
49	30	3	14.85	0.26	2.48	10.7	324.56	162.90	16.30	157.34	70.91	6.18	97.60	1.31
50	31	3	137.62	0.47	5.79	14.1	306.26	143.59	20.75	90.97	106.02	8.75	56.34	0.59
51	32	3	119.60	0.61	7.18	22.2	NaN	NaN	NaN	NaN	NaN	14.99	NaN	NaN
52	33	3	139.56	0.90	3.61	26.5	251.67	75.05	17.80	96.53	172.36	18.33	59.43	0.17
53	34	3	144.49	1.79	1.33	28.2	205.41	70.54	20.81	86.94	209.83	19.61	53.49	0.13
54	35	3	121.12	0.32	1.24	29.4	456.96	181.86	58.15	58.82	786.56	20.54	36.17	0.60
55	36	3	132.04	1.45	0.61	30.3	218.13	75.36	25.02	82.84	204.30	21.18	50.92	0.15
56	37	3	113.13	1.00	0.26	30.6	457.51	177.29	60.09	32.98	581.03	21.40	20.27	0.32
57	38	3	72.97	1.01	0.16	30.7	428.85	171.71	54.67	39.25	409.01	21.48	24.12	0.36
58	39	3	70.27	1.07	0.02	30.6	447.88	170.02	55.16	41.76	311.81	21.43	25.66	0.37
59	40	3	166.48	0.90	0.02	30.7	385.46	150.18	46.96	60.44	213.06	21.51	37.14	0.42
60	41	3	44.38	0.71	0.06	30.9	380.32	159.82	57.76	52.29	254.72	21.60	32.13	0.41
61	42	3	48.71	0.42	0.03	30.9	382.11	156.86	49.37	54.83	178.75	21.61	33.69	0.42
62	43	3	34.73	0.00	0.01	30.8	375.65	173.54	52.24	62.86	142.81	21.57	38.63	0.59
63	44	3	17.43	0.07	0.00	30.8	391.12	162.20	33.23	88.09	85.37	21.57	54.13	0.72
64	45	3	11.87	0.02	0.05	30.9	350.55	160.35	26.29	102.48	61.11	21.60	62.97	0.82
65	46	3	13.88	0.08	0.03	30.8	214.99	66.32	8.90	284.86	22.87	21.56	175.05	0.39

66	47	3	10.01	0.30	0.04	30.8	246.69	97.59	14.10	203.09	25.32	21.56	124.80	0.60
67	48	3	34.70	0.63	0.15	30.7	247.83	105.95	18.15	152.76	36.33	21.47	93.88	0.53
68	49	3	39.37	0.97	0.35	30.4	360.77	158.97	35.28	76.09	122.48	21.26	46.77	0.60
69	50	3	27.00	0.78	0.55	29.7	306.00	138.24	31.15	85.25	88.75	20.73	52.41	0.51
70	51	3	22.66	0.66	1.00	26.1	293.72	153.31	26.63	95.52	72.26	17.99	58.83	0.70
71	52	3	56.70	0.50	1.17	27.7	443.55	221.96	53.81	42.42	186.49	19.16	26.11	0.65

Appendix VI. Acoustic estimate of settling velocity inputs

Year	Day	Datenum	TSS (pumps)	ADV (dB)	log(TSS)	Ctotal_log	Ctotal	w_ADV	w'C'
2013	5	735543.3701	27.39	29.51	1.44	1.59	38.62	0.01	-0.33
2013	5	735543.3875	24.56	31.21	1.39	1.70	49.75	-0.02	0.97
2013	5	735543.4033	25.88	30.57	1.41	1.66	45.25	0.00	-0.17
2013	5	735543.418	34.75	32.47	1.54	1.78	60.06	-0.01	0.84
2013	5	735543.4287	37.01	33.56	1.57	1.85	70.65	0.00	0.32
2013	5	735543.4412	94.41	37.39	1.98	2.10	125.18	0.00	0.07
2013	5	735543.4523	139.41	38.79	2.14	2.19	154.13	0.00	-0.50
2013	5	735543.4634	89.42	37.33	1.95	2.09	124.08	0.01	-1.09
2013	5	735543.4756	84.90	36.09	1.93	2.01	103.15	-0.02	1.67
2013	5	735543.4852	84.85	35.24	1.93	1.96	90.81	0.01	-1.18
2013	5	735543.497	78.18	33.86	1.89	1.87	73.88	0.00	-0.17
2013	5	735543.5064	69.55	32.47	1.84	1.78	60.03	0.00	-0.23
2013	5	735543.5194	45.82	29.23	1.66	1.57	37.07	0.01	-0.31
2013	5	735543.5327	48.76	28.44	1.69	1.52	32.94	-0.01	0.18
2013	5	735543.5451	19.82	27.66	1.30	1.47	29.29	0.00	0.09
2013	5	735543.5593	46.07	28.88	1.66	1.55	35.15	0.00	0.16
2013	5	735543.5703	24.88	26.38	1.40	1.38	24.23	0.00	0.04
2013	5	735543.5815	25.24	26.03	1.40	1.36	22.97	0.00	0.01
2013	5	735543.5978	33.22	27.17	1.52	1.44	27.24	0.00	-0.05
2013	5	735543.6099	22.30	27.23	1.35	1.44	27.48	-0.01	0.30
2013	5	735543.6225	16.88	25.37	1.23	1.32	20.81	0.01	-0.12
2013	5	735543.6354	23.72	28.21	1.38	1.50	31.79	-0.01	0.25
2013	5	735543.6479	18.81	28.61	1.27	1.53	33.76	-0.01	0.22
2013	5	735543.6601	24.42	28.49	1.39	1.52	33.16	0.00	0.15
2013	5	735543.6721	30.29	28.83	1.48	1.54	34.90	0.00	-0.05
2013	5	735543.6842	21.31	29.83	1.33	1.61	40.49	0.00	-0.07
2013	6	735544.4505	103.00	35.15	2.01	1.95	89.62	-0.01	1.14
2013	6	735544.4627	83.77	34.74	1.92	1.93	84.34	-0.01	0.57
2013	6	735544.4746	148.00	36.03	2.17	2.01	102.21	-0.01	0.92
2013	6	735544.4879	211.00	35.94	2.32	2.00	100.80	-0.01	0.75
2013	6	735544.5004	139.47	38.54	2.14	2.17	148.55	0.00	0.52
2013	6	735544.5121	180.53	34.41	2.26	1.90	80.19	-0.01	0.67
2013	6	735544.5248	117.47	32.77	2.07	1.80	62.85	-0.01	0.48
2013	6	735544.5377	125.24	33.49	2.10	1.85	69.99	-0.01	0.46

2013	6	735544.5488	82.57	30.45	1.92	1.65	44.42	-0.01	0.23
2013	6	735544.5611	46.89	29.59	1.67	1.59	39.06	0.01	-0.48
2013	6	735544.5749	43.78	27.90	1.64	1.48	30.39	0.00	0.12
2013	6	735544.586	19.09	23.37	1.28	1.19	15.46	-0.01	0.13
2013	6	735544.598	33.91	24.90	1.53	1.29	19.42	0.00	-0.09
2013	6	735544.6096	28.28	27.13	1.45	1.43	27.06	0.00	-0.01
2013	6	735544.6223	23.67	25.55	1.37	1.33	21.38	0.00	0.03
2014	15	735734.3632	103.06	34.20	2.01	1.92	83.53	0.00	0.37
2014	15	735734.3784	257.43	38.15	2.41	2.30	198.89	-0.02	4.70
2014	15	735734.3934	275.78	38.90	2.44	2.37	234.45	-0.01	3.20
2014	15	735734.4084	189.96	36.15	2.28	2.11	128.12	-0.02	1.97
2014	15	735734.4242	159.58	37.67	2.20	2.25	178.95	-0.02	3.06
2014	15	735734.4392	136.21	37.18	2.13	2.21	160.78	-0.02	2.87
2014	15	735734.4539	60.31	35.47	1.78	2.04	110.42	-0.01	1.29
2014	15	735734.4691	70.57	33.79	1.85	1.88	76.32	-0.01	0.93
2014	15	735734.4842	38.95	32.12	1.59	1.72	52.81	-0.02	1.03
2014	15	735734.4995	37.33	31.46	1.57	1.66	45.68	-0.01	0.48
2014	15	735734.5153	24.49	29.43	1.39	1.47	29.25	0.01	-0.16
2014	15	735734.5314	20.97	28.26	1.32	1.35	22.63	0.00	0.07
2014	15	735734.5469	37.50	27.93	1.57	1.32	21.07	0.00	-0.03
2014	15	735734.5634	12.35	27.93	1.09	1.32	21.08	0.00	-0.01
2014	15	735734.5792	18.90	28.06	1.28	1.34	21.65	0.00	-0.01
2014	15	735734.5953	11.64	27.29	1.07	1.26	18.29	0.00	0.03
2014	15	735734.612	10.28	26.53	1.01	1.19	15.48	0.00	0.01
2014	15	735734.6276	40.63	29.38	1.61	1.46	28.97	0.00	-0.07
2014	15	735734.6432	22.50	28.95	1.35	1.42	26.32	0.00	-0.05
2014	15	735734.6587	22.90	28.30	1.36	1.36	22.84	0.01	-0.20
2014	15	735734.6745	24.12	27.69	1.38	1.30	19.98	0.01	-0.11
2014	15	735734.6886	19.71	28.45	1.29	1.37	23.59	0.01	-0.15
2014	15	735734.7037	17.09	27.04	1.23	1.24	17.31	0.00	0.05
2014	15	735734.7188	22.35	27.48	1.35	1.28	19.09	0.00	-0.08
2014	15	735734.735	21.76	25.86	1.34	1.13	13.36	0.00	-0.04
2014	17	735736.3525	32.11	31.18	1.51	1.63	42.98	-0.01	0.31
2014	17	735736.367	27.43	29.18	1.44	1.44	27.70	-0.01	0.14
2014	17	735736.3812	25.84	27.54	1.41	1.29	19.32	-0.01	0.17
2014	17	735736.3955	13.53	26.21	1.13	1.16	14.44	0.00	0.03
2014	17	735736.4094	13.54	25.50	1.13	1.09	12.34	0.00	0.03
2014	17	735736.425	13.65	23.49	1.14	0.90	7.94	0.00	0.00
2014	17	735736.4477	12.59	27.12	1.10	1.25	17.61	-0.01	0.23
2014	17	735736.4628	155.36	35.29	2.19	2.03	105.98	-0.02	1.74
2014	17	735736.4781	150.96	36.00	2.18	2.09	124.03	-0.02	1.93
2014	17	735736.4941	176.31	37.35	2.25	2.22	166.69	-0.01	1.96
2014	17	735736.5096	152.54	37.17	2.18	2.21	160.42	-0.01	1.71
2014	17	735736.5267	131.24	36.03	2.12	2.10	124.88	-0.01	1.14

2014	17	735736.545	92.83	34.88	1.97	1.99	96.96	-0.01	0.76
2014	17	735736.5599	77.39	33.70	1.89	1.87	74.87	-0.01	0.64
2014	17	735736.5752	56.05	32.86	1.75	1.79	62.25	0.01	-0.76
2014	17	735736.6015	38.71	31.69	1.59	1.68	48.15	0.00	-0.19
2014	17	735736.6446	50.69	30.99	1.70	1.62	41.28	0.01	-0.51
2014	17	735736.6612	36.40	31.00	1.56	1.62	41.35	0.00	0.06
2014	17	735736.6762	39.05	30.18	1.59	1.54	34.50	0.01	-0.23
2014	17	735736.691	42.62	31.27	1.63	NAN	NAN	0.03	NAN
2015	28	736235.3529	87.07	33.32	1.94	1.85	70.63	0.01	-0.37
2015	28	736235.3717	162.01	36.99	2.21	2.05	113.48	0.01	-1.30
2015	28	736235.3878	139.13	34.25	2.14	1.90	79.69	0.03	-2.71
2015	28	736235.403	55.98	34.57	1.75	1.92	83.00	0.01	-1.08
2015	28	736235.4204	80.74	34.69	1.91	1.93	84.35	-0.01	0.61
2015	28	736235.4365	106.73	36.59	2.03	2.03	107.76	-0.01	1.25
2015	28	736235.4514	82.18	36.06	1.91	2.00	100.71	0.00	-0.24
2015	28	736235.4654	56.45	34.22	1.75	1.90	79.39	-0.02	1.35
2015	28	736235.4799	141.75	30.78	2.15	1.71	50.89	-0.01	0.43
2015	28	736235.4944	65.35	29.41	1.82	1.63	42.62	0.00	-0.13
2015	28	736235.5096	30.39	27.44	1.48	1.52	33.07	0.00	-0.02
2015	28	736235.5293	18.71	24.47	1.27	1.35	22.51	0.01	-0.26
2015	28	736235.5483	11.45	22.04	1.06	1.22	16.46	0.00	0.03
2015	28	736235.5636	25.19	21.41	1.40	1.18	15.17	0.00	-0.03
2015	28	736235.5796	24.46	21.98	1.39	1.21	16.33	0.00	-0.08
2015	28	736235.5953	17.73	21.35	1.25	1.18	15.06	0.00	-0.07
2015	28	736235.6115	15.35	22.74	1.19	1.26	18.01	0.00	-0.03
2015	28	736235.6274	16.60	24.61	1.22	1.36	22.93	0.01	-0.14
2015	28	736235.6449	19.00	26.62	1.28	1.47	29.73	0.00	-0.09
2015	28	736235.6598	28.52	27.85	1.46	1.54	34.85	0.01	-0.22
2015	28	736235.6751	34.09	30.21	1.53	1.67	47.31	0.00	-0.07
2015	28	736235.6898	26.30	31.02	1.42	1.72	52.47	0.00	-0.02
2015	28	736235.7058	23.50	31.77	1.37	1.76	57.80	0.01	-0.75
2015	28	736235.7213	27.10	31.67	1.43	1.76	57.13	0.02	-0.98
2015	28	736235.7361	24.03	30.93	1.38	1.71	51.86	0.00	-0.22
2015	28	736235.7513	23.57	29.71	1.37	1.65	44.35	0.01	-0.65
2015	1	736238.3395	30.04	26.41	1.48	1.46	28.92	0.01	-0.33
2015	1	736238.3566	17.87	22.67	1.25	1.25	17.84	0.00	0.05
2015	1	736238.3716	17.79	20.02	1.25	1.10	12.67	0.01	-0.14
2015	1	736238.3874	14.85	18.94	1.17	1.04	11.03	0.02	-0.18
2015	1	736238.4023	137.62	31.48	2.14	1.75	55.72	0.03	-1.45
2015	1	736238.4174	119.60	31.86	2.08	1.77	58.54	0.03	-1.95
2015	1	736238.4324	139.56	34.00	2.14	1.89	77.15	0.04	-3.23
2015	1	736238.4467	144.49	37.19	2.16	2.07	116.55	0.05	-5.41
2015	1	736238.4607	121.12	37.68	2.08	2.09	124.07	-0.20	NAN
2015	1	736238.4758	132.04	35.96	2.12	2.00	99.33	0.02	-2.41

2015	1	736238.4907	113.13	35.97	2.05	2.00	99.51	0.03	-3.41
2015	1	736238.5058	72.97	35.59	1.86	1.98	94.74	0.03	-2.65
2015	1	736238.5211	70.27	34.75	1.85	1.93	84.98	0.01	-1.04
2015	1	736238.5395	166.48	32.12	2.22	1.78	60.50	0.04	-2.45
2015	1	736238.554	44.38	31.14	1.65	1.73	53.33	0.03	-1.57
2015	1	736238.5689	48.71	29.10	1.69	1.61	40.95	0.02	-0.77
2015	1	736238.5839	34.73	NAN	1.54	NAN	NAN	0.02	NAN
2015	1	736238.602	17.43	23.88	1.24	1.32	20.87	0.01	-0.17
2015	1	736238.6193	11.87	18.33	1.07	1.01	10.19	0.00	-0.03
2015	1	736238.6346	13.88	21.93	1.14	1.21	16.23	0.00	0.00
2015	1	736238.6504	10.01	18.72	1.00	1.03	10.71	0.01	-0.15
2015	1	736238.666	34.70	28.33	1.54	1.57	37.07	0.02	-0.74
2015	1	736238.682	39.37	29.18	1.60	1.62	41.38	0.03	-1.16
2015	1	736238.697	27.00	25.83	1.43	1.43	26.86	0.03	-0.78
2015	1	736238.7125	22.66	25.46	1.36	1.41	25.59	0.02	-0.44
2015	1	736238.7271	56.70	31.35	1.75	1.74	54.76	0.02	-0.93
2015	1	736238.7391	46.04	32.33	1.66	1.79	62.16	0.02	-1.22